Disruption of S-adenosylmethionine metabolism in *Drosophila melanogaster* and its impact on chromatin

Dissertation zur Erlangung des Doktorgrades

der Naturwissenschaften an der Fakultät für Biologie der

Ludwig-Maximilians-Universität München

vorgelegt von

Simone Manuela Vollmer

aus Tübingen

Tag der Einreichung: 12. September 2016

Tag der mündlichen Prüfung: 19. Dezember 2016

1. Gutachter: Prof. Dr. Peter Becker

2. Gutachter: Prof. Dr. Dirk Eick

3. Gutachter: Prof. Dr. Kirsten Jung

4. Gutachter: Prof. Dr. John Parsch

5. Gutachter: Prof. Dr. Michael Boshart

6. Gutachter: Prof. Dr. Angelika Böttger

Eidesstattliche Erklärung

Ich versichere hiermit an Eides statt, dass die vorgelegte Dissertation von mir selbständig und ohne unerlaubte Hilfe angefertigt ist.

München, den …… **……**

Simone Vollmer

Table of contents

Summary

The eukaryotic genome is organized in the nucleus in a dynamic structure defined as chromatin. Alterations in chromatin structure are central to many cellular processes such as transcription, replication, DNA repair and cell cycle progression. Chromatin is mainly composed of a repeating unit of DNA and histone proteins. Chemical modifications of these two components are involved in the regulation of chromatin dynamics and gene expression. Many of these modifications are added and removed by enzymes that use cofactors which are derived from metabolism which suggests a direct link between the metabolic state of a cell and the regulation of transcription.

Methylation of DNA and histones is an important epigenetic modification. It is catalyzed by specific methyltransferases that use S-adenosylmethionine (SAM) as a cofactor. SAM is the major methyl group donor and its synthesis is catalyzed by the enzyme S-adenosylmethionine Synthetase (Sam-S) in *Drosophila melanogaster*. This metabolic enzyme is encoded by the *Su(z)5* gene which was isolated in a genetic screen for chromatin modifiers suggesting that Sam-S is directly involved in the regulation of gene expression by changes of chromatin structure.

In this study, different approaches were used to investigate the function of Sam-S in the chromatin of *Drosophila melanogaster* cells. Firstly, using indirect immunofluorescence, the metabolic enzyme Sam-S was found to localize not only to the cytoplasm but also to the nucleus, a prerequisite for potential involvement in chromatin changes. Subsequent proteomic analysis of interaction partners of Sam-S in the nucleus revealed that the enzyme interacts with transcriptional and epigenetic regulators including transcription factors and chromatin modifying proteins. Secondly, knockdown of the endogenous Sam-S in *Drosophila melanogaster* cells led to a major change in cellular SAM concentration. The disruption of SAM metabolism by knockdown of the enzyme interfered with normal cell proliferation and directly affected histone methylation levels with a strong decrease of H3K4me3 and H4K20me3. This decrease had a significant impact on gene expression and genes involved in carbohydrate metabolic processes were affected most. Furthermore, the expression levels of SAM-dependent methyltransferases as well as the levels of transposable elements were altered. Finally, using a heavy methyl SILAC approach, the *Drosophila melanogaster* methylome was determined since methylation of lysine and arginine residues on non-histone proteins has emerged as an important modification in a wide range of cellular functions.

Taken together, the results in this thesis expand our understanding of the link between metabolism and epigenetics through a detailed study of Sam-S's role in controlling gene expression in the model organism *Drosophila melanogaster*.

Zusammenfassung

Das Genom eukaryotischer Zellen liegt in einer dynamischen Struktur im Zellkern vor und wird als Chromatin bezeichnet. Änderungen dieser Chromatinstruktur haben Auswirkungen auf viele zelluläre Prozesse wie beispielsweise die Transkription, die Replikation, die DNA-Reparatur oder den Zellzyklus. Chromatin besteht hauptsächlich aus Nukleosomen, einer wiederkehrenden Einheit aus DNA und Histonproteinen. Chemische Modifikationen dieser zwei Komponenten sind an der dynamischen Regulation der Chromatinstruktur und somit der Genexpression beteiligt. Viele dieser Modifikationen werden von Enzymen angeheftet und entfernt, welche Cofaktoren verwenden, die in Stoffwechselprozessen entstehen. Der Schluss liegt dadurch nahe, dass es eine direkte Verbindung zwischen dem metabolischen Zustand einer Zelle und der Regulation der Transkription gibt.

Die Methylierung von DNA und Histonen ist eine sogenannte epigenetische Modifikation, welche außerhalb der DNA-Sequenz passiert und vererbbar ist. Sie wird von spezifischen Methyltransferasen angeheftet, die S-Adenosylmethionin (SAM) als Cofaktor verwenden. SAM ist der wichtigste Methyldonor in der Zelle und seine Synthese wird durch das Enzym S-Adenosylmethionin-Synthetase (Sam-S) in *Drosophila melanogaster* katalysiert. Dieses metabolische Enzym wird durch das *Su(z)*5-Gen kodiert, welches in einem genetischen Screen nach Faktoren, die Chromatin modifizieren, entdeckt wurde. Dies lässt auf einen direkten Bezug zwischen Sam-S und der Chromatinstruktur schließen.

In der vorliegenden Arbeit wurden verschiedene Experimente in *Drosophila melanogaster* Zellen durchgeführt, um die Funktion von Sam-S im Zusammenhang mit Chromatin zu untersuchen. Zuerst wurde mit Hilfe der Immunfluoreszenz herausgefunden, dass das metabolische Enzym Sam-S nicht nur im Zytoplasma, sondern auch im Zellkern lokalisiert ist. Anschließende Proteomanalysen zeigten, dass Sam-S im Kern sowohl mit Proteinen interagiert, die die Transkription regulieren, als auch mit epigenetischen Regulatorproteinen, die Chromatin modifizieren können. Eine Reduktion des endogenen Sam-S in *Drosophila melanogaster*- Zellen führte zu einer drastischen Veränderung der zellulären SAM-Konzentration. Diese Störung des SAM-Stoffwechsels verlangsamte die Zellproliferation und hatte direkten Einfluss auf die Histonmethylierung. Dabei waren die Level an H3K4me3 und H4K20me3 am stärksten reduziert. Dies führte zu einer signifikanten Änderung der Genexpression, wobei Gene, die in den Kohlenhydrat-Stoffwechsel involviert sind, am stärksten fehlreguliert waren. Darüber hinaus wurde eine Fehlregulation von SAM-abhängigen Methyltransferasen sowie Transposons beobachtet. Da immer öfter ein Zusammenhang von Methylierung von Nicht-Histonproteinen mit verschiedenen Zellfunktionen bekannt wird, wurde das

Drosophila melanogaster Methylproteom bestimmt. Dazu wurden Zellen mit isotopenmarkiertem Methionin inkubiert und mit Hilfe der Massenspektrometrie analysiert.

Die Ergebnisse dieser Arbeit tragen zu einem besseren Verständnis der Rolle des metabolischen Enzyms Sam-S in der Regulation von Genexpression bei und unterstreichen den Zusammenhang zwischen Stoffwechsel und Epigenetik.

1. Introduction

1.1. Chromatin

1.1.1. Chromatin structure

Chromatin is a dynamic structure in the nucleus in which the eukaryotic genome is organized. It consists of DNA, histone proteins, additional DNA-associated proteins and non-coding RNAs (ncRNAs). Based on the extent of spatial compaction, chromatin is usually categorized into the less dense euchromatin and the tightly packed heterochromatin (Elgin and Grewal, 2003; Heitz, 1928). In general, the conformation of euchromatin is more accessible to transcription factors and polymerases and genes are transcriptionally active, while heterochromatin is referred to as a condensed and transcriptionally inert conformation. It is further classified as constitutive or facultative heterochromatin. Both forms are transcriptionally silenced. However, genes located in facultative heterochromatin can be reactivated in distinct cellular situations such as developmental responses or cell cycle stages (Trojer and Reinberg, 2007). In contrast, constitutive heterochromatin is thought to be a more static structure that forms mostly at pericentric regions and telomeres usually consisting of repetitive DNA such as satellite DNA or transposon repeats, respectively (Saksouk et al., 2015).

Nucleosomes form the basic and repeating unit of chromatin and consist of DNA and histone proteins (Kornberg and Thomas, 1974). 147-bp segments are wrapped around a histone octamer and are separated by DNA linkers of various lengths. Dimers of four core histones H2A, H2B, H3 and H4 form the octameric histone protein complex in the nucleosomes (Luger et al., 1997). Another histone, histone H1, binds the linker DNA between two nucleosomes and is involved in the higher order structure of chromatin (Thoma and Koller, 1977). Histones are relatively small proteins with a structured globular domain in the core of the nucleosome and a flexible N-terminal histone tail which protrudes out of the nucleosomal structure (Figure 1.1) and is subjected to a variety of posttranslational modifications (PTMs) (Allfrey and Mirsky, 1964). The nucleosomal structure of chromatin organizes DNA packaging in the nucleus and is a prerequisite for the regulation of genome function.

1.1.2. Regulation of chromatin structure

The cellular machinery employs a variety of mechanisms for dynamic changes in chromatin structure and regulation of gene activity. This includes ATP-dependent chromatin remodeling, incorporation or

replacement of histone variants, ncRNAs, different arrangements of chromosomal domains within the 3D architecture and PTMs of DNA and histone proteins (Bonisch et al., 2008) (Figure 1.1).

Chromatin remodeling

The chromatin remodeling complexes use energy from ATP hydrolysis to catalyze the assembly and disassembly of nucleosomes or to reposition existing ones. In this way, they make DNA more or less accessible for regulatory factors and enzymes (Becker and Horz, 2002). Chromatin remodeling complexes are usually large protein complexes consisting of diverse subunits. ATP hydrolysis is mediated by a highly conserved ATPase domain, related to superfamily 2 DNA helicases (Flaus and Owen-Hughes, 2011) that is characteristic of all remodeling complexes.

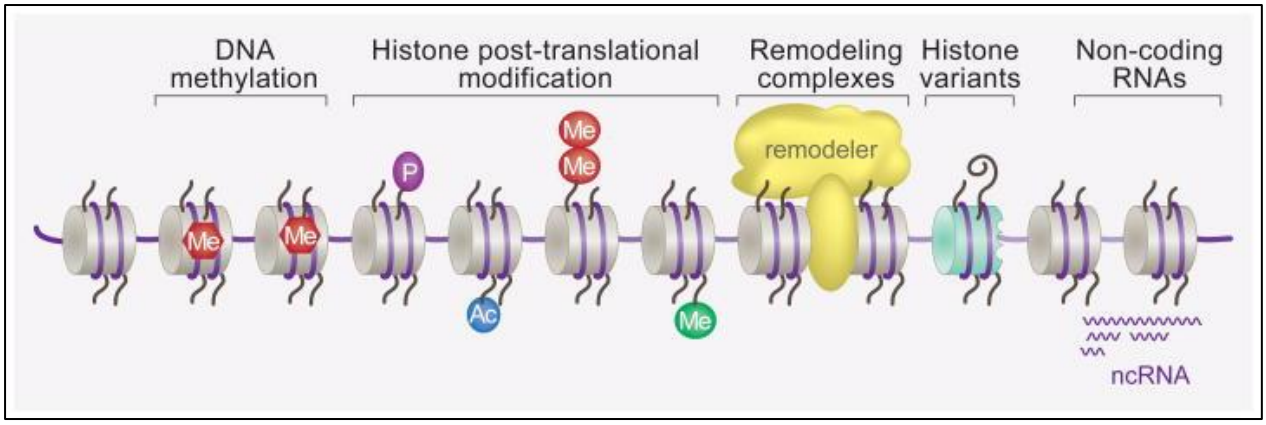

Figure 1.1: Schematic overview of chromatin-mediated gene regulation
Different epigenetic mechanisms regulate the dynamic structure of chromatin. Structural changes may be affected by chemical modifications of DNA and histones, remodeling of nucleosomes or histone variants and by non-coding RNAs (ncRNA). Chromatin structure regulates nuclear processes like transcription and replication by altering the accessibility of DNA to regulatory factors like chromatin modifying complexes, transcription factors or RNA polymerase II (reproduced from Dulac, 2010).

Histone variants

Incorporation or replacement of canonical histones by specialized histone variants can lead to an altered chromatin structure and can influence interaction with other factors like chromatin remodelers, transcription factors or other nucleosomes (Bonisch et al., 2008). Histone variants can either be synthesized and deposited in a cell cycle-dependent manner or incorporated in different chromatin compartments. The mammalian H3, for instance, exists in two replication-dependent variants, H3.1 and H3.2, which are only synthesized and deposited during S-phase. In contrast, H3.3 is also

incorporated in a replication-independent manner outside of S-phase. CENP-A is another variant of H3 and is found at centromeres (Biterge and Schneider, 2014). The histone variants differ slightly in their primary amino acid sequence. In *Drosophila*, three variants of H3 exist: H3 is expressed and synthesized only during S-phase, while H3.3 and centromere identifier (cid, a homologue to mammalian CENP-A), which is the structural component of centromeric chromatin (Ahmad and Henikoff, 2002) are deposited throughout the cell cycle.

Non-coding RNA

Recently, the important role of ncRNAs in the organization of chromatin structure was discovered. It has been shown that they recruit chromatin modifying complexes to particular genomic loci which then affect the chromatin state and modulate gene expression (Rinn and Chang, 2012). The most prominent and best-studied example in which gene regulation is altered by ncRNAs is the dosage compensation of sex chromosomes.

In mammals, one female X chromosome is randomly silenced. The initiation of this X inactivation event depends on the expression of a long ncRNA (lncRNA), the X-inactive-specific transcript RNA (Xist RNA). It accumulates on the inactive X chromosome and induces the formation of repressive domains. Subsequently, it interacts and recruits the polycomb repressive complex 2 (PRC2) which methylates H3K27, a major repressive histone mark. The conversion into repressive compartments leads to the generation of facultative heterochromatin (Maenner et al., 2012).

In contrast, in *Drosophila*, male flies nearly double the expression of their single X chromosome to equal the expression in female flies. There are several binding sites on the male X, where the dosage compensation complex (DCC) binds with variable affinity. The DCC is composed of male-specific lethal (msl) proteins and two long ncRNAs, the so-called RNA-on-the-X RNA (roX RNAs). Those roX RNAs are help to target the DCC to the male X, where it finally spreads and acetylates proximal histone H4 on lysine 16 (H4K16) by its histone acetyltransferase males absent on the first (mof). This acetylation mark along the X chromosome results in an upregulation of X-linked genes (Maenner et al., 2012).

Nuclear architecture

Chromatin is organized in a three-dimensional and dynamic structure. Chromosomes occupy so-called chromosome territories (CTs) which are distinct regions within the nucleus. While gene-rich regions are found frequently within the nuclear interior, gene-poor regions are more often found at the periphery (Lanctot et al., 2007). A recent review (Cremer et al., 2015) presented new insights into the structure–

function relationship within the nucleus. They provide a new model that is based on two spatially co-aligned nuclear compartments, the transcriptionally active and inactive one.

DNA modifications

The four bases of the DNA backbone can undergo chemical modifications resulting in new bases. These new bases affect DNA structure and its functions in gene expression. The most abundant modification is methylation of cytosine. Its impact on gene expression is described in chapter 1.3.1.

Histone modifications

Along with their role as a structural scaffold for DNA packaging, histones are also instrumental in the regulation of chromatin dynamics including chromatin compaction, nucleosome dynamics and transcription. Histone proteins carry many basic amino acids that are subjected to a variety of PTMs (Kouzarides, 2007). The majority of PTMs have been detected on the flexible N-terminal histone tail which protrudes out of the nucleosome. PTMs can influence interactions between nucleosomes and DNA, internucleosomal interactions among adjacent nucleosomes or they may affect interactions between non-histone proteins and chromatin.

The modifications that can occur on histones include acetylation, methylation, phosphorylation, ubiquitination, SUMOylation, ADP ribosylation, citrullination, formylation, biotinylation and deamination (Kouzarides, 2007; Zhao and Garcia, 2015). More recently, new modifications such as propionylation, butyrylation or crotonylation have been described (Kebede et al., 2015). These modifications are reversible and are catalyzed by a multitude of different enzymes. Thereby, different chromatin modifications are added and removed with very different kinetics (Barth and Imhof, 2010). The so-called histone "writers" and "erasers" – proteins that either incorporate or remove PTMs – have therefore become central figures in understanding epigenetic mechanisms (Gillette and Hill, 2015). They are divided into classes depending on the specific modification that they initiate. Histone acetyltransferases (HAT) and deacetylases (HDAC) add and remove acetylation marks, respectively. Similarly, histone methyltransferases (HMT) and demethylases (HDM) catalyze the methylation and demethylation of histones and kinases and phosphatases place and remove phosphorylation marks. Reader proteins are able to recognize specific PTMs or a combination of PTMs on histones or DNA.

Different histone modification patterns are found in chromatin under different activity states. In general, acetylation of lysines and phosphorylation of serines and threonines are associated with transcriptional activation. SUMOylation seems to repress transcription whereas methylation and

ubiquitination are involved in both, activation and repression, depending on the context and residue (Kouzarides, 2007). While trimethylation of histone H3 on lysine 4 (H3K4me3) marks active chromatin states (Vermeulen et al., 2007), trimethylation of H3 on lysine 27 (H3K27me3) is a hallmark for silenced chromatin states (Simon and Kingston, 2009).

In 2000, Strahl and Allis proposed the existence of a histone code which posits that distinct histone modifications act sequentially or in combination and therefore, when read by other proteins, lead to a distinct regulatory outcome (Strahl and Allis, 2000).

Epigenetic events during differentiation and embryogenesis help to create the multiple cell types present in an organism. Subsequently, environmental exposure can produce variations in phenotypes as is observed in the different epigenetic fingerprint patterns of identical twins (Bell and Spector, 2011). Taken together, the dynamic nature of chromatin seems to play a pivotal role in defining the different cell types that make up an organism.

1.2. Metabolic mechanisms meet chromatin

1.2.1. Epigenetic effects of different diets

The honey bee, *Apis mellifera*, represents one example of environmentally controlled differences in phenotypes. Despite their identical DNA sequence, queen and worker bees have strong anatomical, physiological and behavioral differences. The queen bee's life span, for instance, is 20 times longer than that of a worker bee. Despite having large and active ovaries, a worker bee is functionally sterile (Maleszka, 2008). Both the fertile queen and the sterile worker bees develop from genetically identical female larvae. If larvae are fed with royal jelly, it results in the development of a queen bee. The developmental differences are therefore due to a differential diet. It was shown that this phenomenon is mediated epigenetically by DNA methylation. The RNAi-mediated silencing of DNMT3, the enzyme responsible for *de novo* DNA methylation, in newly hatched larvae had a royal jelly-like effect as the majority of DNMT3-silenced larvae developed as queen bees (Kucharski et al., 2008). These findings suggest that DNA methylation influences phenotypes and may be differentially altered by nutritional input.

1.2.2. Epigenetics and metabolism

The honey bee example shows how diet can influence gene expression. Several enzymes of the epigenetic machinery require intermediates of cellular metabolism like phosphate, glycosyl donors,

acetyl and methyl groups (Figure 1.2). Furthermore, recent research revealed that mutations in the metabolic enzymes succinate dehydrogenase, fumarate hydratase and isocitrate dehydrogenase are linked to cancer because they produce metabolites that act as inhibitors for chromatin modifying enzymes, the α-ketoglutarate-dependent dioxygenases (Frezza et al., 2011; Oermann et al., 2012). Together, these findings led to the hypothesis that there is a direct connection between metabolism and chromatin dynamics: chromatin modifying enzymes function in response to changes in the levels of intracellular cofactors which are derived from primary metabolism (Figure 1.2).

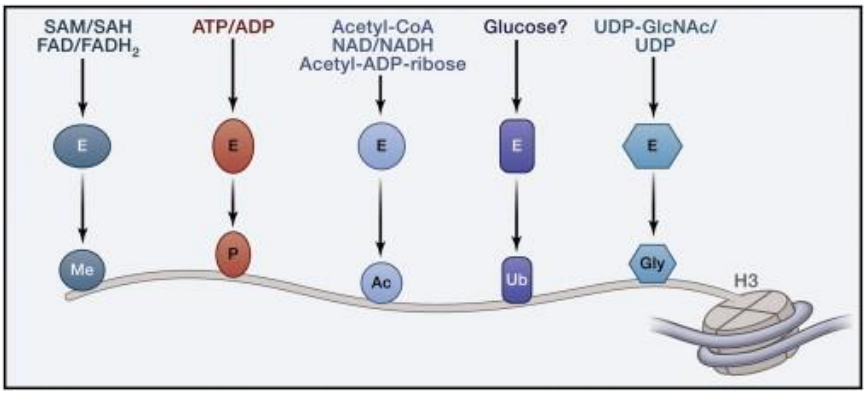

Figure 1.2: Chromatin remodeling enzymes use cofactors from cellular metabolism
Schematic overview of histone H3 and enzymes (E) that modify different residues using cofactors from cellular metabolism which lead to methylation (Me), phosphorylation (P), acetylation (Ac), ubiquitination (Ub) and glycosylation (Gly). These modifications are associated with chromatin structural changes and result in regulation of gene expression (reproduced from Katada et al., 2012).

Three different mechanisms were identified by which cellular metabolism can influence the activity of chromatin modifiers (Meier, 2013). First, competitive inhibitors can modulate the activity of an enzyme. Many chromatin modifying enzymes such as methylatransferases (see chapter 1.4.) are sensitive to feedback inhibition by the cofactor-derived product of their enzymatic reaction. Another example is the lysine acetyltransferase Gcn5, which binds acetyl-coenzyme A (acetyl-CoA) and CoA with similar affinities. Such cofactor-competitive molecules can derive from the enzymatic reaction itself or from rewired metabolic pathways (Wise et al., 2011). Second, cofactor depletion due to rate-limiting levels could disturb enzyme activity. Such depletions can be caused by inhibition of cofactor biosynthesis, nutrient limitations of essential vitamin precursors or overconsumption of competing enzymes. For

instance, 3-deazaneplanocin A (DZNep) is an inhibitor for S-adenosylhomocysteine (SAH) hydrolase, an enzyme involved in the metabolic pathway of the methyl group donor S-adenosylmethionine (SAM). This inhibition and the resulting depletion of SAM were shown to decrease DNA and protein methylation in cancer (Glazer et al., 1986). Third, recent studies discovered that the localization of cofactor biosynthesis in a cell may also affect the activity of chromatin modifiers and that modifiers respond to local changes in cofactor concentration. Acetyl-CoA is produced by two main enzymes, ATP citrate lyase and acetyl CoA-synthetase. Both of these enzymes were found to localize to the nucleus in human cell lines (Wellen et al., 2009). The mammalian methionine adenosyltransferase (MAT) isoenzymes which are responsible for SAM synthesis were also found to localize to the nucleus (Katoh et al., 2011; Reytor et al., 2009; Xia et al., 2010). Both observations indicate that cofactor synthesis may take place where cofactors are then metabolized and thus may have a direct regulatory function.

1.3. Methylation as a regulatory mechanism

In biological systems, methylation can affect diverse processes: gene expression is regulated by the methylation of DNA and histone proteins, while methylation of non-histone proteins has emerged as an important regulator of cellular signal transduction (Biggar and Li, 2015). Furthermore, methylation of phospholipids keeps membranes fluid and methylation of hormones and neurotransmitters controls their action (Fontecave et al., 2004). Therefore, methylation plays an important role in all living cells.

1.3.1. Methylation of nucleic acids

DNA methylation

The best-characterized DNA modification is the addition of a methyl group to cytosine, resulting in 5-methylcytosine (5mC). The human genome contains three DNA methyltransferase (DNMT) enzymes. DNMT3a/3b establishes the 5mC mark and DNMT1 is responsible for maintaining it. DNMT2 has weak DNA methyltransferase activity *in vitro* and it is thought to have evolved into an RNA methyltransferase (Klose and Bird, 2006). DNA methylation is known to occur mostly on CpG islands and is found in repetitive DNA elements leading to a repressed chromatin state. For example, methylated CpG islands are involved in X inactivation or silencing of transposons (Reik, 2007). Several years ago, three additional modifications were identified to occur on DNA: 5-hydroxymethylcytosine (5hmC), 5-formylcytosine (5fC) and 5-carboxylcytosine (5caC). This progressive modification of 5mC is likely

generated by the ten-eleven translocation (TET) enzymes, which are α-ketoglutarate-dependent dioxygenases existing in three isoforms (TET 1-3) (Ito et al., 2011; Tahiliani et al., 2009).

In contrast to mammals, *Drosophila* was long thought to lack DNA methylation as it belongs to the so-called "DNMT2 only" organisms, possessing only the homologue of DNA methyltransferase 2 (dDNMT2/Mt2) (Krauss and Reuter, 2011). But a few years ago, the presence of cytosine methylation in *Drosophila* has been reported in early embryogenesis (Kunert et al., 2003; Lyko et al., 2000). More recently, Phalke et al. found that the presence of 5mC is associated with the silencing of transposons and telomere integrity which is dependent on Mt2 (Phalke et al., 2009). In addition, there is evidence for a single ortholog of the TET proteins, named Tet, in *Drosophila* (Dunwell and Pfeifer, 2014). However, the presence of genomic DNA methylation in this organism is still under debate (Dunwell and Pfeifer, 2014). While some studies showed low levels of DNA methylation (Capuano et al., 2014; Takayama et al., 2014), others failed to replicate these findings (Raddatz et al., 2013). Surprisingly, in contrast to earlier studies, Takayama et al. found that the detected 5mC levels did not change in Mt2 null mutants which could be a hint for the existence of a novel, unidentified methyltransferase (Takayama et al., 2014).

Recently, DNA N^6-methyladenine (6mA) was identified in the *Drosophila* genome which is regulated by the Tet homologue during embryogenesis (Zhang et al., 2015). The function of this modification as an epigenetic mark still has to be analyzed (Heyn and Esteller, 2015). In summary, although the evidence of DNA methylation in *Drosophila* is increasing, its source is still elusive.

RNA methylation

Chemical modifications not only play an important role in modifying and regulating DNA but also RNA. As mentioned above, Mt2 is able to catalyze the methylation of $tRNA^{Asp}$ at cytosine 38 (Goll et al., 2006). Methylation of RNA can be found on different RNA species including tRNA, rRNA, mRNA, snoRNA and miRNA and occurs at a variety of nucleotides and sequences (Motorin and Helm, 2011).

On the one hand, the methylation status of tRNAs or rRNAs has an impact on their structural and metabolic stability, and on the other hand it is important for the efficiency of mRNA decoding. mRNAs are modified co-transcriptionally by the addition of a basic cap structure which is immediately methylated. This 7-methylguanosine cap is required for efficient gene expression and stabilizes the mRNA to promote transcription, translation, splicing, polyadenylation and nuclear export (Motorin and Helm, 2011). A recent study showed that many mRNAs also contain the 5hmC RNA modification (Delatte et al., 2016). This modification is added by the Tet enzyme and marks preferentially

polyadenylated mRNAs promoting translation. In *Drosophila*, both, the Tet enzyme and 5hmC RNA, are found most abundantly in brain tissue. Flies depleted of Tet suffered from brain defects and reduced 5hmC RNA levels indicating that RNA methylation is involved in neuronal activity.

1.3.2. Methylation of proteins

In eukaryotic cells, protein methylation is most prominent on lysine and arginine residues. However, there are many other residues that can be methylated such as histidine, glutamine, asparagine, cysteine and N-terminal and C-terminal residues (Clarke, 2013). Contextually, we categorize protein methylation into histone methylation and non-histone protein methylation.

Histone methylation

Histone methylation occurs mostly on the highly abundant lysine and arginine residues (Figure 1.3). In contrast to acetylation and phosphorylation marks, methylation does not change the charge of the histones. The methylation mark serves as a specific binding site for the so-called reader proteins. Readers contain specific protein domains that recognize the modification on a histone residue like acetylation or methylation along with the state of PTMs such as mono-, di- or trimethylation. Usually, they also interact with the flanking protein sequence in order to distinguish between different sequence contexts (Yun et al., 2011). Methylation is also recognized together with other modifications by combinatory binding modules in histone readers (Strahl and Allis, 2000). Heterochromatin protein 1 (HP1) isoforms, for instance, harbor a methyl lysine binding chromosome organization modifier (chromo) domain which binds to di- and trimethylated H3K9 and mediates heterochromatin formation (Bannister et al., 2001).

Histone lysine methylation is involved in activation and repression, respectively, depending on the residue that is methylated and the position of the methylated nucleosome within the genome (Kouzarides, 2007). In general, methylation at H3K4, H3K36 and H3K79 are linked to gene activation, while methylation at H3K9, H3K27 and H4K20 are linked to gene silencing (Black et al., 2012; Kouzarides, 2007; Lachner et al., 2003; Smith and Shilatifard, 2010). Studies on several histone modifications in *Drosophila* S2 cells led to the definition of nine major chromatin types by which the chromatin landscape can be described. Active genes carry high levels of H3K4me2/me3 and H3K9ac in the promotor regions and the proximal transcriptional start sites (TSS). H3K36me3 is associated with the gene body and found preferentially over exonic regions, while H3K4me1 and H3K36me1 are enriched in different chromatin states involving intronic regions (Kharchenko et al., 2011). In addition,

H3K36me3 is also involved in dosage compensation in *Drosophila melanogaster*. The msl3 subunit of the dosage compensation complex binds to H3K36me3 via its chromo domain and promotes spreading of the DCC along the X chromosome (Bell et al., 2008).

Silenced chromatin like pericentromeric heterochromatin is characterized by high levels of H3K9me2/me3 whereas genes repressed by polycomb group (PcG) proteins have high levels of H3K27me3 (Kharchenko et al., 2011). Silencing of repetitive DNA and transposable elements (TEs) is associated with H3K20me3 (Schotta et al., 2004).

Arginine methylation can occur as monomethylation as well as asymmetric or symmetric dimethylation and is found on H3, H4 and H2A. The methylation events on arginine residues impact the generation of other histone marks and can influence the binding of effector molecules and activate or repress transcription (Di Lorenzo and Bedford, 2011). Transcriptional activators are blocked from binding to H3K4me3 if H3R2 is also methylated and arginine methylation functions, in this case, as a transcriptional repressor (Iberg et al., 2008). Conversely, the asymmetric dimethylation of R3 on H4 (H4R3me2a) is associated with actively transcribed promotors (Wang et al., 2001).

Methylation does not occur exclusively on histones H3 and H4, as it was also described for H2A and H2B. Recently, glutamine methylation on histone H2A was reported as a RNA polymerase I-dedicated modification in yeast and human (Tessarz et al., 2014). In *Drosophila*, N-terminal proline methylation of H2B changes during development with lower levels of mono- and dimethylation in embryos compared to larvae or adult flies. In the same study, cultured cells showed an increased level of H2B methylation in densly growing cells (Villar-Garea et al., 2012). Increased levels of N-terminal H2B methylation was also found in response to cellular stress such as heat shock or arsenite treatment (Desrosiers and Tanguay, 1988).

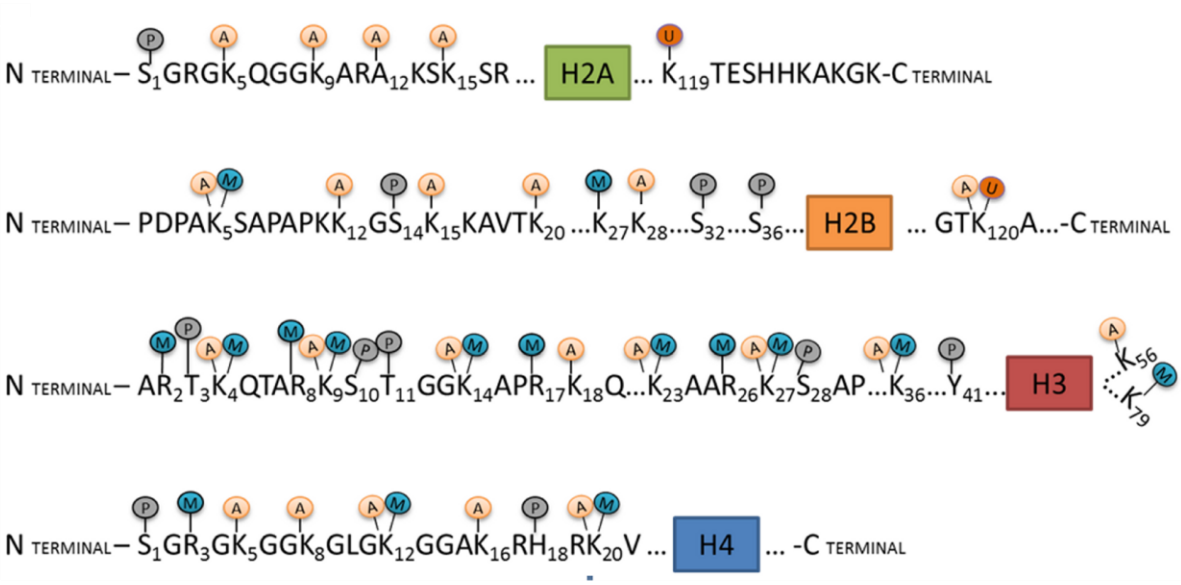

Figure 1.3: Schematic representation of major histone modifications and methylations
Major modifications on the core histones H2A, H2B, H3 and H4 are depicted including phosphorylation (P), acetylation (A), ubiquitination (U) and methylation (M). The N-terminal tails are mainly modified but modifications also occur on the C-terminal tails and the globular domains. N-terminal proline methylation of H2B has only been shown in *Drosophila* to date (reproduced from Xu et al., 2013; published under CC BY 3.0 license: https.//creativecommons.org/licenses/by/3.0/).

Non-histone protein methylation

The methylation of non-histone proteins was discovered in 1959 in the bacterial strain *Salmonella typhimurium* in which the presence of ε-N-methyl-lysine in a natural protein in flagellin was described (Ambler and Rees, 1959). Five years later, the same modification was reported in histones (Murray, 1964). In the beginning, much work was invested in studying histone methylation but recent findings regarding several histone lysine methyltransferases that methylate substrates other than histones have drawn more attention to the methylation of non-histone proteins (Zhang et al., 2012). Non-histone methylation has emerged as a prevalent PTM and plays an important role in regulating cellular signal transduction. For example, arginine methylation of the effector protein rat fibrosarcoma (RAF) in the mitogen-activated protein kinase (MAPK) signaling pathway reduces its signaling capacity and wingless/Int-1 (WNT) signaling is enabled by methylation of GTPase-activating protein-binding protein 2 (G3BP2) at multiple arginine sites (Biggar and Li, 2015).

The first reported non-histone methylation mediated by the lysine methyltransferase Set9 was the methylation of the tumor suppressor protein p53. Methylation positively affects the stability of p53

and the methylated protein is found only in the nucleus (Chuikov et al., 2004). A regulatory demethylation was also reported for p53: The lysine demethylase LSD 1 removes the dimethyl mark from p53K370 (Huang et al., 2007b), emphasizing the possible regulatory function of this modification.
As the importance of non-histone methylation becomes more clear, an important goal is to decipher the methylproteome (methylome) and learn more about its functions in diverse cellular processes, health and disease. With recent advances in proteomic techniques, especially mass spectrometry, the number of known methylated non-histone proteins has increased tremendously (Bremang et al., 2013; Cao et al., 2013).
The above observations indicate that the process of methylation and the enzymes responsible for it play a very important role in many physiological processes in higher organisms and it is therefore instrumental to understand how these mechanisms both maintain and alter the cellular milieu.

1.3.3. Writers and erasers of methylation marks

Methyltransferases

Methyltransferases (MTs) are enzymes that add one or more methyl groups to their substrates such as (histone) proteins, DNA, RNA, lipids and small molecules (Figure 1.4). The methyl donor for almost all cellular methylation reactions and also the cofactor for nearly all methyltransferases is SAM. There is only one exception known: The methionine synthase or homocysteine S-methyltransferase methylates homocysteine to generate methionine and uses 5-methyltetrahydrofolate as the methyl donor in the conversion of homocysteine to methionine (Matthews et al., 2008).
To date, five classes (class I–V) of SAM-dependent methyltransferases are known and categorized according to their structural features (Schubert et al., 2003). Class I possesses a Rossmann-like superfold, which is composed of up to seven β-strands. It is the largest group of MTs and includes all DNA MTs as well as some RNA and protein MTs. For example, the Dot1 histone H3K79 methyltransferase belongs to class I. Members of the less common structural classes include the *E.coli* methionine synthase (MetH) reactivation domain (class II), the precorrinn-4 MTs (class III) and the SPOUT family of RNA MTs (class IV) (Struck et al., 2012).
The largest subset of the protein methyltransferases (PMT) belongs to class V. They are also known as SET-domain protein methyltransferases. The SET domain is named after the *Drosophila* proteins **S**uppressor of variegation 3-9 (Su(var)3-9), **E**nhancer of zeste (E(z)) and **t**rithorax (trx) where the conserved sequence was first recognized. SET domain-containing MTs are able to mono-, di- and trimethylate their substrate on lysine residues (Herz et al., 2013).

Protein methyltransferases are differentiated on the basis of their target amino acid of the methylation event. The majority acts on arginine and lysine residues and are therefore divided into arginine (PRMT) and lysine methyltransferases (PKMT) (Allis et al., 2007). PRMTs belong to class I MTs, while all PKMT MTs belong to the SET domain-containing proteins except for Dot1.

Considering the importance of methylation, it is not surprising that protein methyltransferases emerge as an important group of enzymes both in normal physiology and disease (Copeland et al., 2009). For instance, hDOT1L is involved in mixed lineage leukemia (MLL) (Okada et al., 2005), while EZH2 plays a role in breast and prostate cancer (Varambally et al., 2002). Inhibitors of these enzymes have reached the clinic (Boriack-Sjodin and Swinger, 2016) demonstrating the importance of methylation pathways as effective drug targets.

Demethylases

Protein methylation was long thought to be irreversible until the first lysine demethylase LSD1/KDM1, was identified in 2004. It was shown to demethylate di- and monomethylated histone H3 at lysine 4 and 9 (H3K4 and H3K9) (Metzger et al., 2005; Shi et al., 2004). Since then many protein demethylases have been identified and protein methylation is now considered as a dynamically regulated PTM as phosphorylation (Figure 1.4). Two main classes of protein demethylases exist based on their oxidative demethylation mechanisms. Amine oxidase demethylases, the first group, are flavin-adenine-dinucleotide (FAD)-dependent enzymes which can act only on mono- and dimethylated lysines (Pedersen and Helin, 2010). The second group, the Jumonji C (JmjC) domain-containing demethylases, are Fe(II)- and α-ketoglutarate-dependent dioxygenases. Members of this group, the lysine demethylase 4 proteins (KDM4), were the first demethylases identified to act on trimethylated lysines (Cloos et al., 2006). To date, most known JmjC-containing demethylases act on lysine residues. Only one enzyme was reported to act on arginine residues, the Jumonji domain-containing 6 protein (JMJD6) (Chang et al., 2007). However, another group showed that JMJD6 can be a lysine hydroxylase (Webby et al., 2009), so this contradiction still has to be solved.

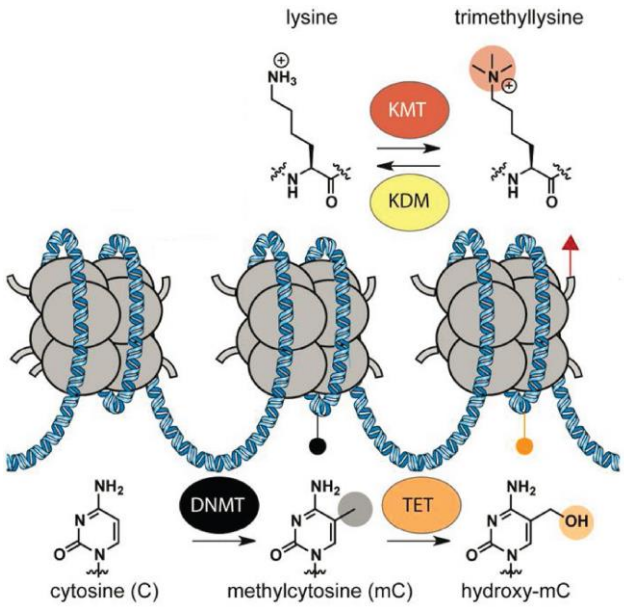

Figure 1.4: Regulation of chromatin structure by methylation
Histone and DNA modifying enzymes modulate the methylation state of arginine, lysine and cytosine residues, respectively. Methylations can affect the accessibility of genomic loci, serve as a binding site for reader proteins or influence neighboring chromatin domains. KMT: Histone lysine methyltransferases; KDM: Histone lysine demethylases; DNMT: DNA methyltransferases; TET: Ten-eleven translocation dioxygenases (adapted with permission from Meier, J.L. Metabolic mechanisms of epigenetic regulation. ACS Cem Biol *8*, 2607-2621. Copyright 2013 American Chemical Society).

In *Drosophila melanogaster*, 13 known or predicted lysine demethylases exist (Holowatyj et al., 2015). Among them, Su(var)3-3 is the only amine oxidase demethylase and the *Drosophila* homologue of LSD1/KDM1 (Di Stefano et al., 2007). The other 12 lysine demethylases belong to the group of JmjC domain-containing demethylases. They are all characterized by a JmjC domain which often exists in combination with other protein domains that are responsible for substrate specificity. The Kdm4 proteins in *Drosophila melanogaster* consist of two homologues, Kdm4a and Kdm4b, and mediate the demethylation of H3K36me2/me3 and H3K9me2/me3. Kdm4a is involved in the organization of heterochromatin and its overexpression causes spreading of HP1a into euchromatin. These two proteins were also shown to interact with each other, which is necessary for the demethylation activity of Kdm4a (Lin et al., 2008) and its targeting to a subset of heterochromatic genes (Lin et al., 2012). Kdm4a also localizes to euchromatic sites where it regulates H3K36 methylation (Lloret-Llinares et al., 2008). A recent study showed that an overexpression of Kdm4a resulted in a global decrease of

H3K36me3 and caused male lethality which might indicate impaired dosage compensation (Crona et al., 2013).

1.4. Methylation and its connection to metabolism: The S-adenosylmethionine cycle

1.4.1. S-adenosylmethionine: one cofactor – many of different methylation reactions

Methyl groups for all methylation reactions come from dietary methyl donors such as methionine, folates and B-group vitamins. On the one hand, methionine is an essential amino acid that is obtained from dietary sources while on the other hand folates and B-group vitamins are involved in the re-methylation of homocysteine which generates methionine inside the cell (Figure 1.5). Subsequently, methionine is converted into SAM by S-adenosylmethionine Synthetase (Sam-S) in an ATP-dependent manner. SAM was discovered in 1951 (Cantoni, 1951) and is the second most widely used substrate after ATP (Cantoni, 1975). It is the universal methyl donor for all methylation reactions that occur in a cell – except for the already mentioned cobalamin-dependent re-methylation of methionine (chapter 1.3.3.). Methyltransferases using SAM to methylate their substrates producing S-adenosylhomocysteine (SAH). SAH is a potent inhibitor for SAM-dependent methyltransferases (Caudill et al., 2001). Therefore, SAH is immediately hydrolyzed to adenosine and homocysteine. Homocysteine can either be re-methylated or is converted to cystathionine, an intermediate in the synthesis of cysteine (also known as transsulfuration) (Chiacchiera et al., 2013; Lu, 2000). In addition, after decarboxylation, SAM serves as a propylamino donor in the polyamine synthesis pathway (Larsson et al., 1996; Lu, 2000) (Figure 1.5).

The ratio of SAM/SAH is crucial for the regulation of methylation and it is used as an indicator of methylation potential (Caudill et al., 2001). A decrease in the SAM/SAH ratio predicts a reduced cellular methylation potential (Cantoni, 1985) which is associated with various diseases such as chronic liver disease (Lu and Mato, 2012), neural defects and developmental abnormalities (Burren et al., 2006; Scott, 1999).

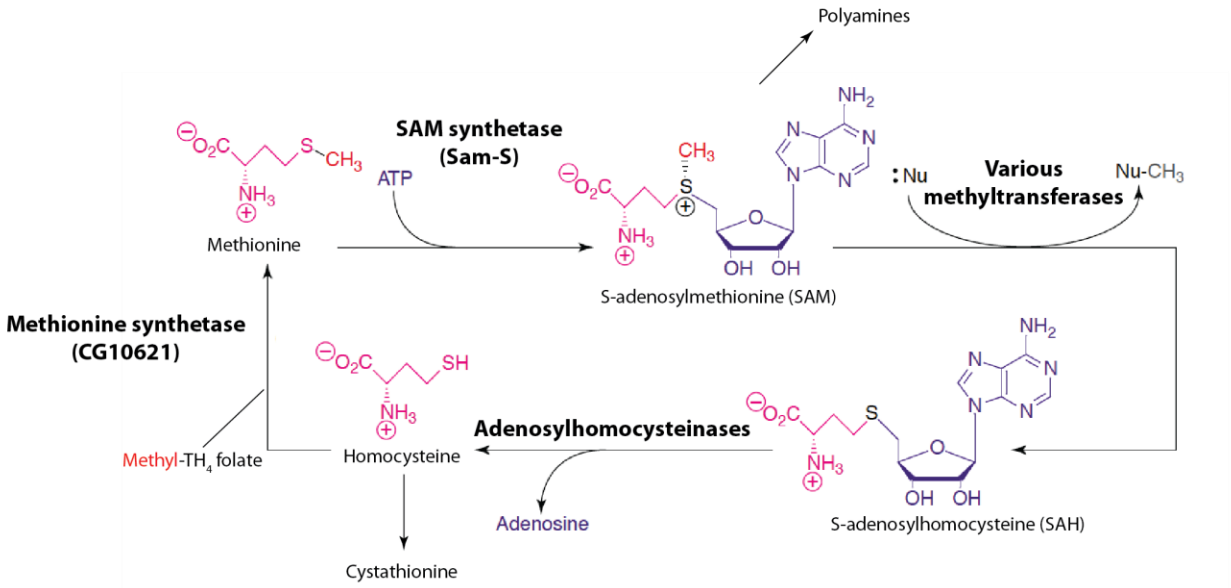

Figure 1.5: The S-adenosylmethionine cycle in *Drosophila melanogaster*
SAM is formed from the reaction of methionine with ATP which is catalyzed by SAM synthetase (Sam-S). Various methyltransferases transfer methyl groups to their substrates including DNA, RNA, proteins, lipids and small molecules. In this reaction, SAM is converted to S-adenosylhomocysteine (SAH). Subsequently, SAH is hydrolyzed by adenosylhomocysteinases to homocysteine and adenosine. Homocysteine is either converted to cystathionine by cystathionine-β-synthase or remethylated to form methionine by a cobalamin-dependent methyltransferase, methionine synthase. After decarboxylation, SAM is involved in the polyamine synthesis pathway and serves as a propylamino donor (adapted from Fontecave et al., 2004).

Recent studies provide evidence that SAM metabolism is directly linked to chromatin state. Aberrant expression of the SAM-dependent nicotinamide N-methyltransferase in cancer cells altered SAM/SAH ratios which changed the methylation landscape including histones (Ulanovskaya et al., 2013). Threonine metabolism in mouse pluripotent stem cells was shown to be coupled to SAM metabolism resulting in the regulation of histone methylation (Shyh-Chang et al., 2013). In mice, methionine restricted diet led to changes in one-carbon metabolism and histone methylation status in the liver (Mentch et al., 2015).

In *Drosophila melanogaster*, reduced levels of either histone demethylases or enzymes that are involved in the SAM cycle have been shown to lead to lethality and defects in wing development and cell proliferation. Disruption of SAM metabolism also affected histone methylation (Liu et al., 2016). It has also been reported that an enhancement of SAM catabolism extended lifespan in flies. This effect was mediated by glycine N-methyltransferase (Gnmt), an enzyme that catalyzes the conversion of

glycine to sarcosine (N-methyl-glycine) (Obata and Miura, 2015). Gnmt was shown to regulate SAM levels in the fat body of *Drosophila*, a counterpart of the liver and white adipose tissue (Obata et al., 2014) and in the liver of mammals (Luka et al., 2009). Furthermore, Gnmt mutations can lead to hepatocellular cancer by affecting SAM levels (Lu and Mato, 2012).

1.4.2. S-adenosylmethionine Synthetase

As mentioned previously, the generation of SAM is catalyzed by the enzyme S-adenosylmethionine Synthetase (see domain organization in Figure 1.6) in the cytosol. In *Drosophila melanogaster*, the analysis of mutations in modifiers of the position effect variegation (PEV) and polycomb group genes is a useful tool to study genes that are involved in chromatin structure. The enzyme Sam-S is encoded by the *Suppressor of zeste* 5 (*Su(z)5*) gene (Larsson et al., 1996) which was isolated as a suppressor of PEV and also acts as an enhancer of Polycomb (Pc) (Kalisch and Rasmuson, 1974; Larsson et al., 1996). These data suggest that Sam-S is involved in the regulation of chromatin structure. According to its annotation in the database Flybase (http://flybase.org), *Su(z)5* is the only known gene to date that encodes for Sam-S in *Drosophila*. Sam-S is essential since homozygous mutants are lethal in the embryonic and early larval stages (Larsson and Rasmuson-Lestander, 1998). Knockdown of Sam-S in the rice plant *Oryza sativa* led to decreased levels in the methylation of DNA and H3K4me3 and resulted in a late-flowering phenotype (Li et al., 2011).

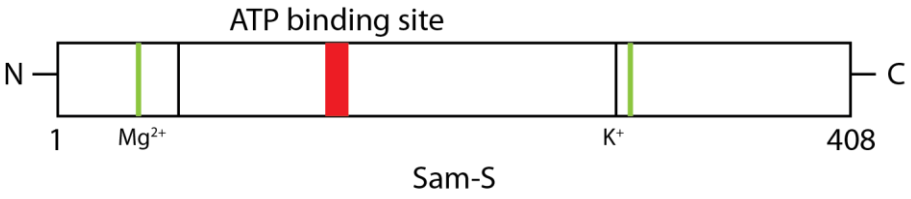

Figure 1.6: S-adenosylmethionine Synthetase in *Drosophila melanogaster*
The enzyme Sam-S catalyzes the formation of SAM from methionine and ATP. It consists of 408 amino acids and harbors a ATP binding domain (red) and several cofactor binding sites for magnesium (Mg^{2+}, green) and potassium (K^{+}, black) (according to http://www.uniprot.org/uniprot/P40320).

In mammals, three isozymes of Sam-S are known, methionine adenosyltransferase I, II and III (MAT I/II/III) (Kotb et al., 1997). Two distinct genes, *MAT1A* and *MAT2A*, have been identified to encode the catalytic subunits α_1 and α_2 of the three enzymes. MAT II is widely expressed and is composed of a dimer of an α_2 catalytic subunit (MAT IIα_2) and its activity is regulated by a β subunit (MAT IIβ), which is encoded by the *MAT2B* gene. MAT I and MATIII form tetramers and dimers, respectively, of the α_1 catalytic subunit and are expressed in the liver (Sakata et al., 2005). Recent studies have shown that MAT isoenzymes are located in the nucleus whereas MAT II serves as a transcriptional co-repressor (Katoh et al., 2011; Reytor et al., 2009; Xia et al., 2010). Furthermore, MAT II was shown to repress the expression of cyclooxygenase 2 (COX-2) by directly interacting with SETDB1, a histone H3K9 methyltransferase. This interaction promoted the trimethylation of H3K9 at the gene locus of COX-2 (Kera et al., 2013). Thus, more and more evidence is accumulating that these enzymes are involved in shaping chromatin structure and its dynamics.

1.5. Aim of the thesis

After ATP, SAM is the second most widely used enzyme substrate and therefore an important molecule that is found in all living cells (Cantoni, 1975). It is the principal biological methyl donor for methyltransferase reactions acting on DNA, RNA, histones and non-histone proteins. Given the importance of methylation in various biological processes such as transcriptional control, the regulation of chromatin structure, DNA repair and signal transduction, the synthesis of SAM should play a key role in cell function.

In *Drosophila melanogaster*, this reaction is catalyzed by the enzyme S-adenosylmethionine Synthetase which is encoded by the *Su(z)5* gene (Larsson et al., 1996). This gene was isolated as a suppressor of PEV and an enhancer of Polycomb (Pc) (Kalisch and Rasmuson, 1974) suggesting that it is involved in the regulation of gene expression and chromatin structure. However, this finding was not followed up. In recent studies, the mammalian homologue, methionine adenosyltransferase, was found to localize to the nucleus (Katoh et al., 2011; Reytor et al., 2009; Xia et al., 2010) and to serve as a transcriptional co-repressor (Katoh et al., 2011). That metabolic enzymes are localized to the nucleus was also reported for ATP citrate-lyase and acetyl-Co A synthtetase (Wellen et al., 2009) as well as for the NAD^+ synthase nicotinamide mononucleotide adenylyltransferse-1 (Zhang et al., 2009). However, the nuclear function of these metabolic enzymes is still unclear.

In this work, the model organism *Drosophila melanogaster* was used to investigate basic biological properties of Sam-S. To date, *Su(z)5* is the only known gene that encodes for Sam-S. To gain more insights into the nuclear function of Sam-S, the following questions were asked:

1. Where does Sam-S localize to?
2. Which proteins does Sam-S interact with?
3. Which genes are regulated by Sam-S?

Different approaches were used to investigate Sam-S in *Drosophila* Schneider L2-4 cells. Firstly, monoclonal antibodies were raised against the protein and used in indirect immunofluorescence to verify its localization to the nucleus. In addition, these antibodies were also used to immunoprecipitate endogenous Sam-S and its interaction partners were analyzed using a proteomic analysis by tandem mass spectrometry (LC-MS/MS). Secondly, following knockdown of endogenous Sam-S in L2-4 cells by RNA interference (RNAi), a quantitative analysis of histone methylation levels was performed using LC-MS/MS. The impact of Sam-S knockdown on gene expression was investigated on a microarray and responder genes were verified by quantitative real-time PCR (qPCR).
Upon Sam-S knockdown, L2-4 cells were depleted of SAM in order to investigate to what extent the SAM/SAH ratio was affected and how protein levels of SAM-metabolizing enzymes changed. Two methods were established to answer the following questions:

4. How is the SAM/SAH ratio changed upon Sam-S knockdown?
5. What happens to SAM-metabolizing enzymes upon changes in metabolite concentration?

First, a LC-MS/MS method after Burren et al. was established to measure endogenous levels of SAM and SAH (Burren et al., 2006). Second, the company caprotec developed a method which enables the purification of proteins that share the same function (Lenz et al., 2010). This method was used to purify SAM-metabolizing proteins from L2-4 cells.
Finally, since methylation is an important PTM for the regulation of gene expression and cellular signal transduction (Biggar and Li, 2015), we adopted a heavy methyl SILAC approach (Ong et al., 2004) to identify methylation sites in the *Drosophila melanogaster* proteome. Taken together, our analyses aimed to a better understanding of the important function of methylation as a PTM as well as its regulation via metabolism.

2. Results

2.1. Characterization of monoclonal antibodies

2.1.1. Antibodies against the methyltransferase Enhancer of zeste

FLAG-tagged Enhancer of zeste (E(z)) was expressed with the baculovirus system in Sf21 cells. It was purified using ANTI-FLAG® M2 affinity gel (Sigma) and used for production of monoclonal antibodies by Dr. Elisabeth Kremmer, Helmholtz Zentrum Munich (Figure 2.1 A). Antibodies were prescreened by ELISA and two positive ones were further analyzed by western blot on nuclear extracts from *Drosophila* Schneider L2-4 cells (L2-4 cells). Only one antibody specifically recognized the endogenous E(z). It showed a signal in the nuclear extract with the expected molecular weight. This specific band disappeared when E(z) was knocked down (Figure 2.1 B). Two protein bands remained which were identified as Centrosomal protein 190 kD (Cp190) by mass spectrometry (data not shown). Since the antibody showed this cross-reactivity with Cp190 (*), it was only used for straightforward western blot applications.

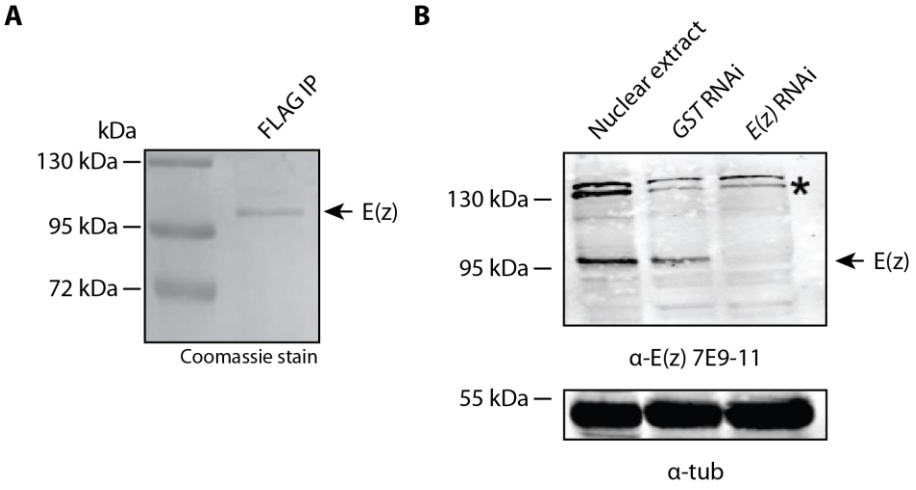

Figure 2.1: E(z) antibody showed cross-reactivity with Cp190
(A) The methyltransferase E(z) was expressed in Sf21 cells with the baculovirus system and purified via its FLAG-tag. Purified protein was used for generation of monoclonal antibodies in mouse (by Dr. Elisabeth Kremmer). **(B)** The monoclonal antibody α-E(z) 7E9-11 was tested on nuclear extracts from L2-4 cells in western blot. It specifically recognized endogenous E(z). *GST* RNAi served as a control. The antibody also showed a cross-reactivity with Cp190 (indicated by asterisk (*)).

2.1.2. Antibodies against the metabolic enzyme S-adenosylmethionine Synthetase

To investigate S-adenosylmethionine Synthetase in *Drosophila melanogaster*, monoclonal antibodies were generated in mouse and rat against the protein in collaboration with Dr. Elisabeth Kremmer, Helmholtz Zentrum Munich. The monoclonal antibodies were raised against GST-tagged Sam-S. Recombinant expression and purification from bacterial lysates on glutathione sepharose beads was done by André Hansbauer (Figure 2.2 A). Dr. E. Kremmer tested hybridoma cell supernatants and received 49 positive clones.

These clones were analyzed by western blot on whole cell extracts from L2-4 cells (data not shown). Two antibodies, one generated in mouse (Sam-S 4A2) and one in rat (Sam-S 4A7), respectively, specifically detected Sam-S as indicated by a signal at the expected molecular weight. This signal disappeared when Sam-S was knocked down (Figure 2.2 B). These two antibodies were further characterized for their suitability in different applications.

In order to test if the antibodies were able to immunoprecipitate endogenous Sam-S, both antibodies were bound to a mixture of Protein A and G sepharose beads and subsequently incubated with L2-4 cell extracts in separate experiments. Antibody-free beads served as a negative control. Both antibodies immunoprecipitated endogenous Sam-S as confirmed by western blot analysis (Figure 2.2 C).

Next, antibodies were tested in immunofluorescence microscopy. A L2-4 cell line that stably expressed a FLAG-HA-tagged version of Sam-S was generated. The expression of FLAG-HA-Sam-S was induced 24 h before harvesting. Cells were mixed in a 1:1 ratio with wild-type L2-4 cells. Afterwards, cells were immunostained and Sam-S was detected with an epifluorescence microscope. Both antibodies were able to detect the tagged version of Sam-S as well as the endogenous protein. Therefore we concluded that both antibodies are suitable for IF microscopy (Figure 2.2 D).

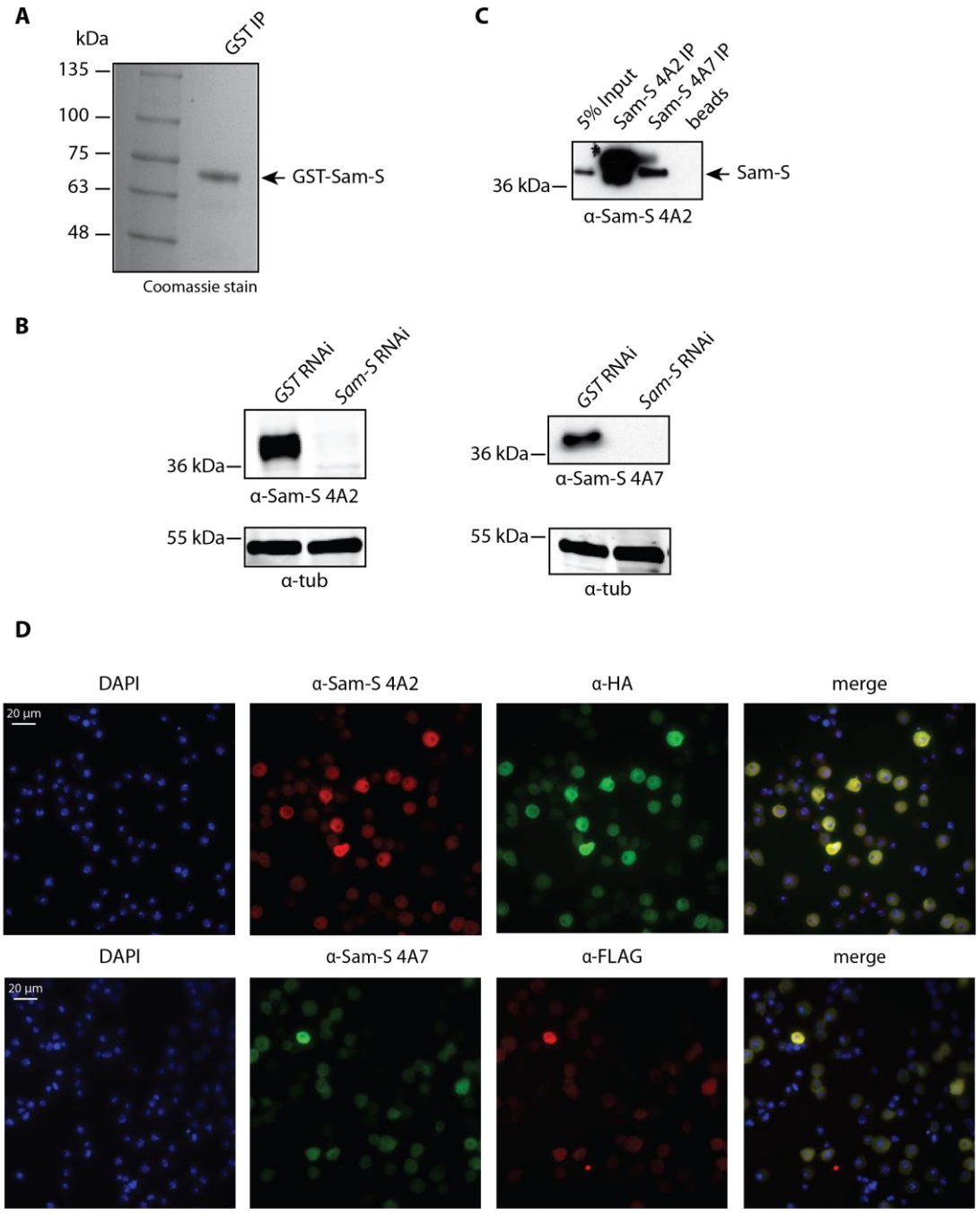

Figure 2.2: Characterization of Sam-S antibodies
(A) Sam-S was bacterially expressed and purified using GST beads (performed by André Hansbauer). Purified protein was used for generation of monoclonal antibodies in mouse and rat (by Dr. Elisabeth Kremmer). **(B)** The monoclonal antibodies α-Sam-S 4A2 (mouse) and 4A7 (rat), respectively, were tested on whole cell extracts from L2-4 cells depleted from Sam-S in western blot analysis. *GST* RNAi served as a control. **(C)** Both antibodies were bound to Protein A/G sepharose beads to test them in immunoprecipitation (IP). Antibody-free beads served as a negative control (beads). **(D)** Immunofluorescence was tested with a 1:1 mixture of wild-type L2-4 cells and cells expressing FLAG-HA-tagged Sam-S. Expression was induced 24 h before harvesting.

2.2. Subcellular localization of S-adenosylmethionine Synthetase in *Drosophila melanogaster*

To elucidate where the *Drosophila melanogaster* Sam-S is localized in the cell, an immunofluorescence microscopy analysis was performed using the previously described L2-4 cell line that stably expressed the FLAG-HA-tagged version of Sam-S. Immunostaining against the HA-tag was performed and showed that Sam-S is not only localized to the cytoplasm but also to the nucleus. As a control, wild-type L2-4 were used and DNA was stained by DAPI (Figure 2.3 A). To verify this result further, an immunofluorescence confocal microscopy analysis was performed by Dr. Teresa Barth using the antibody Sam-S 4A7 against the endogenous protein. This analysis also showed the subcellular localization of the enzyme to the nucleus and the cytoplasm (Figure 2.3 B).

Furthermore, following biochemical fractionation of subcellular compartments, a minor fraction of the endogenous Sam-S was also found in the nuclear fraction (Figure 2.3 C). A similar observation has been reported for the mammalian isoenzymes, methionine adenosyltransferases I, II and III which were also found in the cytoplasm and in the nucleus (Katoh et al., 2011; Reytor et al., 2009; Xia et al., 2010).

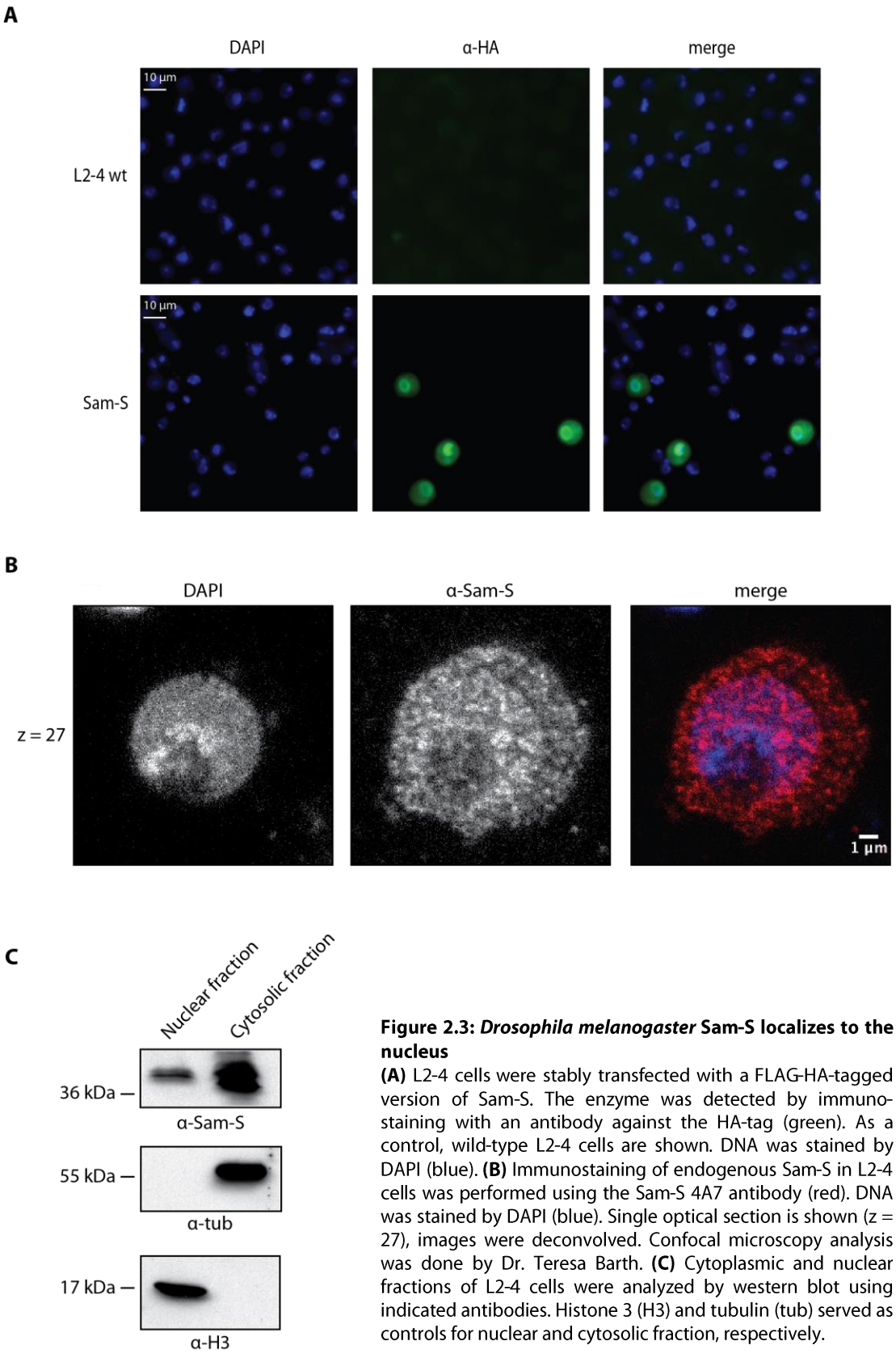

Figure 2.3: *Drosophila melanogaster* Sam-S localizes to the nucleus
(A) L2-4 cells were stably transfected with a FLAG-HA-tagged version of Sam-S. The enzyme was detected by immunostaining with an antibody against the HA-tag (green). As a control, wild-type L2-4 cells are shown. DNA was stained by DAPI (blue). **(B)** Immunostaining of endogenous Sam-S in L2-4 cells was performed using the Sam-S 4A7 antibody (red). DNA was stained by DAPI (blue). Single optical section is shown (z = 27), images were deconvolved. Confocal microscopy analysis was done by Dr. Teresa Barth. **(C)** Cytoplasmic and nuclear fractions of L2-4 cells were analyzed by western blot using indicated antibodies. Histone 3 (H3) and tubulin (tub) served as controls for nuclear and cytosolic fraction, respectively.

2.3. Investigation of S-adenosylmethionine Synthetase and its nuclear function

2.3.1. Sam-S interacts with various proteins involved in the regulation of transcription and chromatin organization

To gain insights into the nuclear function of Sam-S, a nuclear extract from L2-4 cells was prepared and Sam-S interacting proteins were purified using the Sam-S 4A2 antibody bound to a mixture of Protein A and G sepharose beads. As a control antibody-free sepharose beads were used. Bound proteins from both samples were eluted from the beads by boiling in SDS sample buffer and subsequently were separated by SDS-PAGE. Following silver staining of the proteins in the gel, a higher number of protein bands was observed in the lane corresponding to the Sam-S-specific co-immunoprecipitation (co-IP) in comparison to the control IP (Figure 2.4 A and B).

In order to learn more about the nature of the proteins interacting with Sam-S, the gel lanes for Sam-S IP and control IP samples were cut into eight fractions and the Sam-S-associated proteins were analyzed by LC-MS/MS. MS data were mapped to protein sequences using the MaxQuant software (version 1.2.2.5) (Cox and Mann, 2008). For protein quantitation, iBAQ intensities were used which are based on the abundance of the identified peptides of each protein hit. iBAQ intensities of three independent replicates were averaged and the $\log_2$ fold enrichment over the negative control was calculated. By comparing the two data sets, there were 145 proteins exclusively found in the purified Sam-S samples but not in the negative control. In total, 225 proteins were considered as potential interaction partners of Sam-S as they showed a $\log_2$ fold enrichment factor above two. Sam-S was the top hit with a $\log_2$ fold enrichment factor of 28. Figure 2.4 C shows a selection of Sam-S-interacting proteins and their assigned biological function. The open source Database for Annotation, Visualization and Integrated Discovery (DAVID) bioinformatics tool (Huang et al., 2007a) was used to do a gene ontology (GO) term enrichment analysis using the Sam-S-associated proteins as input. GO terms such as chromatin organization, regulation and initiation of transcription and regulation of RNA metabolic processes were the most significant hits (Figure 2.4 C). Among the proteins that were related to transcriptional regulation were components of the PcG complexes (Sce, pho), the DCC complex (msl-1, msl-3), the Sin3 complex (Sin3A, Bin1) and the TATA-binding protein (TBP)/TBP-associated factors (TAF) complex (Taf subunits, Tbp). A histone demethylase, Kdm4a, was also identified as a potential interactor of Sam-S. Identified proteins involved in chromatin structure included the chromatin insulator Cp190, mod(mdg4), a component of the gypsy chromatin insulator complex, and putzig (pzg), a component of the TATA-binding protein-related factor 2 (TRF2)/DNA replication-related element factor (DREF) complex. Within this complex, pzg resembles regulators of

insulator function. Taken together, these results suggest that Sam-S is involved in the regulation of chromatin structure and gene expression by interacting with transcriptional and epigenetic regulators

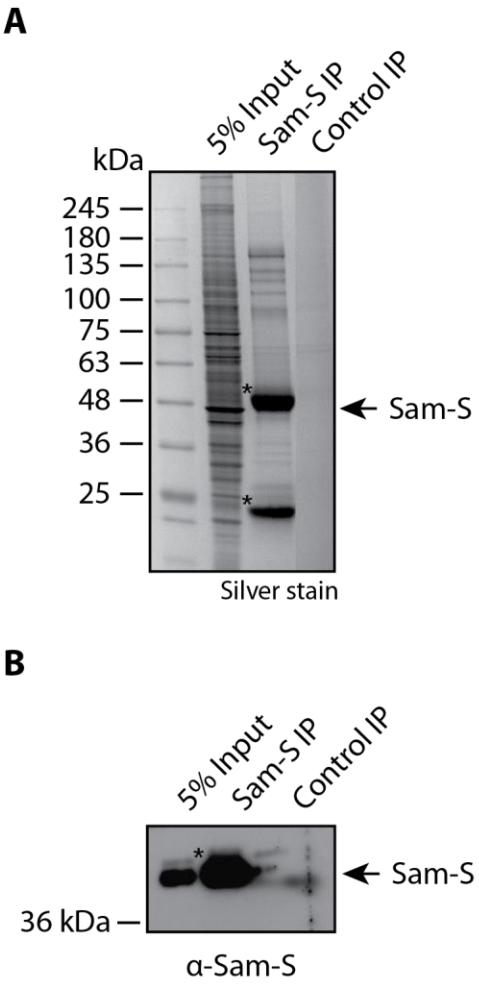

C

Flybase ID	Name	log_2 IP (Sam-S/Control)
FBgn0005278	Sam-S	28
REGULATION OF TRANSCRIPTION		
FBgn0029775	Vsx1	21
FBgn0001994	crp	20
FBgn0039209	CG13624	18
FBgn0011763	Dp	18
FBgn0004606	zfh1	17
FBgn0033233	Kdm4A	17
FBgn0001185	her	16
FBgn0032475	Sfmbt	16
FBgn0002783	mor	15
FBgn0000212	brm	14
FBgn0000210	br	13
FBgn0033749	achi	5
FBgn0001990	wek	4
FBgn0027378	MRG15	4
FBgn0000541	E(bx)	4
FBgn0013263	Trl	4
FBgn0001291	Jra	2
PcG omplexes		
FBgn0002521	pho	18
FBgn0003330	Sce	18
DCC complex		
FBgn0005617	msl-1	15
FBgn0002775	msl-3	3
Sin3 complex		
FBgn0022764	Sin3A	3
FBgn0024491	Bin1	2
Transcription initiation		
FBgn0010356	Taf5	24
FBgn0010280	Taf4	23
FBgn0000617	e(y)1 (=Taf9)	23
FBgn0024909	Taf7	22
FBgn0022724	Taf8	22
FBgn0011290	Taf12	21
FBgn0011836	Taf2	21
FBgn0032847	Taf13	21
FBgn0010355	Taf1	6
FBgn0026262	bip2 (=Taf3)	5
FBgn0011291	Taf11	4
FBgn0003687	Tbp	4
Regulation of RNA metabolic process		
FBgn0022984	qkr58E-3	23
FBgn0086895	pea	13
FBgn0085444	CG34415	3
CHROMATIN ORGANIZATION		
FBgn0028965	A16	18
FBgn0000283	Cp190	10
FBgn0044324	Chro	8
FBgn0259785	pzg	8
FBgn0015602	BEAF-32	4
FBgn0024227	ial	4
FBgn0085451	CG34422	4
FBgn0002781	mod(mdg4)	2

Figure 2.4: Sam-S interacts with various chromatin-related proteins
(A) Endogenous Sam-S was purified from L2-4 cells using a Sam-S-specific antibody bound to sepharose beads. Antibody-free sepharose beads served as a control. Sam-S-interacting proteins were separated by SDS-PAGE and visualized by silver nitrate staining. **(B)** Western blot analysis of Sam-S and control IP using indicated antibody. Asterisk (*) indicates heavy chain from antibody. **(C)** Sam-S-interacting proteins were analyzed using LC-MS/MS and categorized after their assigned biological function in a gene ontology (GO) term enrichment analysis with the DAVID bioinformatics tool. Table shows a chosen selection of identified proteins with log_2 fold enrichment over the negative control.

2.3.2. SAM depletion interferes with cell proliferation but not cell cycle

According to the information on Flybase (http://flybase.org), *Sam-S* is the only known gene to date that encodes for Sam-S protein in *Drosophila melanogaster*. In order to further elucidate its nuclear function, a transient knockdown of Sam-S was performed in L2-4 cells by RNAi in the following experiments. Subsequently, the effects of SAM depletion on histone modifications and resulting gene expression were characterized (see chapter 2.4.3. and 2.4.4.).

Sam-S knockdown – RNA level

L2-4 cells were either treated with double-stranded RNA (dsRNA) against *Sam-S* or against the bacterial *glutathione S-transferase* (*GST*) as a negative control. After five days, cells were harvested and analyzed. After cells were harvested, total RNA was purified using the RNeasy Kit (Qiagen). Compared to the negative control, a reduction of roughly 90% of the *Sam-S* mRNA expression could be achieved (Figure 2.5 A).

Sam-S knockdown – Protein level

The efficiency of the knockdown was also confirmed on the protein level. For this purpose, a whole cell extract was prepared from harvested cells, separated by SDS-PAGE and analyzed by western blot (Figure 2.5 B). A representative blot shows that Sam-S protein cannot be detected any more after five days.

Quantitative analysis of SAM and SAH

Since the ratio of SAM/SAH is important for a cell (Cantoni, 1985), endogenous SAM and SAH levels were analyzed to see if the ratio is altered upon Sam-S depletion. For this experiment, a LC-MS/MS assay was established according to that previously described by Burren et al. (Burren et al., 2006) (see chapter 2.5.).

As expected, the measurement of SAM and SAH levels revealed that the SAM/SAH ratio was changed dramatically upon Sam-S knockdown. After five days, SAM levels were strongly reduced (log_2 fold change: - 4.3) whereas SAH levels were slightly increased (log_2 fold change: 2.0). This led to a SAM/SAH ratio of 50.3 (+/- 11.1) in the control compared to a ratio of 0.6 (+/- 0.07) in the knockdown condition (Figure 2.5 C). The average of two independent replicates was taken and the log_2 fold change over the control was calculated.

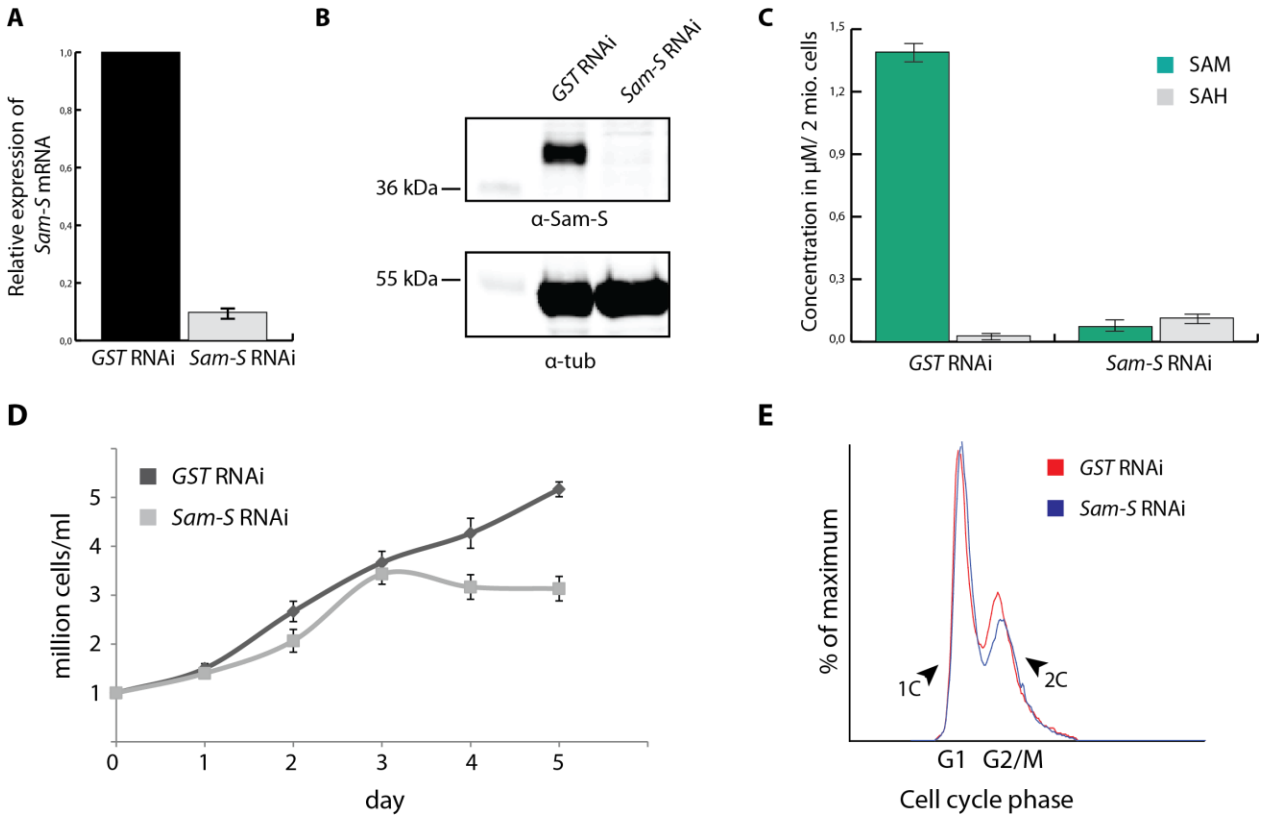

Figure 2.5: Sam-S knockdown affects cell growth but not cell cycle
Sam-S was transiently knocked down in L2-4 cells by RNA interference (RNAi) for five days. Effects of *Sam-S* RNAi on mRNA level **(A)**, protein level **(B)** and SAM/SAH ratio **(C)** is shown. RNAi of bacterial *gluthathione S-transferase* (*GST*) was used as a negative control. SAM/SAH ratio was measured using LC-MS/MS. **(D)** Cell proliferation upon Sam-S knockdown was monitored over five days. Cells were counted using the Casy® cell counter system. **(E)** To follow the RNAi treated cells through the cell cycle, propidium iodide signals of labeled DNA were measured by fluorescence-activated cell sorting (FACS). 1C: one chromatid chromosome; 2C: two chromatid chromosome.

Cell proliferation

To investigate if Sam-S knockdown and protein depletion of the protein affects cell proliferation and cell cycle, cells were seeded in different batches and treated with dsRNA against *Sam-S*. Control cells were treated with dsRNA against *GST*. Every 24 h, cells were harvested and counted using the Casy® cell counter system. The resulting growth curve is illustrated in Figure 2.5 D. Three independent batches of cells were counted independently for each time point. After four days, the Sam-S-deficient cells clearly showed a reduced number in comparison to control cells, indicating that Sam-S depletion interferes with normal cell growth. After five days, Sam-S knockdown led to a decrease in cell number of roughly 40%.

Fluorescence-activated cell sorting

To investigate if the cell cycle is affected upon Sam-S knockdown, flow cytometry analysis of cultured L2-4 cells was performed. After five days of treatment with dsRNA against *Sam-S* or *GST* as a control, cells were harvested. The DNA content as a measure for the cell cycle state was measured by fluorescence-activated cell sorting (FACS) analysis of propidium iodide signals. Three biological replicates were analyzed for *GST* RNAi cells and *Sam-S* RNAi cells. The profiles for DNA content of the individual replicates were highly reproducible. In the FACS profiles, G1-phase corresponds to a DNA content of one chromatid chromosomes (1C) while G2/M-phase corresponds to two chromatid chromosomes (2C). S-phase is represented between those two states. A representative plot of control versus Sam-S-depleted cells is demonstrated in Figure 2.5 E. No significant difference in cell cycle progression was observed upon *Sam-S* RNAi.

2.3.3. Disruption of SAM metabolism affects histone methylation pattern

As shown before, the protein level of Sam-S was substantially reduced which led to a dramatic change in the SAM/SAH ratio. Cell growth was affected upon depletion but so far an effect on the cell cycle could not be detected. However, a potential role for Sam-S in gene regulation was hypothesized due to co-immunoprecipitation results (chapter 2.3.1.). In order to investigate this function further, several experiments were carried out. A quantitative analysis of posttranslational modifications of histones after knockdown of Sam-S was performed since they have a major impact on gene expression.

For investigation of the global histone modification pattern, histones were extracted from control and knockdown cells as described in chapter 4.2.6.3. After SDS-PAGE, gels were stained with Coomassie Brilliant Blue G250 and bands corresponding to H2B, H3 and H4 were excised (Figure 2.6 A). Histone bands were then prepared for mass spectrometry analysis (Villar-Garea et al., 2008) to quantify their posttranslational modifications. Histones from three independent replicates were analyzed and the histone modification pattern of control and knockdown cells was compared. Figure 2.6 shows the analysis of posttranslational modifications from histone H2B (Figure 2.6 B), H3 (Figure 2.6 D) and H4 (Figure 2.6 C).

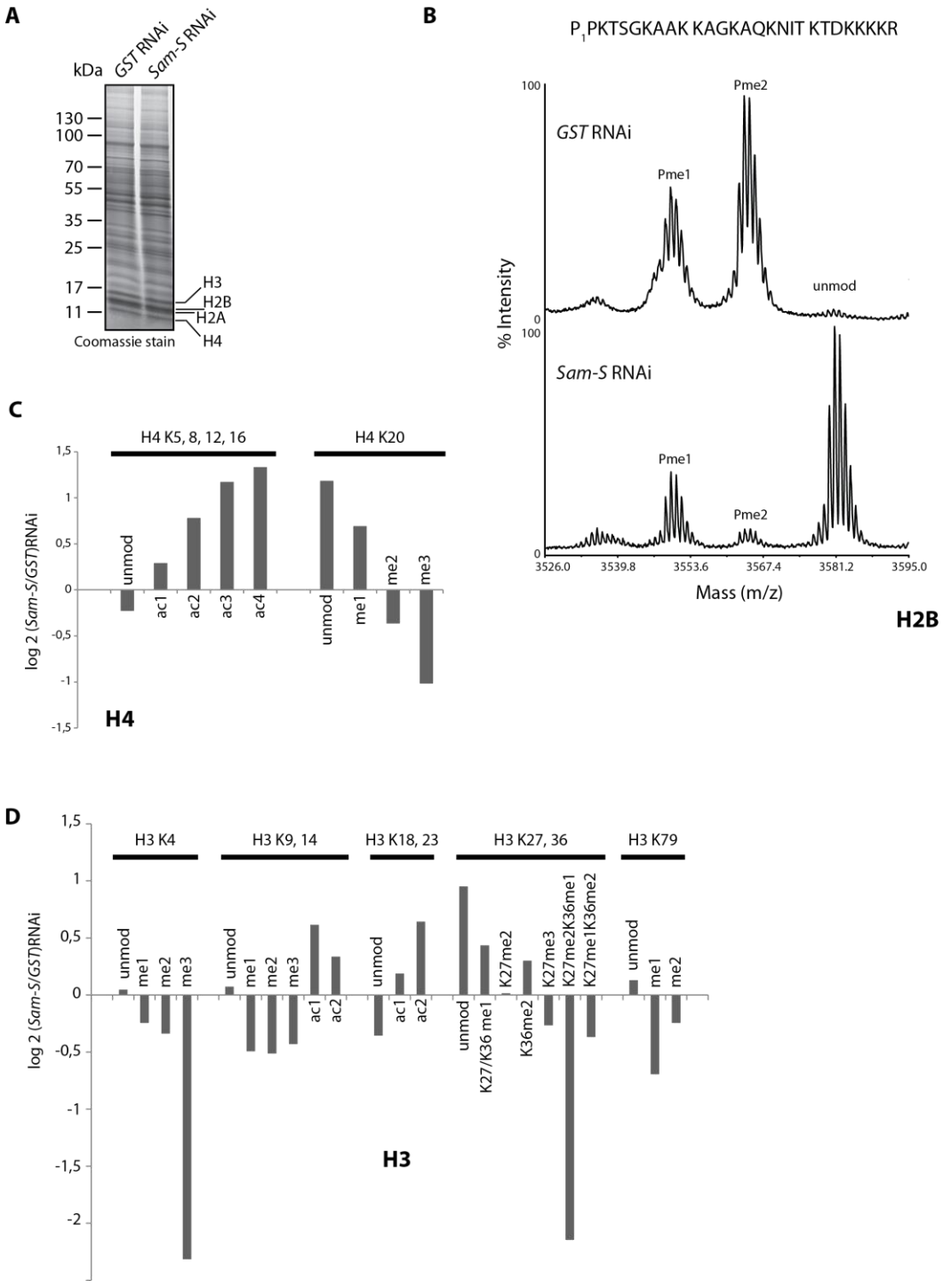

Figure 2.6: Histone modification pattern changed upon SAM depletion
(A) Nuclei were prepared from L2-4 cells. Histones were extracted by benzonase treatment and separated by 18% SDS-PAGE. After electrophoresis, gel was stained with Coomassie Brilliant Blue G250 and bands corresponding to H2B, H3 and H4 were excised. Histones were digested with trypsin and peptides were subjected to mass spectrometry analysis. **(B)** MALDI-TOF spectra of H2B. Signals of the peptide 1–28 are displayed. Unmod: unmodified proline; Pme1/Pme2: mono- and dimethylated proline. MALDI-TOF analysis was performed by Dr. Ignasi Forné. LC-MS/MS analyses of histone modifications of H4 **(C)** and H3 **(D)** are shown, respectively. The $\log_2$ fold change compared to the control is displayed. Unmod: unmodified peptide; me1/2/3: mono-, di- and trimethylated peptide; ac1/2/3/4: mono-, di-, tri- and tetraacetylated peptide.

In *Drosophila melanogaster*, the N-terminal proline at position 1 of H2B was detected in a mono- and dimethylated form (Villar-Garea et al., 2012). In the control, dimethylated proline (Pme2) was the most prominent modification which was completely lost upon Sam-S knockdown. Furthermore, the monomethylation state (Pme1) was also strongly decreased in the knockdown background in comparison to the control. The most abundant peptide found in Sam-S-depleted cells was the unmodified H2B peptide containing proline 1 which was not detected in the control (Figure 2.6 B). MALDI-TOF analysis of histone H2B was performed by Dr. Ignasi Forné.

Among other modifications, the core histone H4 can be methylated at arginine 3 (H4R3) and lysine 20 (H4K20) and acetylated at lysine 5, 8, 12 and 16 (H4K5/8/12/16) (Kouzarides, 2007). In presented mass spectrometry experiments, two peptides (4–17, 20–23) of H4 could be detected and modifications on lysine residues were quantified. Depletion of Sam-S resulted in a decreased di- and trimethylation level of H4K20 (~1.3- and 2.0-fold change, respectively) and an increased level of monomethylation on this residue (1.6-fold change). Furthermore, the unmodified H4K20 peptide was enriched by 2.2-fold. The peptide 4–17 was found to be hyperacetylated upon Sam-S knockdown and contained increased levels of acetylation marks on all lysine residues (between ~1.2-fold to 2.5-fold enrichment for ac1 and ac4, respectively, Figure 2.6 C).

The core histone H3 can be modified at various residues (Kouzarides, 2007). In this study, five peptides were examined which are rich in arginine and lysine residues that can be methylated and acetylated. These peptides are: 3–8 (K4), 9–17 (K9/14), 18–26 (K18/23), 27–40 (K27/36) and 73–83 (K79). Sam-S depletion resulted in a strong decrease of H3K4me3 and H3K27me2K36me1 levels (4.5-fold and 5.0-fold change, respectively). H3K79me1 was decreased by 1.6-fold whereas most of the other methylation marks were only slightly but reproducibly decreased and some were modestly enriched (H3K27/36me1, H3K27me2 and H3K36me2). Acetylation marks on H3 were also enriched in the knockdown situation as was observed for H4 (Figure 2.6 D).

Taken together, nearly all methylation marks were reduced upon Sam-S knockdown, although to various levels. In contrast to methylation, all acetylation marks were enriched on H3 and H4 residues in comparison to the control. These data reveal that Sam-S regulates global histone methylation which is involved in the regulation of gene expression.

2.3.4. Disruption of SAM metabolism results in an altered gene expression profile

The quantitative analysis of posttranslational modifications showed that global histone methylation levels decreased upon depletion of Sam-S. To investigate its impact on the regulation of gene expression, an analysis of the genome-wide gene expression was performed.

To identify Sam-S-regulated genes, total mRNA was purified and checked for quality with the Bioanalyzer. Compared to the negative control, a reduction of roughly 90% of the *Sam-S* mRNA expression could be achieved (Figure 2.5 A). The gene expression profiles between the control and *Sam-S* knockdown were then compared using a DNA microarray analysis (Figure 2.7 A). Out of the 18800 probe sets (analyzing over 18500 transcripts), the expression levels of 6671 genes were altered, 1734 genes were changed by >1.5-fold of which 676 probes showed a down- and 1058 probes an upregulation, respectively. The open source DAVID bioinformatics tool (Huang et al., 2007a) was used to generate a gene ontology analysis. In the group of downregulated genes GO terms such as glucose metabolic process or protein amino acid phosphorylation were the most significant hits (Figure 2.7 B). In the group of upregulated genes the most significant GO terms were connected to ncRNA processing, rRNA processing and tRNA metabolic process (Figure 2.7 C).

In order to investigate if there is a correlation between low SAM levels and the expression levels of SAM-metabolizing enzymes, the list of altered genes was searched against the list of all (putative) methyltransferases from the Pfam and Superfamily databases (python alignment, see chapter 4.2.6.2.). The comparison found 166 annotated MTs on the DNA microarray, from which 35 probes showed a down- and 85 probes showed an upregulation, respectively. A GO term analysis with the DAVID bioinformatics tool was performed as well. Histone methylation and chromatin organization were significant hits for downregulated MTs (Figure 2.7 B) while significant hits for the upregulated MTs were, consistent with the former GO term analysis, ncRNA metabolic process and RNA modification (Figure 2.7 C).

A

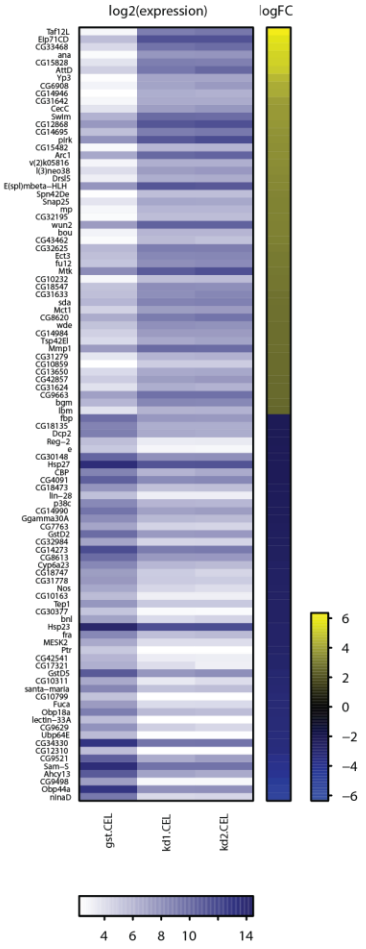

B

GO terms of down-regulated genes	
Term	**P-value**
Glucose metabolic process	1.5(E-7)
Protein amino acid phosphorylation	3.0(E-6)
Monosaccharide metabolic process	3.8(E-6)
Cellular carbohydrate catabolic process	4.4(E-6)
GO terms of down-regulated methyltransferases	
histone methylation	8.8(E-10)
chromatin organization	6.5(E-5)

C

GO terms of up-regulated genes	
Term	**P-value**
ncRNA processing	8.1(E-15)
Ribosome biogenesis	5.5(E-12)
rRNA processing	1.6(E-9)
RNA modification	6.4(E-9)
tRNA metabolic process	2.5(E-6)
GO terms of up-regulated methyltransferases	
ncRNA metabolic process	9.9(E-21)
RNA modification	9.7(E-19)

Figure 2.7: Gene expression profile is altered upon SAM depletion
Total mRNA was purified from L2-4 cells. **(A)** DNA microarray analysis of gene expression in control (*GST*) and *Sam-S* knockdown cells (kd1/2). Data analysis was performed by Dr. Tobias Straub. Heat map shows genes that were either down- (blue) or upregulated (yellow). Log_2 fold enrichment over the negative control was calculated. Gene ontology (GO) term enrichment analysis with the DAVID bioinformatics tool was performed. Tables show significant hits for down- **(B)** and upregulated **(C)** genes.

Expression levels of methyltransferases

To confirm the results from the DNA microarray, a quantitative real-time PCR was performed for various genes. As a reference, the housekeeping gene *tubulin 97E* (*tub*) was used. The average of three biological replicates was taken and the expression levels of selected genes in the control were normalized to one.

First, the reduction of *Sam-S* gene expression was confirmed upon RNAi treatment. Compared to the negative control, a reduction of roughly 90% of the *Sam-S* mRNA expression could be reproduced.

Furthermore, gene expression levels of enzymes of the metabolic pathway of SAM were analyzed (Figure 2.8 A). Interestingly, the mRNA level of *CG10623*, a putative methionine synthase, was also significantly reduced although it is a putative methyltransferase that is not SAM-dependent. The mRNA level of the major *Adenosylhomocysteinase (Ahcy)*, however, was only reduced modestly (Figure 2.8 A). Ahcy catalyzes the hydrolysis of SAH to homocysteine and adenosine (Caggese et al., 1997).

Next, the expression level of several histone methyltransferases was analyzed since the microarray analysis showed the tendency to affect their expression upon Sam-S depletion. Using qPCR, this could be confirmed for nearly all selected enzymes except for *Suppressor of variegation 3-9 (Su(var)3-9)*, a H3K9 MT. In contrast to the microarray results, the mRNA level of this enzyme showed no change in expression levels.

The two enzymes of a bifunctional methyltransferase complex (Villar-Garea et al., 2012), namely Ntmt, which methylates H2BP1, and Art8, which methylates H3R2, showed a modest reduction of their mRNA levels compared to the control. Significantly reduced were the mRNA levels of the H4K20 MTs *histone methyltransferase 4-20 (Hmt4-20)* and *pr-set7*. However, the strongest reduction was found for the H3K4 MTs *trithorax (trx)* and *trithorax-realted (trr*) (Figure 2.8 B) which was consistent with the strong downregulation of H3K4 trimethylation (Figure2.6 D).

For the group of upregulated genes and MTs, GO terms like ncRNA processing as well as rRNA processing and tRNA metabolic processes were enriched (Figure 2.7 C). Therefore, the expression levels of DNA and RNA MTs were analyzed by qPCR. Consistent with the microarray analysis, qPCR analysis showed a significant elevation for the DNA/ tRNA MT *Methyltransferase 2 (Mt2)* and the rRNA MT *CG11837*. However, *Sam-S* knockdown also resulted in a significant reduction for the tRNA MT *CG33468* and mRNA *MT CG6379*.

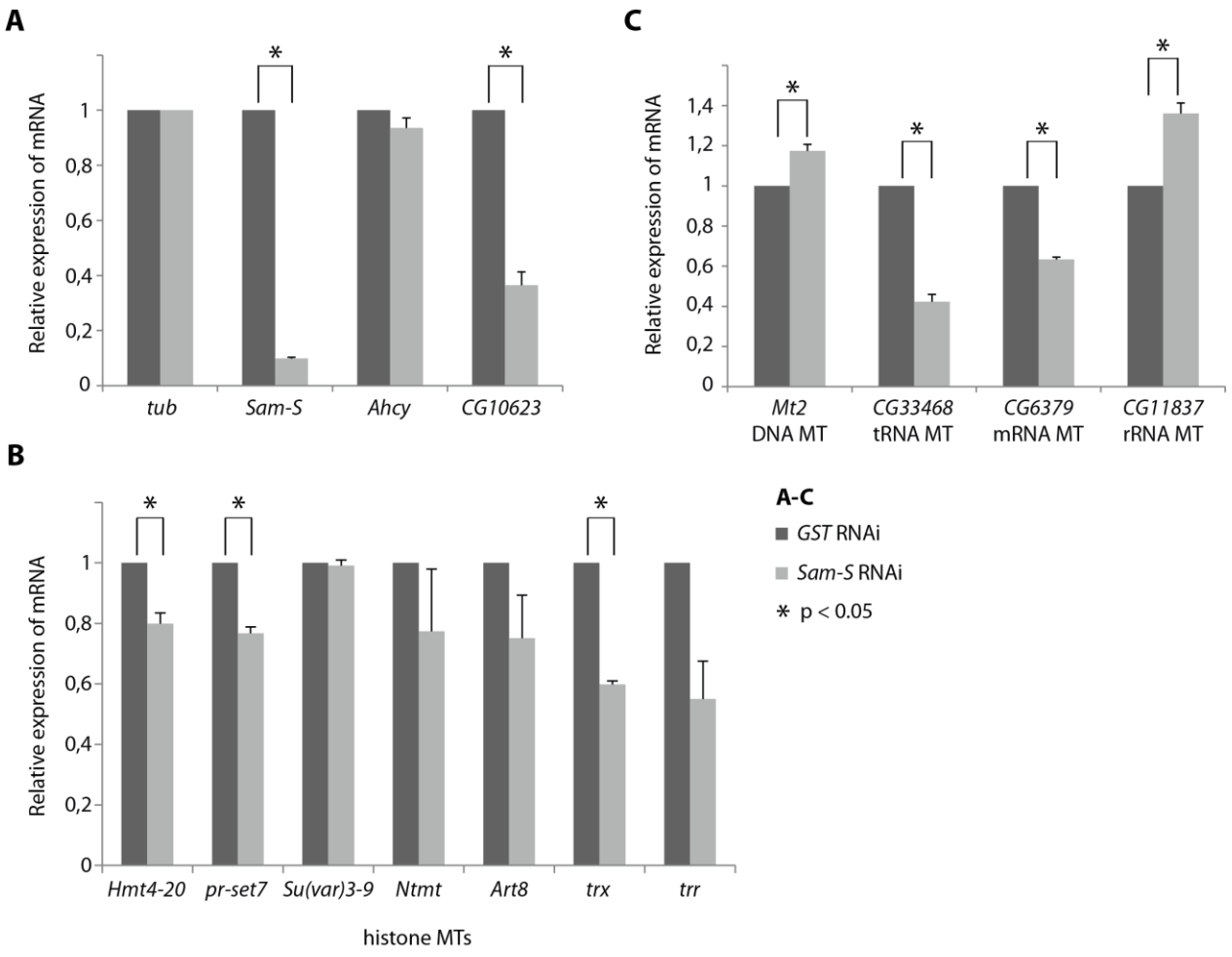

Figure 2.8: Expression levels of methyltransferases were altered due to SAM limitation
Total mRNA was purified from L2-4 cells and expression levels of mRNA were analyzed using qPCR. The housekeeping gene *tubulin 97E* (*tub*) served as a control. Shown is the fold change after normalization to *tubulin 97E* mRNA levels. Error bars indicate standard deviation of three biological replicates. Asterisk (*) indicates statistical significance with $p \leq 0.05$. Investigated were genes involved in SAM metabolism **(A)**, several histone methyltransferases **(B)**, DNA methyltransferase Mt2 and various RNA methyltransferases (MT) **(C)**.

In summary, the results from the DNA microarray analysis could be confirmed by qPCR for the majority of investigated MTs. However, it is important to keep in mind, that over the last years discrepancies between gene expression levels and protein levels have become an area of concern (Foss et al., 2007; Ghazalpour et al., 2011). In order to test if such a discrepancy was also seen within this analysis, another approach, the Capture Compound™ Mass Spectrometry, was established. The results are described in chapter 2.5.

Expression levels of transposable elements

Methylation is well known to be a signal for transcriptionally inactive chromatin (Kouzarides, 2007; Schotta et al., 2004). Especially, retrotransposon silencing is reported to be controlled by the DNA methyltransferase Mt2 and the trimethylation of K20 within H4 (Phalke et al., 2009), a histone mark which was decreased upon Sam-S depletion (Figure 2.6 C). In order to investigate a potential function for Sam-S within the silencing of transposable elements, the copy number of various TEs and their expression levels were determined upon *Sam-S* RNAi.

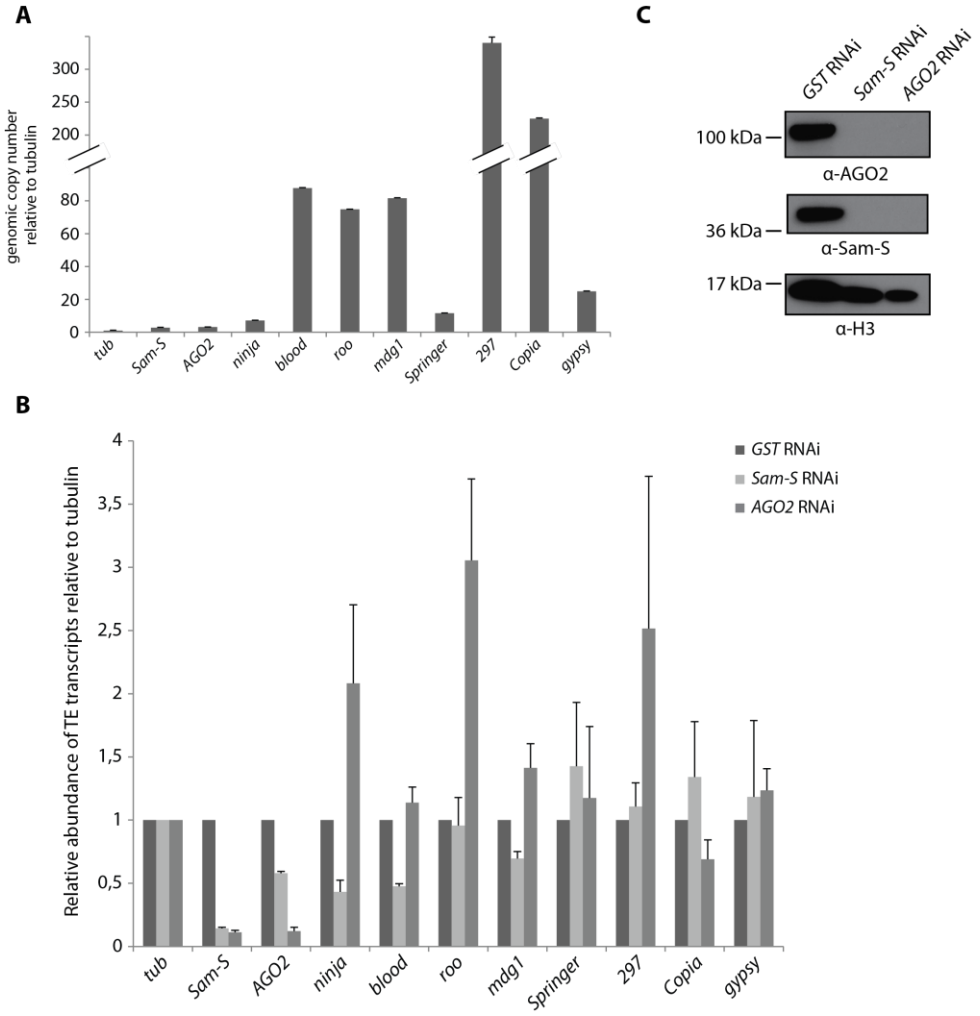

Figure 2.9: Expression levels of transposable elements were changed upon Sam-S depletion
(A) Genomic DNA was isolated from L2-4 cells. Genes of various retrotransposons were quantified using qPCR. The genomic copy numbers were normalized to *tubulin 97E* (*tub*). **(B)** Total mRNA was purified from L2-4 cells and expression levels of mRNA were quantified using qPCR. Abundance of transcripts from transposable elements after *Sam-S* and *AGO2* RNAi, respectively, are shown. *GST* RNAi served as a control. Shown is the fold change relative to *tubulin 97E*. Error bars indicate standard deviation of three biological replicates. **(C)** L2-4 cells depleted of Sam-S and AGO2, respectively, were analyzed by western blot using indicated antibodies. Histone 3 (H3) served as a control.

First, the genomic copy number of selected class I TEs, so-called retrotransposons, was determined. Genomic DNA was isolated from L2-4 cells and quantified using qPCR. The genomic copy number of various retrotransposons relative to *tubulin 97E* (*tub*) is depicted in Figure 2.9 A. Copy numbers ranged from 7 for *ninja* to 354 for the retrotransposon *297*. The single copy genes *tub*, *Sam-S* and *AGO2* ranged from 1 to 3 as expected.

For quantitation of TE transcript abundance, the same cDNA as for MTs analyses was used for qPCR experiments. The expression levels were normalized to *tubulin 97E*. The average of three biological replicates was taken and the expression levels of TEs in the control were set to one. A knockdown of *Argonaute 2 (AGO2)*, a crucial component of the RNAi machinery, served as a positive control since AGO2 is known to function in the silencing of transposable elements (Czech, 2008; Chung, W.-J:, 2008). The knockdown of *Sam-S* resulted in a bidirectional misregulation of TEs. An increase was observed for the TEs *Springer, 297, Copia, gypsy*, while the TEs *ninja, blood, mdg1* were reduced (Figure 2.9 B). As expected, in an *AGO2* knockdown, all TE transcripts (except *Copia*) showed an increase in expression levels (Figure 2.9 B).

Besides this result, a very interesting observation was made. The mRNA level of *AGO2* was strongly affected in the *Sam-S* knockdown and *vice versa*. This was also present on the protein level as determined by western blot analysis from the knockdown cells (Figure 2.9 C).

2.4. Quantitative analysis of S-adenosylmethionine and S-adenosylhomocysteine in tissue culture cells by liquid chromatography tandem mass spectrometry

In order to quantify endogenous levels of SAM and SAH in cultured cells, a liquid chromatography tandem mass spectrometry approach was established in collaboration with the Metabolomics platform (head: Dr. Cornelia Prehn) of the Genomic Analysis Center (GAC, head: Prof. Dr. Jerzy Adamski) at the Helmholtz Zentrum München GmbH in Neuherberg.

The metabolites SAM and SAH were acid extracted from L2-4 cells and directly prepared for LC-MS/MS analysis as described in chapter 4.2.6.4. As an internal standard, deuterium-labeled SAM ($^2H_3$-SAM) was used for absolute quantitation of SAM and SAH since this minor structural difference had no effect on linearity and precision (Burren et al., 2006). Metabolites were measured using multiple reaction monitoring (MRM) (Kitteringham et al., 2009).

The MRM method is a sensitive method for quantitative measurement of a target molecule (targeted metabolomics). Two stages of mass filtering are applied. First, the mass of the molecule of interest is

preselected (parent ion) in the mass spectrometer. Second, a fragmentation of the parent ion is induced which results in a specific product ion spectrum for each target molecule. These product ions are then used for quantitation. This targeted method decreases the limit of detection (LOD) compared to methods where only the parent ions are used for quantitation.

The LC-MS/MS method after Burren et al. was then used to determine the concentration of SAM and SAH in L2-4 cells (Burren et al., 2006). The method was established and partially validated as follows:

2.4.1. Chromatography

Prior to mass spectrometry analysis, the metabolites SAM and SAH were separated on a pentafluorophenylpropyl (PFPP) column. Since SAM is a polar compound, it is minimally retained on standard reverse-phase columns. Therefore, the PFPP column was chosen due to its additional ion-exchange properties (Burren et al., 2006). Representative chromatograms of the internal standard $^{2}H_{3}$-SAM (Figure 2.10 A), SAM (Figure 2.10 B) and SAH (Figure 2.10 C), dissolved in a matrix of L2-4 cells, are depicted in Figure 2.10. The two metabolites were clearly separated in retention times and did not co-elute as required for quantitative analysis.

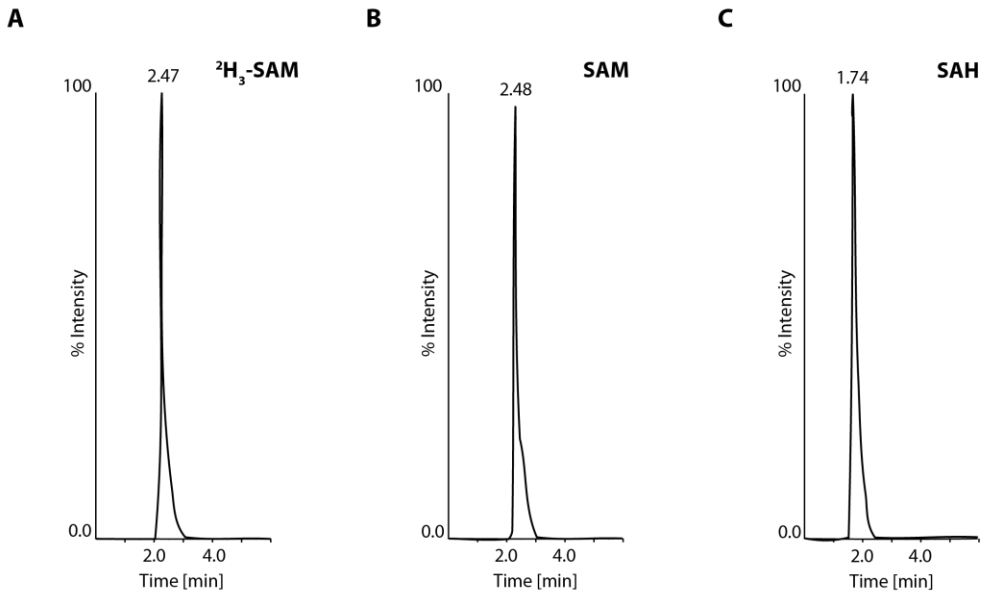

Figure 2.10: Chromatograms of SAM and SAH
LC-MS/MS chromatograms were obtained in the MRM mode. Representative chromatograms are shown for $^{2}H_{3}$-SAM **(A)**, SAM **(B)** and SAH **(C)** in a matrix of L2-4 cells. Retention times are indicated above peaks.

2.4.2. Mass spectra

The expected parent ions (red, Figure 2.11) for $^{2}H_{3}$-SAM, SAM and SAH were m/z 402.2, 399.2 and 385.2, respectively. The obtained mass spectra fit with the theoretical masses and detected product ions were similar to published data (Burren et al., 2006; Krijt et al., 2009).

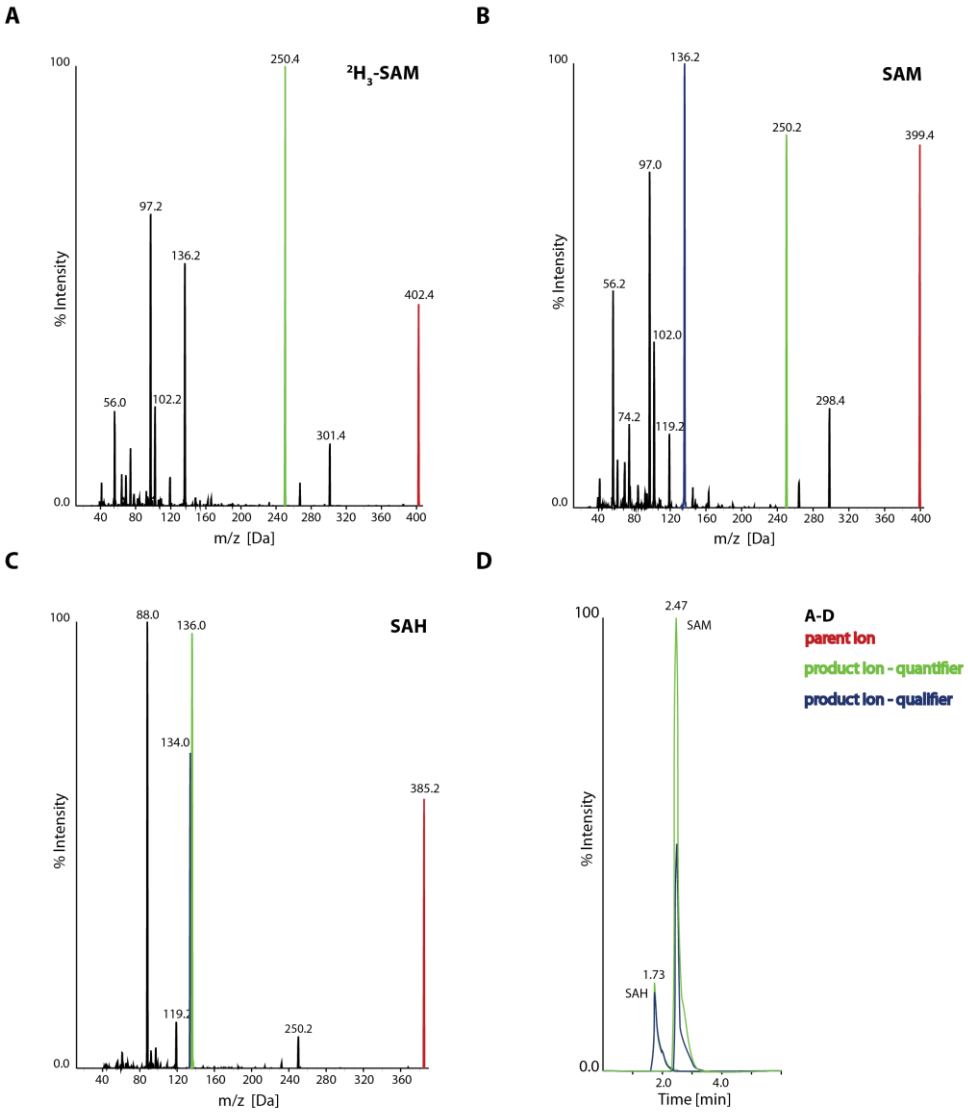

Figure 2.11: Product ion spectra for protonated molecules used for quantitation
Representative product ion spectra are shown. The panels show multiple reaction monitoring for the transitions m/z 402.2 –> 250.0 (green) for $^{2}H_{3}$-SAM **(A)**; 399.2 ->250.0 (green) and 399.2 -> 136.2 (blue) for SAM **(B)** and 385.2 -> 136.0 (green) and 385.2 -> 134.0 (blue) for SAH **(C)**. Product ions used for quantitation are depicted in green (quantifier) and product ions used for confirmation are depicted in blue (qualifier). **(D)** LC-MS/MS chromatograms for quantifier (green) and qualifier (blue), respectively, obtained in the MRM mode. Retention times for SAM and SAH are indicated above peaks.

A representative product ion spectrum for each molecule is shown in Figure 2.11. Each spectrum resulted from a compound optimization and the final MRM transitions were taken as follows: $^{2}H_{3}$-SAM: 402.2 –> 250.0 (Figure 2.11 A); SAM: 399.2 ->250.0 (quantifier, green) and 399.2 -> 136.2 (qualifier, blue) (Figure 2.11 B) and SAH: 385.2 -> 136.0 (quantifier, green) and 385.2 -> 134.0 (qualifier, blue) (Figure 2.11 C). The product ion at m/z 136.1 is thought to correspond to the adenine backbone (Struys et al., 2000). For SAM and SAH, a second product ion (qualifier) was included in the measurement to ensure that the product ion, which was used for quantitation (quantifier), originated from the correct parent ion (Figure 2.11 D). Since both product ions derive from the same parent ion, quantifier and qualifier must have the same retention time thereby increasing confidence that the proper molecule is quantified.

2.4.3. Validation of established method: selectivity, linearity and precision

The MRM method was established on a different mass spectrometer than the previously published method in Burren et al. (Burren et al., 2006). Therefore, a few parameters were validated.

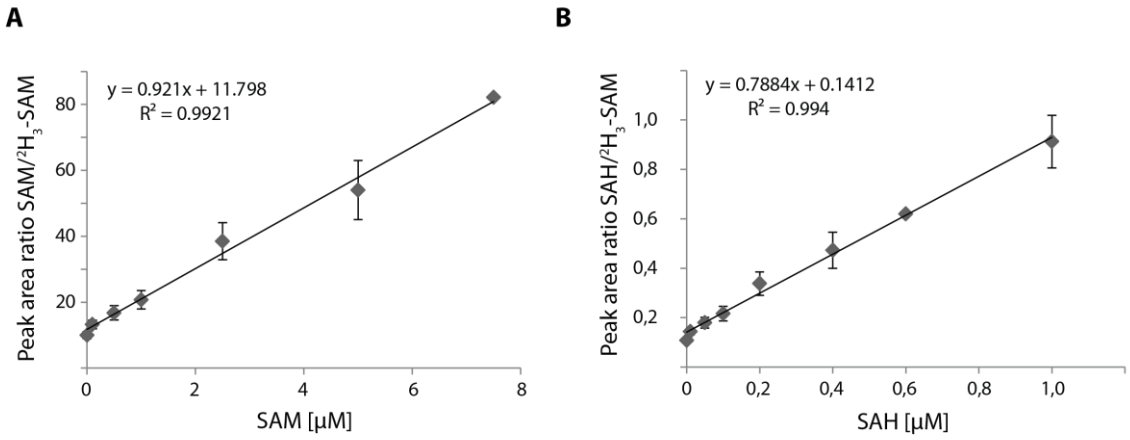

Figure 2.12: Calibration curves for SAM and SAH used for quantitation
Calibrators, SAM and SAH, were spiked in a matrix of L2-4 cells with 1 µM of the internal standard $^{2}H_{3}$-SAM in each sample. Peak area ratios are plotted against SAM **(A)** and SAH **(B)** concentration. Data points for SAM correspond to a concentration of 0.1, 0.5, 1.0, 2.5, 5.0 and 7.5 µM. Data points for SAH correspond to a concentration of 0.01, 0.05, 0.1, 0.2, 0.4, 0.6 and 1.0 µM. Each sample was run in triplicates, error bars indicate standard deviation.

Selectivity is the ability to determine analytes in a biological sample under given conditions in the presence of other components of similar behavior. SAM and SAH could be detected and quantified in a

matrix of L2-4 cells. Selectivity is therefore ensured. The lower limits of quantitation (LLOQ) for SAM and SAH were 8.0 nmol/l and 0.2 nmol/l, respectively. This was determined from a matrix prepared from of $0.1*10^6$ L2-4 cells.

For linearity, calibration curves were measured in a matrix of L2-4 cells to include quenching effects from the matrix in the quantitation. The calibration curves for both metabolites were linear through a range sufficient for the analysis (Figure 2.12 A and B). For SAM the concentration range was linear between 0.1–7.5 µM, for SAH between 0.01–1.0 µM. The coefficient of linear correlation (R^2) was 0.9921 and 0.994 for SAM and SAH, respectively. All samples for the calibration curve contained 1 µM of the internal standard $^2H_3$-SAM and were run in triplicate. Calibration curves were then used to quantify endogenous levels of SAM and SAH. Analysis of an analyte can be suppressed or enhanced by other components of the matrix. To avoid possible matrix effects, the calibration curve was dissolved in a matrix background of L2-4 cells. The measured endogenous SAM and SAH levels in $2*10^6$ cells were 1.39 µM and 0.03 µM, respectively, resulting in a SAM/SAH ratio of 50.3 (+/- 11.1) (Figure 2.5 C).

Precision describes the closeness to the true value when repeated and individual measurements under unchanged conditions are performed. To determine it, three different concentrations of SAM and SAH were measured at least three times. The intra-assay coefficients of variations (CVs) ranged from 3.45% to 7.35% for SAM and 1.61% to 8.00% for SAH, respectively (Table 1).

Table 1: Intra-assay precision of the LC-MS/MS method for L2-4 cells
The precision was determined by repeated assay (n= 3) of a matrix of L2-4 cells spiked with different concentrations of SAM and SAH. STDEV: Standard deviation; CV: coefficient of variation.

SAM		**SAH**	
Mean concentration (µM +/- STDEV)	CV (%)	Mean concentration (µM +/- STDEV)	CV (%)
2.72 +/- 0.02	7.35	0.40 +/-0.01	2.50
5.21 +/- 0.21	4.03	0.62 +/-0.01	1.61
9.85 +/- 0.34	3.45	1.00 +/-0.08	8.00

Heat precipitation of proteins during sample preparation had no effect on SAM or SAH stability. SAM and SAH were spiked in before and after heat treatment and showed no difference in quantitation (data not shown).

In summary, a LC-MS/MS method was established that enabled the sensitive and precise quantitation of endogenous levels of SAM and SAH in *Drosophila* tissue culture cells.

2.5. Profiling of SAM-dependent methyltransferases by Capture Compound™ Mass Spectrometry

Regulation of methyltransferases upon Sam-S knockdown could be observed at the mRNA level (chapter 2.3.4.). However, there are discrepancies reported between gene expression levels and protein levels (Foss et al., 2007; Ghazalpour et al., 2011). In addition, different SAM binding affinities of (histone) methyltransferases (Brown et al., 2014; Copeland et al., 2009; Horiuchi et al., 2013; Patnaik et al., 2004; Xiao et al., 2003) suggest that SAM concentration may play a role in their regulation. In order to test for correlations between metabolite concentration and enzyme activity, protein levels of MTs had to be investigated. Since western blot analyses are limited to existing antibodies, the Capture Compound™ Mass Spectrometry (CCMS) (Koster et al., 2007) is a technology that enables a functional isolation of subproteomes. First, this method had to be established.

2.5.1. Capture Compound™ Mass Spectrometry technology

The CCMS enables the isolation of a subset of proteins from a protein mixture that shares a common function (Koster et al., 2007). This chemical proteomics technology is based on a trifunctional molecule called Capture Compound™ (CC) (Figure 2.13 A and B). This compound consists of three different functionalities: a selectivity function which interacts with target proteins, a photo-activatable reactivity function to covalently trap interacting proteins and a sorting function that enables the isolation of the captured proteins via a biotin tag.

In this work, the isolation of SAM-metabolizing methyltransferases was the subproteome of interest. SAH is an inhibitor for all SAM-dependent methyltransferases and binds strongly to these enzymes. It was used for selectivity due to its higher stability than SAM (Dalhoff et al., 2010). The SAH-Capture Compound™ (SAH-CC) was available with two different photo-reactive cross-linkers: fluorinated aryl azide (aa) (Figure 2.13. A) and benzophenone (bp) (Figure 2.13 B). In general, benzophenones have a few advantages: they are chemically more stable than aryl azides and can be repeatedly excited at 350 nm thereby avoiding protein-damaging wavelengths (Dorman and Prestwich, 1994). In contrast, aryl azides are smaller in size and therefore have steric advantages but are activated at 315 nm which is close to the absorption wavelength at which proteins absorb UV light at 280 and 200 nm (Smith and Collins, 2015).

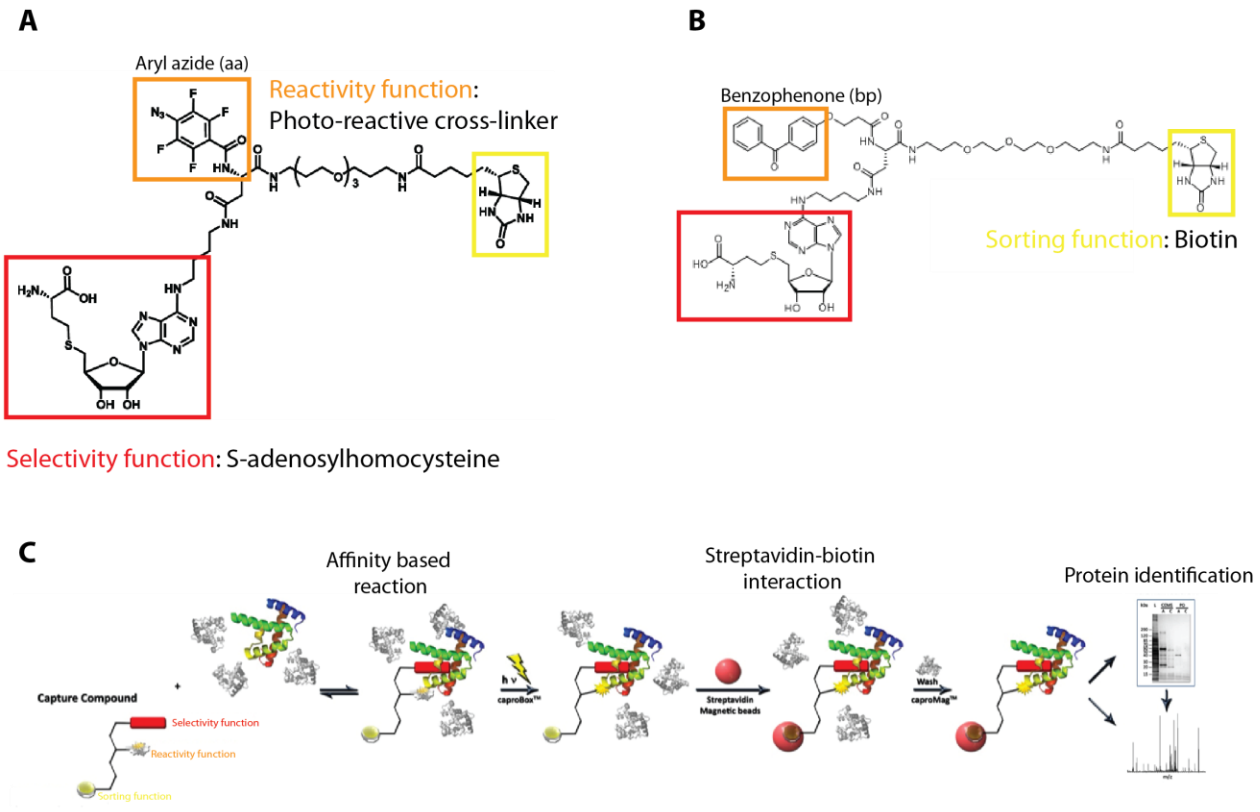

Figure 2.13: The technology of Capture Compound™ Mass Spectrometry (CCMS)
CCMS is based on a trifunctional molecule, the so-called Capture Compound™ (CC). This compound consists of three different functionalities: a selectivity function (red), a reactivity function (orange) and a sorting function (yellow). SAH was used as the selectivity function to isolate methyltransferases and other SAH-binding proteins. Fluorinated aryl azide **(A)** and benzophenone **(B)** were used as reactivity function, respectively. **(C)** Shematic overview of the workflow of CCMS: first, an affinity-based reaction reaction takes place between the selectivity function and target proteins. Second, upon UV irradiation a covalent bond is formed with bound proteins. Third, target proteins are isolated via the biotin tag with streptavidin-coated magnetic beads. Analysis of captured proteins is performed by LC-MS/MS.

The workflow for isolation of SAM-dependent MTs by CCMS was accomplished in three steps and is illustrated in Figure 2.13 C. First, SAH-CCs were incubated with nuclear extract from L2-4 cells. In this step, the affinity-driven interaction between SAM/SAH-binding proteins and the SAH-CC took place. Second, the reactivity functional group was activated by UV light and the captured protein was covalently bound to the SAH-CC. This allows the isolation of weak interaction partners and stringent washing conditions. Finally, the biotin function was used to isolate the SAH-CC-protein complex from the nuclear extract using streptavidin-coated magnetic beads. Subsequent analysis of the subproteome was done using LC-MS/MS.

2.5.2. SAH-Capture Compounds™ form covalent bonds to target proteins upon UV irradiation

One feature that both SAH-CCs share is the formation of a covalent bond to the target protein which also enables the isolation of weak interaction partners. Two known SAM-binding proteins were chosen, the N-terminal methyltransferase (Ntmt) and Su(var)3-9 Δ213, to demonstrate covalent-binding properties. Therefore, recombinant MTs were incubated with SAH-CC_{aa} and SAH-CC_{bp}, respectively, and subsequently were photo-activated with the appropriate wavelength. As negative controls, samples were either not irradiated or no SAH-CC_{aa} was added.

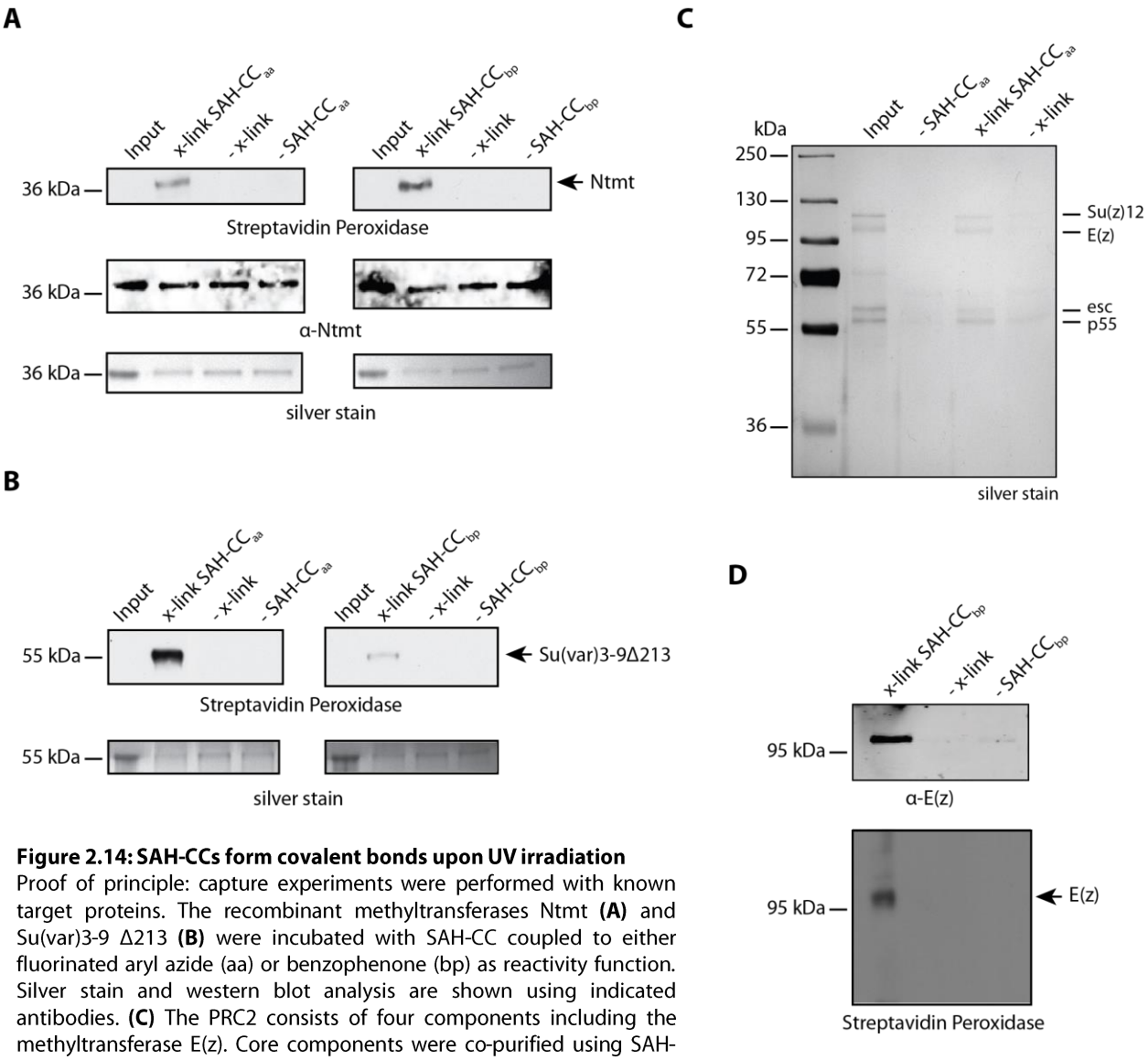

Figure 2.14: SAH-CCs form covalent bonds upon UV irradiation
Proof of principle: capture experiments were performed with known target proteins. The recombinant methyltransferases Ntmt **(A)** and Su(var)3-9 Δ213 **(B)** were incubated with SAH-CC coupled to either fluorinated aryl azide (aa) or benzophenone (bp) as reactivity function. Silver stain and western blot analysis are shown using indicated antibodies. **(C)** The PRC2 consists of four components including the methyltransferase E(z). Core components were co-purified using SAH-CC_{aa} while only E(z) was covalently bound **(D)**.

Capture experiments were analyzed by SDS-PAGE and western blot analyses (Figure 2.14). Streptavidin peroxidase enables the detection of biotinylated proteins. If a protein is covalently bound to the SAH-CC, it carries a biotin-tag. Both SAH-CCs were able to bind to recombinant Ntmt and Su(var)3-9 Δ213. Both MTs carried a biotin-tag after irradiation (Figure 2.14 A and B). Furthermore, under denaturing conditions (SDS-PAGE), biotinylation was lost when no UV irradiation was performed and therefore no covalent bond was formed, emphasizing the need of the cross-link (x-link).

Different binding affinities could be observed for the two different compounds. While Ntmt seemed to have a higher affinity for SAH-CC_{bp} than SAH-CC_{aa} (Figure 2.14 A), Su(var)3-9 Δ213 was bound at a modest level to the SAH-CC_{bp} and at a higher extent to the SAH-CC_{aa} (Figure 2.14 B).

To show that proteins interacting with a certain methyltransferase are co-purified, recombinant PRC2 was used as a known target of SAH-CC. The PRC2 consists of four core components: the H3K27 methyltransferase E(z), Suppressor of zeste 12 (Su(z)12), extra sex combs (esc) and p55. The complex was recombinantly expressed with the baculovirus system and purified via the FLAG-tag of E(z). A capture experiment was performed and demonstrated that the whole complex could be bound (Figure 2.14 C). This experiment also confirmed that only the SAM-dependent methyltransferase E(z) is bound to the SAH-CC_{aa} since it was the only component of the complex that carried the biotin-tag (Figure 2.14 D).

2.5.3. Comprehensive profiling of SAM-dependent methyltransferases in *Drosophila melanogaster*

The *in vitro* experiments showed that MTs were bound with different affinities to the different SAH-CCs. Therefore, two independent capture experiments with SAH-CC_{aa} and SAH-CC_{bp}, respectively, were performed.

To investigate the protein interaction profile, SAH-CCs were incubated with nuclear extracts from L2-4 cells. Photo-cross-linking was performed with the appropriate wavelength and irradiation time for each SAH-CC (for details see chapter 4.2.6.2.). Subsequently, captured proteins were isolated via the biotin-tag with streptavidin magnetic beads and separated by SDS-PAGE (Figure 2.15 A and B). A tryptic in-gel digestion was performed and obtained peptides were subjected to LC-MS/MS analysis. Finally, a computational analysis with the MaxQuant software (Cox and Mann, 2008) was done. For this purpose, the average of the iBAQ intensities of three independent replicates was taken and the $\log_2$ fold enrichment over the negative control was calculated. A list of (putative) methyltransferases was compiled from the Pfam and the Superfamily databases and compared to the list of enriched proteins.

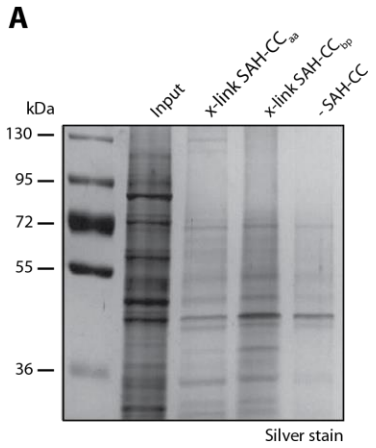

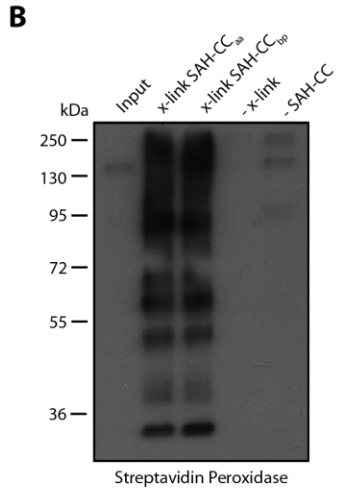

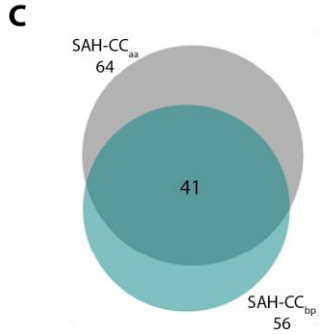

D

SAH-CC$_{aa}$ and SAH$_{bp}$ capturing experiments:

Flybase ID	Name	log$_2$ IP (x-link/ctrl) SAH-CC$_{aa}$ (SAH-CC$_{bp}$)	Flybase ID	Name	log$_2$ IP (x-link/ctrl) SAH-CC$_{aa}$ (SAH-CC$_{bp}$)
FBgn0037834	Art1	3 (5)	FBgn0039407	CG14544	4 (3)
FBgn0032329	Art8	2 (3)	FBgn0003062	Fib	2 (2)
FBgn0033948	CG12863	4 (4)	FBgn0039139	Ime4	4 (5)
FBgn0015925	csul	3 (9)	FBgn0026079	Nsun2	4 (2)
FBgn0000629	E(z)	2 (4)	FBgn0026309	aft	7 (3)
FBgn0086908	egg	6 (2)	FBgn0031189	CG14618	2 (2)
FBgn0040372	G9a	3 (6)	FBgn0029714	CG3527	5 (2)
FBgn0025639	Hmt4-20	6 (4)	FBgn0025629	CG4045	5 (3)
FBgn0039559	Mes-4	6 (5)	FBgn0032873	CG2614	5 (5)
FBgn0040022	Set1	4 (3)	FBgn0037543	CG10903	11 (4)
FBgn0011474	Set8 (pr-set7)	6 (4)	FBgn0034422	CG7137	6 (3)
FBgn0023518	trr	6 (2)	FBgn0031494	CG17219	7 (8)
FBgn0032016	CG7818	10 (4)	FBgn0040964	CG18661	14 (6)
FBgn0023522	CG11596	8 (7)	FBgn0024558	Dph5	9 (2)
FBgn0052732	CG32732	3 (4)	FBgn0027495	Smyd4-4	10 (5)
FBgn0031003	CG7889	10 (7)	FBgn0038869	Smyd5	7 (7)
FBgn0031485	CG9634	9 (2)	FBgn0036398	upSET	2 (3)
FBgn0029693	CG6379	4 (6)	FBgn0037061	CG12975	13 (2)
FBgn0032430	CG6388	4 (2)	FBgn0011763	Dp	7 (5)
FBgn0033741	CG8545	8 (4)	FBgn0011020	Sas-4	5 (5)
FBgn0033473	CG12128	7 (5)			

E

SAH-CC$_{aa}$ capturing experiment:

Flybase ID	Name	log$_2$ IP (x-link/ctrl)
FBgn0005386	ash1	4
FBgn0264495	gpp	8
FBgn0038396	CG5013	7
FBgn0036856	CG9666	8
FBgn0031777	CG9154	3
FBgn0039627	CG11837	3
FBgn0037347	CG1427	5
FBgn0035035	CG3570	9
FBgn0034351	CG5190	6
FBgn0033686	Hen1	7
FBgn0001974	l(2)35Bd	9
FBgn0261381	mtTFB1	5
FBgn0259704	Nsun5	5
FBgn0266195	Tgs1	7
FBgn0263144	bin3	3
FBgn0037200	CG11109	6
FBgn0035537	CG11342	7
FBgn0037368	CG1239	8
FBgn0036838	CG3808	4
FBgn0032724	CG10428	5
FBgn0000289	cg	4
FBgn0001977	CIAPIN1	8
FBgn0026702	l(1)G0045	3

F

SAH-CC$_{bp}$ capturing experiment:

Flybase ID	Name	log$_2$ (x-link/ctrl)
FBgn0038306	Art3	6
FBgn0034817	Art7	4
FBgn0032727	CG10623	7
FBgn0086768	Pcmt	3
FBgn0033457	Ntmt	2
FBgn0028507	CG3793	6
FBgn0029823	CG3011	7
FBgn0038471	CG5220	3
FBgn0052281	CG32281	5
FBgn0037116	Als2	4
FBgn0026566	CG1307	3
FBgn0030447	CG2200	5
FBgn0027607	CG8230	2
FBgn0005649	Rox8	6
FBgn0036571	Strumpellin	3

B-D

- Protein MT
- DNA MT
- RNA MT
- Putative MT

Figure 2.15: Comprehensive profiling of methyltransferases in *Drosophila* L2-4 cells
Methyltransferases (MT) were captured from nuclear extracts of L2-4 cells in two independent experiments with either SAH-CC$_{aa}$ or SAH-CC$_{bp}$. **(A)** Captured proteins were separated by SDS-PAGE and visualized by silver nitrate staining. A capture experiment without SAH-CC served as a control. **(B)** Western blot analysis of capture experiments using streptavidin peroxidase to detect biotinylation. Capture experiment without x-link and SAH-CC served as a control. **(C)** Venn diagram gives proportions and total numbers of all identified MTs and their overlap in the two different capturing experiments. Diagram was created with BioVenn (http://cmbi.ru.nl/cdd/biovenn/). Tables show MTs which were either identified in both capture experiments **(D)** or were specific for the SAH-CC$_{aa}$ **(E)** and SAH-CC$_{bc}$ **(F)** capture experiment, respectively. The log$_2$ fold enrichment over the negative control is shown. MTs were categorized as indicated.

The identified methyltransferase profile for each SAH-CC is depicted in Figure 2.15 D-F. In total, 79 methyltransferases were identified from 170 (putative) MTs annotated in the Pfam and the Superfamily databases of which 130 are expressed at low levels in *Drosophila* Schneider S2 cells according to Flybase (http://flybase.org; RNA-Seq profile search). 64 and 56 MTs could be identified for SAH-CC_{aa} and SAH_{bp}, respectively, with a $\log_2$ fold enrichment of >2. There was an overlap of 41 MTs which were captured with both SAH-CCs (Figure 2.15 C). Captured MTs were categorized depending on their substrate in protein MTs (blue), RNA MTs (orange) and DNA MTs (red). Identified proteins with an annotated methyltransferase activity and an unknown substrate were categorized as putative MTs (black). Methyltransferases identified in both capturing experiments included protein MTs like the histone MTs E(z), G9a, pr-set7 and Hmt4-20, RNA and putative MTs, respectively (Figure 2.15 D). Apart from MTs that were identified in both capture experiments, there were specific MTs for each compound (Figure 2.15 E and F). For instance, Ntmt was only identified in the SAH-CC_{bp} experiment which was consistent with the *in vitro* observation where it showed higher affinity to this Capture Compound™ (Figure 2.14 A). Interestingly, DNA MTs were only captured with SAH-CC_{aa} (Figure 2.15 E). SAH-CCs not only captured SAM-binding proteins but also bound defined subproteomes consisting of other ATP and purine nucleotide binding proteins (data not shown; appendix list).

As also shown in *in vitro* experiments, interacting proteins of SAM-dependent MTs could be identified (e.g. the core components of PRC2, Figures 2.14 C and 2.16 A). Another histone methyltransferase complex with its eight subunits could be identified, the complex of proteins associated with Set 1 (COMPASS) (Figure 2.16 B). It is a histone H3K4 methyltransferase complex responsible for di-and trimethylation in *Drosophila* with Set1 as the MT (Mohan et al., 2011).

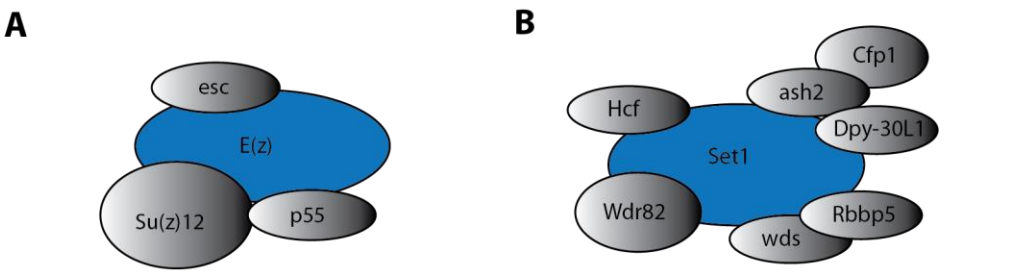

Flybase ID	Name	log_2 IP (x-link/ctrl)	
		SAH-CC_{aa}	SAH-CC_{bp}
FBgn0000588	esc	3	5
FBgn0020887	Su(z)12	7	5
FBgn0015610	p55	2	3

Flybase ID	Name	log_2 IP (x-link/ctrl)	
		SAH-CC_{aa}	SAH-CC_{bp}
FBgn0039904	Hcf	3	3
FBgn0000139	ash2	7	8
FBgn0040066	wds	2	2
FBgn0036973	Rbbp5	9	-
FBgn0030121	Cfp1	5	-
FBgn0032030	Wdr82	2	-
FBgn0032293	Dpy-30L1	8	-

Figure 2.16: Co-purification of histone methyltransferase complexes
SAM-dependent methyltransferases and their interacting proteins were purified from the nuclear extract of L2-4 cells in two independent experiments with either SAH-CC_{aa} or SAH-CC_{bp}. The log_2 fold enrichment over the negative control (ctrl) is shown. **(A)** The PRC2 consists of four components including the H3K27 methyltransferase E(z), extra sex combs (esc), Suppressor of zeste 12 (Su(z)12) and p55. **(B)** COMPASS consists of eight subunits including the methyltransferase Set1 responsible for H3K4 methylation. Hcf: Host cell factor; ash2: absent, small or homeotic discs2; Cfp1: CXXC finger protein 1; Dpy-30L1: Dpy-30-like1; Rbbp5: Retinoblastoma binding protein 5; wds: will die slowly; Wdr82: WD repeat domain 82.

2.6. Identification of lysine and arginine methylation in the *Drosophila melanogaster* proteome

Methylation is a posttranslational modification that is known to play an important role in the regulation of chromatin via histone and DNA methylation (Fontecave et al., 2004). Recent studies also showed its importance in other biological pathways involving non-histone proteins (Biggar et al., 2015). Since little is known about methylation sites in *Drosophila melanogaster* beyond histones, a heavy methyl stable isotope labeling by amino acids in cell culture (hmSILAC) was combined with high-resolution mass spectrometry proteomics to identify new methylation sites on lysines and arginines. This was done in collaboration with the laboratory of Dr. Tiziana Bonaldi, IFOM-IEO Campus in Milan since a pipeline had already been established for identifying methylation sites in the human proteome (Bremang et al., 2013).

2.6.1. Incorporation of heavy methionine

Before samples could be analyzed by LC-MS/MS, the proper conditions for hmSILAC labeling had to be set up. Since the concentration of L-methionine in the *Drosophila* Schneider medium (GIBCO) is rather high (0.8 g/l), three different concentrations of L-methionine, 0.5, 1 and 2 g/l, were tested. L2-4 cells were metabolically labeled with mentioned concentrations of either heavy ($^{13}CD_3$, Met-4) or the light ($^{12}CH_3$, Met-0) L-methionine for nine replication cycles. Samples were mixed in a 1:1 ratio and analyzed in the lab of Dr. Tiziana Bonaldi for incorporation of heavy L-methionine. Labeling with 1g/l of Met-4 resulted in an incorporation rate of 95 % (Figure 2.17 A) which is sufficient for a qualitative analysis of methylation sites. Surprisingly, there was no significant difference between the incorporation of Met-4 when labeled with 2 g/l and 0.5 g/l of Met-4, respectively (incorporation rate 93.6 % and 92.9 %, respectively; data not shown).

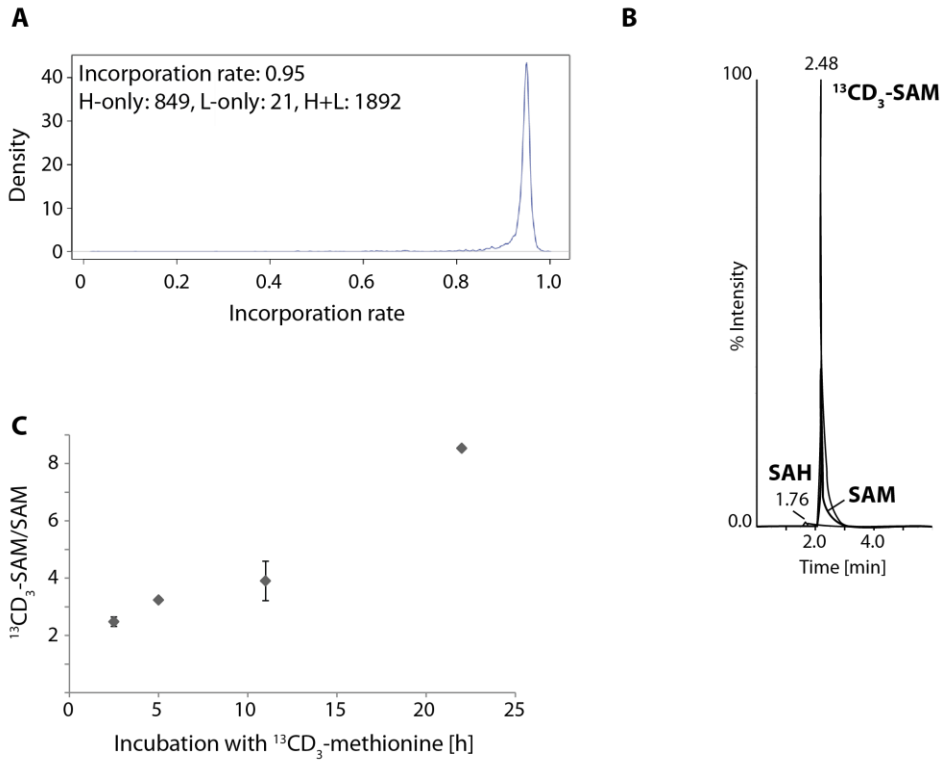

Figure 2.17: Heavy methionine is incorporated in SAM
(A) L2-4 cells were metabolically labeled with heavy $^{13}CD_3$-methionine (H) or light $^{12}CD_3$-methionine (L) for nine replication cycles. Shown is the incorporation rate when labeling was performed with 1g/l. **(B)** Heavy $^{13}CD_3$-methionine is incorporated in heavy $^{13}CD_3$-SAM. A representative LC-MS/MS chromatogram obtained in the MRM mode is shown. Retention times are indicated above peaks. **(C)** Time course of $^{13}CD_3$-methionine incorporation in $^{13}CD_3$-SAM in L2-4 cells.

In a second approach, the rate of heavy $^{13}CD_3$-methionine incorporation into SAM was tested. L2-4 cells were incubated with Met-4 for 2.5, 5, 11 and 22 h. Afterwards, cells were harvested and incorporation was analyzed using the established LC-MS/MS method in the MRM mode. A representative chromatogram of $^{13}CD_3$-SAM is shown in Figure 2.17 B confirming that heavy $^{13}CD_3$-SAM elutes at the same time as endogenous SAM. The huge concentration differences between SAM and SAH can be appreciated in this chromatogram. The expected mass for $^{13}CD_3$-SAM was m/z 403.2 and the MRM transition $^{13}CD_3$-SAM: 403.2 –> 250.0 was used for quantitation. Over time, heavy $^{13}CD_3$-methionine gets incorporated in heavy $^{13}CD_3$-SAM, which did not reach a plateau after 22 h (Figure 2.17 C).

2.6.2. Workflow of the hmSILAC and preparation for MS analysis

L2-4 cells were metabolically labeled with either heavy L-methionine or the light version of the amino acid for at least nine replication cycles. After this time, heavy and light cells were mixed in a 1:1 ratio and a subcellular fractionation was performed. The cytosolic and nuclear fractions were then sent to the laboratory of Dr. Tiziana Bonaldi for further analysis (Figure 2.18 A).

Due to limitations in the protein levels, 5 mg and 1.2 mg for the cytosolic and nuclear fraction, respectively, no affinity enrichment with antibodies against lysine- and arginine-methylated proteins could be performed. Still, each subcellular fraction could be subjected to either SDS-PAGE separation followed by tryptic in-gel digestion or tryptic in-solution digestion followed by isoelectric focusing (IEF) of the peptides depending on their isoelectric point (pI). Independent of which strategy was used, all obtained peptides were prepared the same for subsequent LC-MS/MS analysis on a high resolution Orbitrap mass spectrometer (Figure 2.18 B). Sample preparation was done as described in Bremang et al. (Bremang et al., 2013). Raw data were then analysed using the MaxQuant software and searched against a *Drosophila melanogaster* proteome derived from the UniProt database (14/06). Output from the MaxQuant searches was postprocessed using a pipeline developed in-house (Perl) for detecting hmSILAC pairs. LC-MS/MS and data analysis was done by Dr. Michael Bremang, IFOM-IEO Campus in Milan.

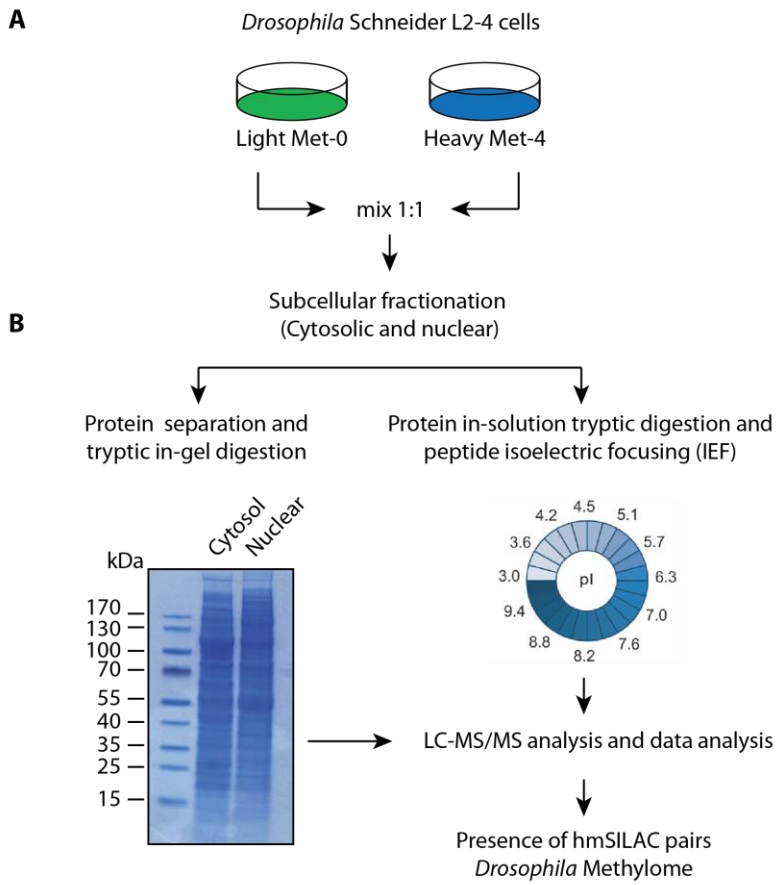

Figure 2.18: Workflow of the heavy methyl SILAC approach
(A) L2-4 cells were grown separately in light (Met-0) and heavy (Met-4) methionine-containing media, respectively. After labeling, cells were harvested and mixed in a 1:1 ratio followed by a separation into cytosolic and nuclear fractions. **(B)** Each fraction was then subjected either to protein separation by SDS-PAGE followed by in-gel digestion or to in-solution digestion and peptide separation by isoelectric focusing (IEF). All peptides were subjected to LC-MS/MS analysis, raw data were processed using MaxQuant software and hmSILAC pairs were identified using an analysis pipeline developed in the Bonaldi laboratory. Analyses were performed by Dr. Michael Bremang (reproduced from Bremang et al., 2013 with permission from the Royal Society of Chemistry).

2.6.3. The *Drosophila melanogaster* methylome

After data analysis, peptide pairs were arranged in classes. A confident identification required the identification of sequenced peptides in both the heavy and the light form. In addition, the localization probability of the modified site was >0.75. HmSILAC pairs meeting these criteria were assigned to class A. Those peptide pairs were further classified depending on their score. An hmSILAC pair with a score higher than 62 for at least one peptide was classed as A1, and classed as A2 for a score less than 62 (Figure 2.19 A). The class A methylome consisted of 76 modifications on 66 sites, associated with 48

unique proteins. The majority of these methylation sites were novel, since there is a limited annotation of these sites for *Drosophila melanogaster*.

A

Non-histone proteins

Class A1+A2 only	K	R	Total
Modifications	**26**	**50**	**76**
Sites	23	43	66
Peptides	25	42	65
Proteins	21	29	48

Class B only	K	R	Total
Modifications	**91**	**82**	**173**
Sites	91	80	171
Peptides	78	68	159
Proteins	74	62	121

B

Histone proteins

Class A1+A2 only	K	R	Total
Modifications	**9**	**2**	**11**
Sites	9	2	11
Peptides	6	2	8
Proteins	3	1	4

A+B
Class A1: hmSILAC H/L pair detected, Score >62,
Class A2: hmSILAC pair detected, Score <63
Class B: only heavy form of modified peptide detected

C

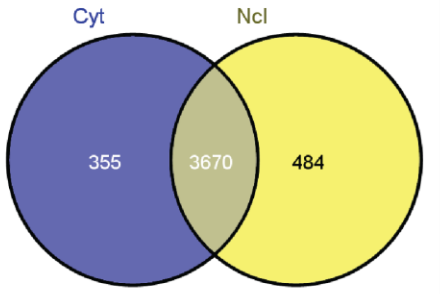

D

GO terms of Class A methylome

Term	P-value
RNA processing	8.3(E-4)
Chromosome organization	2.6(E-3)
RNA splicing	3,7(E-3)
mRNA metabolic process	4.6(E-3)
Cell cycle checkpoint	6.4(E-3)
mRNA processing	1.6(E-2)
Posttranscriptional regulation of gene expression	2.5(E-2)

Figure 2.19: The *Drosophila melanogaster* methylome
L2-4 cells were labeled with heavy ($^{13}CD_3$) and light ($^{12}CD_3$) L-methionine. Methylation sites were analyzed using LC-MS/MS. A confident identification required the identification of sequenced peptides in both the heavy and the light form. **(A)** Numbers of identified methylation sites on non-histone proteins is shown. Identified methylation sites were categorized in class A and class B depending on the identification confidence. **(B)** Identified methylation sites on histone proteins are shown. **(C)** Venn diagram gives total numbers of all identified proteins in the nuclear and cytosolic fraction. Diagram was created with BioVenn (http://cmbi.ru.nl/cdd/biovenn/). **(D)** Gene ontology (GO) term enrichment analysis with the DAVID bioinformatics tool was performed. Table shows significant hits. All analyses were performed by Dr. Michael Bremang.

A third class, class B, consisted of modified peptides that where only detected in the heavy form. This provides some evidence for *in vivo* methylation but represents intermediate confidence identification. The class B methylome consisted of 173 modifications on 171 sites, associated with 121 proteins

(Figure 2.19 A). The new analysis pipeline (currently being developed) aims to find the light and unsequenced identifications of these heavy peptides in the light form to re-classify them into class A.

Since the aim was to investigate methylation sites on non-histone proteins, the protocol for subcellular fractionation ensured that the nuclear fraction was depleted from histone proteins. Still, a few methylation sites could also be identified on histone H3 and H1 with high confidence (Class A1, appendix list) (Figure 2.19 B).

From the analysis of the cytosolic and nuclear proteomes, 4025 and 4154 proteins, respectively, were obtained. Surprisingly, the overlap seemed high (>80%), which signalled an incomplete separation of nuclear and cytosolic proteins (Figure 2.19 C).

In summary, the class A methyl-proteome consisted of 76 modifications on 48 proteins. The majority of these are novel, given the limited methyl-site annotation of *Drosophila melanogaster*. There is, however, a clear enrichment for biological processes (Gene Ontology) which were observed in the HeLa methylome (Bremang et al., 2013) and, as expected, many orthologous proteins (Figure 2.19 D).

3. Discussion

In *Drosophila melanogaster*, the analysis of mutations in modifiers of the position effect variegation and polycomb group genes is a useful tool to study genes that are involved in chromatin structure. The *Suppressor of zeste* 5 gene was isolated in such a screen as a suppressor of PEV and an enhancer of Polycomb (Kalisch and Rasmuson, 1974). Later, it was shown that this gene encodes for S-adenosylmethionine Synthetase, a metabolic enzyme (Larsson et al., 1996). These data suggest that Sam-S is involved in the regulation of chromatin structure. However, this finding had not been followed up. In this work, the molecular function of Sam-S in the context of chromatin was further analyzed in *Drosophila melanogaster* L2-4 cells.

3.1. Nuclear function of Sam-S

3.1.1. Nuclear localization of Sam-S in *Drosophila melanogaster*

S-adenosylmethionine is involved in many biological processes ranging from the regulation of gene expression, methylation of hormones and neurotransmitters and the synthesis of spermidine and spermine (Larsson et al., 1996; Lu, 2000). SAM is synthetized from methionine and adenosine triphosphate in a single reaction by Sam-S (Lu, 2000). This enzyme is present in the cytosol while SAM-metabolizing enzymes are widely distributed throughout the cell. Transfer of SAM to other cell compartments is carried out by specific transporters (Horne et al., 1997). In recent studies, the mammalian homologues, methionine adenosyltransferase I/II/III, were also found in the nucleus (Katoh et al., 2011; Reytor et al., 2009; Xia et al., 2010). MAT II was shown to be involved in gene expression as a transcriptional co-repressor of Maf oncoprotein in mouse cells (Katoh et al., 2011). Other metabolic enzymes like ATP citrate-lyase, acetyl-CoA synthetase and NAD^+ synthase nicotinamide mononucleotide adenylyltransferse-1 were also reported to localize to the nucleus in human cell lines (Wellen et al., 2009; Zhang et al., 2009). Taken together, these data suggest a role for metabolic enzymes in the regulation of gene expression.

In this study, the subcellular localization of Sam-S in *Drosophila melanogaster* was examined by confocal microscopy and subcellular fractionation. Both techniques confirmed the nuclear localization of the enzyme in L2-4 cells (Figure 2.3) which further supports the hypothesis of epigenetic regulation by subcellular localization of cofactor biosynthesis (Meier, 2013). MATs/Sam-S may be recruited to locations where SAM is needed during enhanced DNA and histone methylation and ensure an adequate supply of the methyl donor. In relation to this hypothesis, an interesting *in vitro* observation in our laboratory (by André Hansbauer) was made. When Sam-S-dependent histone methyltransferase

(HMTase) assays were performed (assay includes methionine, ATP, Mg^{2+}, Sam-S, substrate and an appropriate methyltransferase), the activity of the histone methyltransferase Su(var)3-9 was increased compared to HMTase assays where only SAM was added (assay includes SAM, substrate and an appropriate methyltransferase). The enzyme Su(var)3-9 methylates H3K9 and is able to establish all states of methylation, either the mono-, di- and trimethylation (Ebert et al., 2004; Eskeland et al., 2004). While in the SAM-containing HMTase assay only mono- and dimethylation could be observed (see also (Eskeland et al., 2004)), trimethylation could be detected when Sam-S was present together with ATP and methionine (Figure 3.1). It may be that the interaction between Sam-S and Su(var)3-9 increases methylation activity due to conformational changes or a concomitant phenomenon like substrate channeling. The stable SAM concentration could also be the reason for increased enzyme activity. However, further experiments have to be done to confirm this hypothesis.

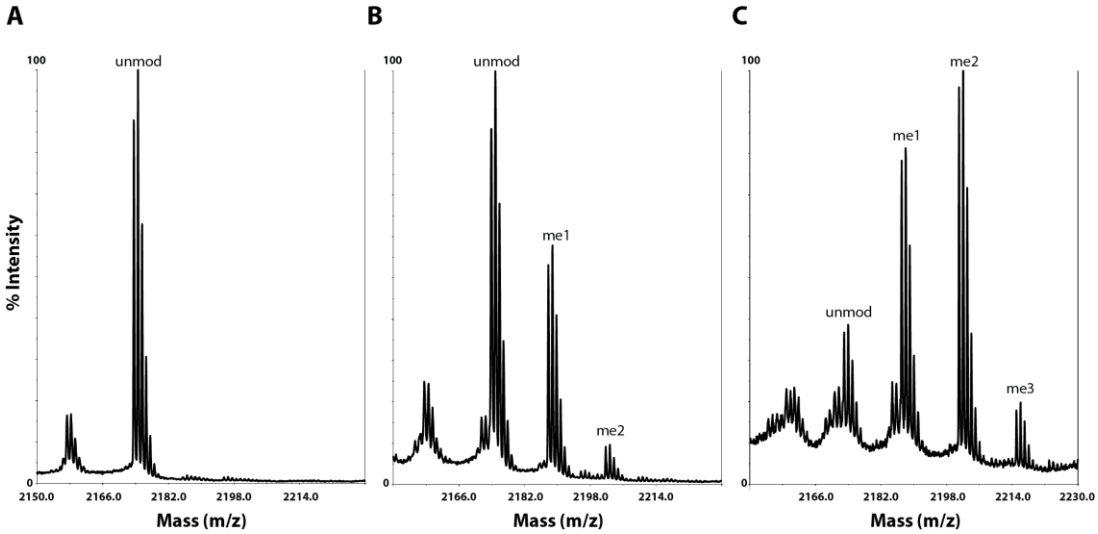

Figure 3.1: Sam-S boosts activity of the methyltransferase Su(var)3-9 *in vitro*
In vitro histone methyltransferase (HMT) assays were performed (by André Hansbauer) with the H3K9 methyltransferase Su(var)3-9. Analyses were done by MALDI-TOF, H3 peptide (amino acid 1–20) was used as substrate. **(A)** As a negative control, the assay was performed without Su(var)3-9. **(B)** HMTase assay was performed using SAM as a methyl donor. Mono- and dimethylation could be observed. **(C)** Increased activity of Su(var)3-9 was observed in a Sam-S-dependent HMT assay using methionine, ATP, Mg^{2+} and Sam-S as the source of methyl groups. Mono-, di- and trimethylation could be observed.

Furthermore, due to its small size, SAM is able to diffuse across the nuclear pore (Kramer et al., 2007) but there is the possibility that its high instability requires *in situ* synthesis for methylation reactions for

a discrete transcriptional outcome. However, to correlate Sam-S occupancy with distinct histone methylation levels, genomic analyses will be required to understand if Sam-S localizes to specific loci or if it is distributed equally throughout the genome.

3.1.2. SAM limitation and its effect on cell proliferation

A recent study in murine pre-B-cells showed a cell cycle arrest in G1-phase upon limiting levels of SAM (Lin et al., 2014). These low SAM levels were accompanied by activation of the mitogen-activated protein kinase 38 (MAPK38) and subsequent phosphorylation of its downstream MAPK-activated protein kinase-2 (MK2). Therefore, SAM limitation could be linked to the p38-MK2 pathway which has been proposed earlier as a third cell cycle checkpoint module following DNA damage (Reinhardt and Yaffe, 2009). In addition, a metabolic cell cycle checkpoint that responds to limiting levels of SAM was demonstrated.

In this study, a link between normal cell growth and low SAM levels could be observed in *Drosophila* L2-4 cells. Upon Sam-S knockdown and decreasing SAM levels, cells did not proliferate as fast as controls and total cell number decreased after four days by 30% (Figure 2.5 D). Recently, the same effect on cell proliferation was reported in *Drosophila* S2 cells after Sam-S knockdown (Liu et al., 2016). In these experiments, the cell number decreased about 20%. Alterations in different pathways could lead to this decrease in cell number. Possibly the decrease in histone methylation for some genes could directly affect expression of proteins involved in pathways important for cell proliferation. Interestingly, genes involved in glucose metabolic pathways, protein phosphorylation pathways and cellular carbohydrate catabolic processes were indeed found to be downregulated (Figure 2.7 B) in L2-4 cells upon *Sam-S* RNAi. However, analysis of histone methylation levels at single gene loci will be required to understand if this is a direct effect. Another explanation for the decreased cell proliferation could be an effect of apoptosis. However, few dead cells were observed in the cell growth assay.

In contrast to murine pre-B-cells, neither an effect on cell cycle progression was observed nor could a cell cycle arrest be detected in L2-4 cells (Figure 2.5 E). It is possible that *Drosophila* L2-4 cells do not have a comparable metabolic checkpoint and therefore react to limiting levels of metabolite concentration in decreased cell proliferation. One reason may be that L2-4 cells are less sensitive to low SAM concentration than mouse cells and a putative checkpoint is not triggered at the conditions that were used in this study. The underlying mechanism for how metabolite concentration is monitored and connected to cell proliferation, however, remains elusive.

3.1.3. Sam-S and its interacting proteins in the nucleus

The mammalian homologue methionine adenosyltransferases IIα (MAT IIα) was shown to interact with chromatin-related proteins including the PRC1complex, the NuRD and Swi/Snf complexes as well as the methyltransferases G9a, Ehmt1 and ALL1/KMT2A (Katoh et al., 2011). In addition, work by Kera et al. identified the H3K9 methyltransferases SETDB1 and Suv39h1 as interacting partners (Kera et al., 2013). MAT IIβ was shown to interact with proteins including MAT IIα, DEAD box polypeptide 1, pre-mRNA cleavage factor 1 and HuR, an mRNA binding protein, in a human colon cancer cell line (Xia et al., 2010).

In *Drosophila melanogaster*, Sam-S was included in a large-scale analysis which was performed by the Artavanis-Tsakonas lab (Guruharsha et al., 2011). They used co-affinity purification coupled to mass spectrometry analysis to examine protein associations of nearly 5000 FLAG-HA-tagged *Drosophila melanogaster* proteins. Stringent statistical analysis led to the generation of a *Drosophila* Protein interaction Map (DPiM) encompassing 556 protein complexes. They identified 194 Sam-S interacting proteins. The co-immunoprecipitation of Sam-S presented in this study led to the identification of 227 potential interaction partners (Figure 2.4) of which 15 were also enriched in the DPiM. The limited overlap could result from different reasons: in contrast to the L2-4 cell line, Guruharsha et al. used a different *Drosophila* cell line, namely the S2R+ line. Although both cell lines derive from the original *Drosophila* Schneider S2 cell line, they most likely have slightly different genomic and proteomic patterns (Cherbas and Gong, 2014; Guruharsha et al., 2011). While Guruharsha et al. used whole cell extract from transiently transfected cells with induced expression of a FLAG-HA-tagged version of Sam-S (Guruharsha et al., 2011), the co-IP presented here was performed using a nuclear extract and an antibody against the endogenous Sam-S. Furthermore, the technical equipment and different software tools for data analysis can cause additional variance between the two Sam-S co-IPs. Therefore, the interaction partners identified in this study were considered as potential candidates and are discussed further.

The purification of Sam-S from a nuclear extract from L2-4 cells provided some evidence for its function in chromatin biology since potential interactors had known transcriptional and epigenetic function. These included the transcription initiation factors Taf1-5, 7-9 and 11-13, the dosage compensation complex and polycomb group proteins. Tafs are known to regulate transcription by interacting with activators and histone modifications, to bind to promoters and act as a scaffold for the assembly of RNA Polymerase II and other proteins like Tbp (Malkowska et al., 2013). The DCC is composed of male-specific-lethal proteins of which two proteins were identified in this co-IP, namely

msl-1 and msl-3. The DCC is responsible for the upregulation of X-linked genes from the male X chromosome (Maenner et al., 2012). On the one hand, these observations suggest a role for Sam-S in active transcription while on the other hand, proteins were identified with known repressive function like the PcG proteins (Simon and Kingston, 2009) and Sin3a (Silverstein and Ekwall, 2005). Consistent with this result, the mammalian homologues of these proteins were also identified in the MAT IIα immunoprecipitation (Katoh et al., 2011). Furthermore, Kdm4a was identified as a potential interacting protein which is also reported to be involved in transcriptional repression of genes (Klose et al., 2006; Lin et al., 2008). Kdm4a is, however, also reported to be involved in transcriptional activation of genes required for lifespan control and male-specific sex determination and courtship behavior (Lorbeck et al., 2010).

In contrast to the identified MAT IIα interactors (Katoh et al., 2011; Kera et al., 2013), no methyltransferase was identified in the present study. One explanation is that the association and disassociation of Sam-S and methyltransferases is transient, consequently causing a dynamic regulation of histone methylation at specific loci. This is further supported by Katoh et al. since they found G9a, Ehmt1 and ALL1/KMT2A only in their single-step purification but not in a further purified complex by western blot analyses (Katoh et al., 2011).

Taken together, these data support Sam-S involvement not only in transcriptional repression and but also in activation. However, further studies will be required to understand how Sam-S and its interaction with other nuclear and chromatin-related proteins are regulated in the context of single genes.

3.1.4. Histone methylation is decreased upon SAM depletion and results in an altered gene expression profile

Methylation can affect diverse biological processes including the regulation of gene expression which is controlled by the methylation of DNA and histone proteins. As the level of methyl donor SAM is important for histone methylation (Brosnan and Brosnan, 2006), it does not come as a surprise that Sam-S may be involved in the regulation of histone methylation by controlling SAM levels. Interestingly, reduction of Sam-S affected different histone marks in a different way (Figure 2.6). This variability may be the result of the different SAM binding affinities of methyltransferases accompanied by their different sensitivity to SAM levels (Katada et al., 2012). Another possibility could be the presence of different methyltransferases at specific chromatin regions which results in different histone methylation levels. In L2-4 cells, reduction of Sam-S led to decreased global histone

methylation levels with H3K4me3, H3K27me2K36me1, H4K20me3 and H2BP1me2 being most strongly affected (Figure 2.6). Given that, on the one hand, H3K4me3 is tightly associated with active genes (Barski et al., 2007) while on the other hand, H4K20me3 is associated with repression of transcription (Wang et al., 2008) it is most likely that the gene expression profile was altered. As shown by microarray analysis, the expression levels of 6671 genes were altered, 1734 genes were changed by >1.5-fold of which 676 probes showed a down- and 1058 probes an upregulation, respectively (Figure 2.7 A). A similar experiment was performed in iMEFs cells where *MAT2α* was transiently knocked down (Kera et al., 2013). There, 1597 genes were altered by >2-fold of which 821 and 776 probes showed a down- and upregulation, respectively. When a gene ontology analysis was performed, the affected genes were not enriched for specific GO terms. In contrast, the group of downregulated genes presented in this study was associated with GO terms such as glucose metabolic process, protein amino acid phosphorylation and cellular carbohydrate catabolic processes (Figure 2.7 B). This is possibly the reason – or consequence – for the decreased cell proliferation discussed previously (Figure 2.5 D; see chapter 3.1.2.).

The observed decrease in H3K4me3 levels is consistent with recent studies where H3K4me3 was reported to be globally reduced upon Sam-S (Liu et al., 2016) and MAT II (Kera et al., 2013) knockdown. Both studies showed different gene-specific H3K4me3 levels suggesting that Sam-S/MAT II contributes locally and globally to histone methylation levels. Upon restriction of methionine, similar to this study, H3K4me3 also exhibited the largest change among other histone methylation marks such as H3K9me3 and H3K27me3 in HCT116 cells (Mentch et al., 2015). This study also showed that this effect is dynamic and reversible. In contrast to the present study, quantitative western blot analyses were used to investigate histone methylation levels in the other studies and therefore, the analyses were restricted to a few modifications according to antibody limitations. Here, the advantage of mass spectrometry analysis is that more modifications can be analyzed at the same time and even a combination of modifications on the same petide can be investigated (Feller et al., 2015).

Consistent with the decrease of H3K4me3, the expression levels of the H3K4 methyltransferases *trx* and *trr* were significantly reduced (Figures 2.6 D and 2.8 B). The same observation was made for H2BP1me2 and the responsible MT Ntmt (Figures 2.6 B and 2.8 B). Villar-Garea et al. showed that an increased level of H2B methylation occurs when cells reached a high density (Villar-Garea et al., 2012). The complete loss of H2BP1me2 after Sam-S depletion may therefore be the effect of reduced cell proliferation accompanied by decreased cell density in tissue culture cells. However, this hypothesis needs further study.

Retrotransposon silencing is reported to be controlled by the methyltransferase Mt2 and H4K20me3 (Phalke et al., 2009; Schotta et al., 2004). Upon *Sam-S* knockdown, the expression level of the H4K20 methyltransferase *Hmt4-20* was significantly reduced (Figure 2.8 B). This reduction results in a decreased level of H4K20me3 (Figure 2.6 C). Therefore, the expression levels of several transposable elements were monitored upon *Sam-S* knockdown. The knockdown of *Sam-S* resulted in a bidirectional misregulation of TEs. As expected, an increase of expression level was observed for the TEs *Springer, 297, Copia* and *gypsy*. The TEs *ninja, blood* and *mdg1* showed reduced expression levels (Figure 2.9 B). This could be explained by secondary effects of Sam-S including reduction or silencing of a TE transcription factor which could be due to the observed upregulation of the methyltransferase *Mt2* upon *Sam-S* knockdown.

The mRNA and protein levels of *AGO2* were strongly affected in the *Sam-S* knockdown and *vice versa* (Figure 2.9 B and C). Whether this mutual dependency is a direct or indirect effect is still unknown. Since *AGO2* knockdown shows an upregulation of almost all TEs, it is most likely an effect on the level of transcription or transcript (mRNA) stability, e.g. interaction with transcription factors or RNA degrading machinery. Supporting this idea, recent work in human T47D cells did not identify the mammalian homologue MAT as a potential interactor when AGO2 immunoprecipitation was performed (Kalantari et al., 2016).

In contrast to methylation, all acetylation marks were enriched on H3 and H4 residues compared to controls (Figure 2.6 C and D). Kera et al. also found H3K9 acetylation increased at the COX-2 promoter region (Kera et al., 2013). It is possible that the reduction of methylation allows the acetylation mark to be placed at the same residue. Alternatively, histone deacetylases may transiently interact with Sam-S and its recruitment may be lost upon Sam-S knockdown.

RNA methylation also plays an important role in the regulation of gene expression. The methylation status of tRNAs and rRNAs, for instance, has an impact on structural and metabolic stabilization on the one hand, and is important for the efficiency of mRNA decoding on the other hand (Motorin and Helm, 2011). Interestingly, in this study, the GO analysis of Sam-S interactors showed significant enrichment of proteins involved in the regulation of RNA metabolic processes (Figure 2.4). Furthermore, the expression levels of tRNA and mRNA methyltransferases were significantly reduced. The effect of SAM depletion on RNA methylation, however, was not investigated and could be a part of future studies.

3.2. LC-MS/MS as a sensitive method to quantify SAM and SAH in *Drosophila* cells

SAM and SAH are important metabolites in one-carbon metabolism. SAM is the major methyl donor for transmethylation reactions in the cell and is involved in many biological processes (Fontecave et al., 2004). The ratio of SAM/SAH is crucial for the regulation of methylation reactions and this ratio is used as an indicator for methylation potential (Caudill et al., 2001). In order to see how the SAM/SAH ratio is changed upon Sam-S knockdown, a highly sensitive method for a targeted absolute quantitation of SAM and SAH was established. Various methods for the determination of SAM and SAH have been published to date. Amongst others, sensitive LC-MS/MS methods are described but require time-consuming sample preparation (Gellekink et al., 2005; Struys et al., 2000). More recently, sensitive LC-MS/MS methods were developed with rapid and simple sample preparation (Burren et al., 2006; Krijt et al., 2009). The limits of detection of all four methods were in the nanomolar range. A more recent study described the development of a LC-MS/MS method which enables the quantitation of the SAM cycle metabolites L-met, SAM, SAH and Hcy (Gardner et al., 2013).

In this study, the LC-MS/MS method from Burren et al. was successfully established (Burren et al., 2006) in collaboration with the Metabolomics platform of the Genomic Analysis Center at the Helmholtz Zentrum, München (chapter 4.2.6.4.). This method enabled the specific and simultaneous quantitation of SAM and SAH in *Drosophila* tissue culture cells. Parameters including sensitivity, linearity and precision were validated and comparable to the method reported by Burren et. al. (Burren et al., 2006). The obtained sensitivity was also in the nanomolar range (8.0 nmol/l and 0.2 nmol/l for SAM and SAH, respectively), calibration curves for both metabolites were linear throughout a concentration range (0.1–7.5 µM and 0.01–1.0 µM for SAM and SAH, respectively) sufficient for the analysis and intra-assay precision ranged from 3.45% to 7.35% for SAM and 1.61% to 8.00% for SAH, respectively (see chapter 2.5.).

The analysis of absolute SAM and SAH concentrations revealed an altered SAM/SAH ratio upon *Sam-S* knockdown. It changed dramatically from a ratio of 50.3 (+/- 11.1) in the control to a ratio of 0.6 (+/- 0.7) in the knockdown condition (Figure 2.5 C). While SAM levels were strongly reduced (log_2 fold change: -4.3), SAH levels were only slightly increased (log_2 fold change: 2.0). Since SAH is still metabolized by the enzyme Ahcy, its levels are not changed as much as SAM levels. Interestingly, unchanged SAM levels were reported upon *Sam-S* RNAi in *Drosophila* day-5 male flies in the fat body (Obata and Miura, 2015). SAM level was measured relative to the control. In that study, *Sam-S* RNAi led to a reduction of Gnmt protein, a predominant regulator of SAM levels. Unchanged SAM levels were

explained by a possible transcriptional or posttranscriptional regulation of Gnmt expression for maintaining SAM levels (Obata and Miura, 2015).

In sum, in this study, the use of a sensitive LC-MS/MS method enabled the precise and simultaneous quantitation of nanomole quantities of SAM and SAH in tissue culture cells and could potentially be applied to any tissue.

3.3. Improvements and limitations of Capture Compound™ Mass Spectrometry

In order to correlate changes in metabolite concentration to enzyme activity, Capture Compound™ Mass Spectrometry was considered as an appropriate approach. This technology enables a functional isolation of subproteomes and is based on trifunctional affinity probes (Koster et al., 2007). For establishment of this novel methodology, initial steps were performed in an earlier study (Vollmer S., Diploma thesis, 2008) where three MTs were identified when capture experiments were performed following manufacturer's instructions. To establish CCMS and improve the number of captured methyltransferases, a few changes were made in this work compared to the standard protocol.

First, the SAH-CC was used with two different photo-reactive cross-linkers, fluorinated aryl azide and benzophenone, respectively (Figure 2.13 A and B). Each cross-linker has different advantages. Benzophenones are chemically stable due to their inertness to solvents. Furthermore, they are activated by a long wavelength at 350 nm and thereby lower the risk of protein damage (Smith and Collins, 2015). The disadvantages are the longer irradiation time (90 min) and the size of the benzophenone group. The long irradiation time can increase non-specific reactions while the rather bulky size can affect the interaction between the SAH-CC and the target protein. This steric hindrance can also lead to increased non-specific capture. In contrast, fluorinated aryl azides are smaller in size and have a shorter irradiation time (5 min). The shorter wavelength required for activation at 315 nm can cause damage to proteins. Another disadvantage is that azides can be reduced to amines by thiols in solvents and buffers (Staros et al., 1978).

Second, given that methyltransferases have a wide range of binding affinities to SAM and SAH, respectively (Brown et al., 2014; Copeland et al., 2009; Horiuchi et al., 2013; Patnaik et al., 2004; Xiao et al., 2003), the concentration of SAH-CC was increased to 45 µM compared to 5 µM in the manufacturer's instructions (Dalhoff et al., 2010) in order to gain binding saturation and a higher number of captured MTs.

Third, the antiviral compound 3-deazaneplanocin (DZNep) was added to each reaction. DZNep inhibits the enzyme adenosylhomocysteinase (Chiang, 1998) and thereby prevents SAH-CC from being

metabolized. Ahcy13 was therefore only slightly enriched in the capture experiment with SAH-CC_{bp} as an SAH-binder (data not shown).

After CCMS was performed with the optimized protocol, 79 methyltransferases were identified in total (Figure 2.15) from 170 (putative) MTs annotated in the Pfam and the Superfamily databases. 130 MTs are expressed in *Drosophila* Schneider S2 cells according to Flybase with low expression levels (http://flybase.org; RNA-Seq profile search). L2-4 cells derive from the original *Drosophila* Schneider S2 cell line, and may have slightly different genomic and proteomic patterns (Cherbas and Gong, 2014). In this work, MTs were captured from a nuclear extract of L2-4 cells. Capture experiments from whole cell extracts will enable the identification of cytoplasmic MTs as well. Using only nuclear extracts also explains why the number of captured MTs and expressed MTs differ. For instance, the putative DNA/tRNA methyltransferase Mt2 is reported to be mostly cytoplasmic (Krauss and Reuter, 2011) and, consistent with that, was not identified in the capture experiments. Other nuclear proteins like the histone methyltransferase Su(var)3-9 and trx are expressed in S2 cells, however, were not captured which is most likely due to limiting protein amounts in the nucleus. Most MTs were enriched and identified in both capture experiments while a few MTs could only be captured with either SAH-CC_{aa} or SAH-CC_{bp} (Figure 2.15). This difference in binding behavior is possibly due to steric hindrance caused by the different sizes of the photo-reactive cross-linkers with regard to the active site of the enzymes. Therefore, using both SAH-CCs is suggested for further studies.

In addition to the expected identification of MT targets a number of specifically captured proteins could be identified which, however, where not annotated as SAM/SAH-binding proteins. The majority of these enriched non-target proteins were ATP and purine nucleotide binding proteins which can be explained by the structural similarities between SAH and ATP. For instance, Sam-S, an ATP-binding protein, was enriched in the capture experiment with SAH-CC_{bp}.

In summary, even though CCMS was improved in this work, it will need further optimization with respect to quantitative analyses and background reduction. Due to current technical limitations, CCMS was not used in a knockdown experiment in this work to test changes in enzyme activity during SAM depletion. This is, however, a suggested application for CCMS in the future.

3.4. Methylome

Recent studies showed the emerging importance of methylation of non-histone proteins. It is involved in cellular signal transduction like WNT, MAPK and JAK-STAT signaling pathways (Biggar and Li, 2015). Non-histone methylation can also lead to changes in activity like automethylation of PRMT 8 which

regulates its activity by impeding SAM sensitivity (Dillon et al., 2013). Since little is known about methylation sites in *Drosophila melanogaster* beyond histones, an hmSILAC approach was performed in this work. The class A methylome consisted of 76 modifications on 66 sites, associated with 48 unique proteins (Figure 2.19 A). The majority of these methylation sites were novel, since there is a limited annotation of these sites in the context of *Drosophila melanogaster*. The ratio of lysine/arginine modifications (1:2) was less than what was observed in the HeLa methylome (1:4) (Bremang et al., 2013) which may reflect differences between organisms. The class B methylome consisted of 173 modifications on 171 sites, associated with 121 proteins (Figure 2.19 A). In contrast to class A, class B consisted of modified peptides that were only detected in the heavy form which represents an intermediate confidence for identification. Still, it provides some evidence for *in vivo* methylation. A new analysis pipeline (currently being developed) aims to find light and unsequenced identifications of these heavy peptides to re-classify them. In a similar study, Bremang et al. identified 501 different methylation types on 397 distinct lysine and arginine sites associated with 139 unique proteins in HeLaS3 cells with the same method (Bremang et al., 2013). Due to limitations in protein amount of the cytosolic and nuclear fraction, it was not possible to perform an immuno-affinity enrichment of methylated proteins using antibodies which recognize methyl-K or methyl-R. Including this step in further experiments will increase the identification of methylation sites. There was, however, a clear enrichment of biological processes (GO terms) that were also observed in the HeLa methylome and many orthologous proteins.

Lysine and arginine methylation on histone and non-histone proteins has emerged as an important modification in a wide range of cellular functions. Deciphering the methylome and determining the function of these modifications will be a crucial topic of future research. Taken together, new methylation sites in *Drosophila melanogaster* were identified and further studies will be needed to increase the identification of methylated proteins.

4. Materials and Methods

4.1. Materials

4.1.1. Cell lines

Name	Description
Drosophila Schneider L2-4 cells	Clonal isolate from *Drosophila* Schneider S2 cells (Schneider, 1972); received from Patrick Heun
Sf21 cells	Cells developed from ovaries of the fall armyworm, *Spodoptera frugiperda* (Vaughn et al., 1977)
E.coli strain	DH5α (New England Biolabs, #C2987) genotype: *fhuA2Δ(argF-lacZ)U169 phoA glnV44 ϕ80 Δ(lacZ)M15 gyrA96 recA1 relA1 endA1 thi-1 hsdR17*

4.1.2. Plasmids

Plasmid	Insert	Application
pMT	FLAG-HA-Sam-S (N-terminal)	Overexpression of Sam-S in L2-4 cells ($CuSO_4$ inducible; Hygromycin resistance) drived from Thomae et al., 2013
pMK33-CFH-BD	FLAG-HA-Sam-S (C-terminal)	Cloning of Sam-S, bought from *Drosophila* Genomics Resource Center (DGRC)
pFastBac 1 pFastBac HT B pFastBac HT B pVL1393 (Martinez-Balbas et al., 1998)	FLAG-E(z) his-Su(z)12 HA-esc myc-p55	Recombinant expression of PRC2 with the baculovirus system

4.1.3. Recombinant enzymes

Name	Description
Su(var)3-9 Δ213	Deletion mutant (amino acids 1–213 are missing; (Eskeland et al., 2004)
Ntmt	Bacterial expression and purification described in Villar-Garea et al., 2012
PRC2	Expressed and purified as described in chapter 4.2.4.5.

4.1.4. Enzymes

Name	Company
NotI	New England Biolabs
Phusion® High-fidelity DNA polymerase	New England Biolabs
T4 DNA ligase	New England Biolabs
Taq Polymerase	VWR
Trypsin	Promega
XbaI	New England Biolabs

4.1.5. Oligonucleotides

All oligonucleotides were ordered from Sigma Aldrich and dissolved in water to reach a stock concentration of 100 µM. Primer design:

Name	Sequence 5'–3'
	Cloning of Sam-S
Su(z)5 fw Not1	TTTGCGGCCGCCCGCAAAAGACAAACGGACATAGC
Su(z)5 rev Xba1	TTTTCTAGATTAGTTGTCAATCTCCAGAGGCTTGGC

	RNAi: TTAATACGACTCACTATAGGGAGA… (T7-promotor)
Sam-S RNAi for	…TGCCAACTCTTATGGGCTTT
Sam-S RNAi rev	…TCTGCGCATACCGGTAAAAT
E(z) for	…ATCAAGGAGGCGTGGATA
E(z) rev	…TGATTTCGCCAACGTCTC
AGO2 for	…AAGATTATGAACTTGCTGCAATACTTCCAG
AGO2 rev	…TGCGTCAAAATTCCATGCTGCAG

	qPCR – proteins
Tub97E for	GAGCAAGAACAGCAGCTACTTTGT
Tub97E rev	CACCTTGACGTTGTTGGGAAT
Sam-S for	ACTCCTCCAAGGGTTTCGAT
Sam-S rev	GATCTCAGGCGATTGTTGGT
AhCy for	GGAGTACATGTGGTGCATCG
AhCy rev	TACTGGGGGAACTTTTCGTG
CG10621 for	ACGCTATCTCACCGAGTGCT
CG10621 rev	ATGGAGGCAATGATCAAAGG
AGO2 for	AGCTGAATGACTTCGGGAAC
AGO2 rev	TAGTGTCTAGGCTGCGTTCG
Hmt4-20 for	GACAAGATCGAATGCCTGGT
Hmt4-20 rev	TCATTTTTGCCAGAGTGCAG
PrSet7 for	CACAATGATGGCACACAACA
PrSet7 rev	TTCTCAATGGTGCGAGTTTG
Suv3-9 for	AGCCAGCTTCGTCTTCCAT
Suv3-9 rev	GCCGCTACTATTGCTTGGAC
S for	TCAAGCCCAGTCCTTCAAAC
S rev	GTTCACCTCGTCCACATCCT
Trr for	CGTCCATTCTCATGCACATC
Trr rev	TGATCTGTAGCCCCGAAAAC
Trx for	ACACCCTCAAACGACAAAGG
Trx rev	CAAAGGTAGCCAAAGGTTGC
Ntmt for	CAGGGATCGAATGTGTTCCT

Ntmt rev	GAGTCACCCGACCAATGC
Art8 for	GCCGTAGAAGCATCCAATGT
Art8 rev	ATTCCTCAACACGCGACTG
Mt2 for	AGGGACACGGAAGACAAGC
Mt2 rev	TCTCGAAACCCTTGACGTTT
CG6379 for	ATGAAAGCAACCAGGACTCG
CG6379 rev	TCTGACCTTCCACCGAAAAG
CG33468 for	GCGACTGGAAAGGTATTTGC
CG33468 rev	CACTTCGGTTGGAATGTACTCA
CG11837 for	GTGATCGCCTGTGAGATTGA
CG11837 rev	AGCTCCGCCTTTAGGAAGTC

qPCR – transposons

(Ghildiyal et al., 2008; Klenov et al., 2007; Padeken et al., 2013)

ninja for	GCCATCACCGACTACCATT
ninja rev	TCACCCCATCCGACGCTCTT
blood for	TGCCACAGTACCTGATTTCG
blood rev	GATTCGCCTTTTACGTTTGC
roo for	CGTCTGCAATGTACTGGCTCT
roo rev	CGGCACTCCACTAACTTCTCC
mdg1 for	CACATGTTCTCATTCCCAACC
mdg1 rev	TTCGCTTTTTATATTTGCGCTAC
Springer for	CCATAACACCAGGGGCA
Springer rev	CGAGTGCTGGTCTGTCA
297 for	AAAGGGCGCTCATACAAATG
297 rev	TGTGCACATAAAATGGTTCG
Copia for	GCATGAGAGGTTTGGCCATATAAGC
Copia rev	GGCCCACAGACATCTGAGTGTACTACA
gypsy for	CTTCACGTTCTGCGAGCGGTCT
gypsy rev	CGCTCGAAGGTTACCAGGTAGGTTC

4.1.6. Antibodies

Primary antibodies (Species)	Supplier	Application and Dilution
α-FLAG M2 (mouse)	Sigma	Western blot 1:1000 Immunofluorescence 1:200
α-HA, monoclonal (rat)	Dr. E. Kremmer	Immunofluorescence 1:50
α-Sam-S 4A2, monoclonal (mouse)	Dr. E. Kremmer	Western blot 1:20 Immunofluorescence 1:5
α-Sam-S 4A7, monoclonal (rat)	Dr. E. Kremmer	Western blot 1:20 Immunofluorescence 1:5
α-Su(var)3-9 (rabbit)	Prof. G. Reuter	Western blot 1:1000
α-Ntmt, monoclonal (rat) (Villar-Garea et al., 2012)	Dr. E. Kremmer	Western blot 1:20
α-E(z) 7E9, monoclonal (mouse)	Dr. E. Kremmer	Western blot 1:20
α-Ago2 (rat)	abcam	Western blot 1:250
α-H3 (rabbit)	abcam	Western blot 1:2000
α-tubulin (mouse)	Sigma	Western blot 1:3000
Streptavidin-HRP	Roche	Western blot 1:2000

secondary antibodies (Species)	Supplier	Application and Dilution
α-mouse/rat/rabbit (IRDye® 680/800CW)	Li-COR	Western blot 1:10000
α-mouse/rat/rabbit HRP-coupled	VWR	Western blot 1:5000
α-mouse Rhodamine-Red-X (ultra-high pre-absorbed) (Especially for very critical co-stainings with α-rat ab!)	Jackson Immuno Research	Immunofluorescence 1:200
α-rat Alexa488	Jackson Immuno Research	Immunofluorescence 1:200
α-rat Cy3 (pre-absorbed)	Jackson Immuno Research	Immunofluorescence 1:500

4.1.7. Antibiotics

Name	Company	Stock concentration
Ampicillin	Roth	100 mg/ml (dilution 1:1000)
Hygromycin B	Invitrogen	50 mg/ml
Penicillin/Streptomycin	PAA	10 mg/ml Streptomycin; 10000 Units/ml Penicillin G (dilution 1:100)
Gentamicin	PAA	10 mg/ml (dilution 1:100)

4.1.8. Inhibitors

Name	Company	Stock concentration
Aprotinin	Genaxxon	1 mg/ml in H_2O
DZNep	Inhibits S-Adenosylhomocysteine hydrolase (Glazer et al., 1986)	100 mM in H_2O
Leupeptin	Genaxxon	1 mg/ml in H_2O
Pepstatin A	Genaxxon	0.7 mg/ml in EtOH
PMSF	Sigma	34 mg/ml in isopropanol

All protease inhibitors were diluted 1:1000

4.1.9. Capture Compounds™

Capture Compound™	Company	Stock concentration
SAH-CC_{aa}; Fluorinated aryl azide (aa)	Caprotec	100 µM
SAH-CC_{bp}; Benzophenone (bp)	Caprotec	190 µM

4.1.10. Purification beads

Name	Description
Dynabeads® MyOne™ Streptavidin C1 (life technologies)	Magnetic beads (diameter: 1 µm) Binding specificity: biotin labeled proteins/DNA binding capacity: ~ 20 µg of biotinylated IgG/ mg of Dynabeads (diameter: 1 µm)
ANTI-FLAG® M2 affinity gel (Sigma)	Agarose beads Binding specificity: FLAG octapeptide (DTKDDDDK) binding capacity: ≥ 0.6mg/ml

4.1.11. Chemicals

Reagent	Company
1 kb DNA ladder	New England Biolabs
Acetonitrile	Roth
Agarose	Bio&Sell
Ambion® MEGAscript® RNAi kit	Life Technologies
Ammonium acetate	Merck
Ammonium bicarbonate	Roth
Bovine serum albumin	Sigma
Coomassie Brilliant Blue G250	Serva
$CuSO_4$	Sigma
DAPI	Life Technologies
Dimethyl sulfoxide	Sigma
Dithiothreitol	Roth
Fetal calf serum	Sigma
Fetal calf serum, dialyzed	Sigma
Formaldehyde methanol-free	VWR
Formic acid	Sigma
Glycine	VWR

HEPES	VWR
Heptafluorobutyric acid	Sigma
Image-iT FX signal enhancer	Invitrogen
$^{13}CD_3$-methionine	Sigma
Normal goat serum	Dianova
Nitrocellulose membrane	GE Healthcare
Propionic anhydride	VWR
Protein assay Dye Reagent Concentrate	Biorad
S-adenosylhomocysteine	Sigma
S-adenosylmethionine	Sigma
[$^2H_3$]- S-adenosylmethionine	CDN Isotopes
Spike tides	JPT technologies

4.1.12. Equipment

Device	**Company**
Axiovert 200M epifluorescence microscope	Zeiss
Bioanalyzer	Agilent Technologies
BIO-LINK™ UV-crosslinker	Peqlab
CaproBox®	Caprotec
Casy® cell counter	OMNI Life Science
Digital Sonifier	Branson
BD FACSCanto™ II	BD Biosciences
Geldocument system G:Box	Syngene
LightCycler® system	Roche
LTQ Orbitrap XLTM	Thermo Fisher Scientific
Nanodrop	Peqlab
Odyssey® Imager	Li-Cor Biosciences
TCS SP5 II confocal microscope	Leica
TripleTOF 6600 QTOF Mass Spectrometer	Sciex
Voyager-DETM STR Workstation (MALDI-TOF)	Applied Biosystems

4.2. Methods

4.2.1. Tissue culture

4.2.1.1. Cultivation and passaging of cells

Drosophila Schneider L2-4 cells were cultivated in Schneider's *Drosophila* medium (GIBCO) supplemented with 10% fetal calf serum (FCS) and Pen/Strep (100 U/ml Pen G; 0.1 mg/ml Strep) at 26°C. They were grown in culturing flasks (Greiner) and diluted every 3–4 days to 1.5–2*10^6 cells/ml.

Sf21 cells were cultivated in Sf-900-II medium (Invitrogen) supplemented with 10% FCS and gentamycin (0.1 mg/ml) at 27°C. They were grown in shaker flasks (Cellspin, Integra Bioscience) and diluted every 2–3 days to 1–1.2*10^6 cells/ml.

Cells were counted using the Casy® cell counter. 50 µl of cell suspension was diluted in 5 ml of Casy® solution and measured with the appropriate settings. The resulting concentration was an average of three measurements.

4.2.1.2. Preparation of frozen cell stocks

L2-4 cells from a medium cell culture flask (75 cm^2) with ~80% confluence were harvested and centrifuged at 300x g for 4 min at 4°C. 1.5 ml freezing medium was added to the cell pellet, cells were carefully resuspended and 0.5-ml stocks were aliquoted into cryovials. Cells were frozen slowly and then put at -20°C for 30 min, followed by over night incubation at -80°C before they were stored in liquid nitrogen. Frozen cell stocks were thawed rapidly in hand and 0.5 ml cells were diluted in 10 ml fresh medium in a culturing flask (25 cm^2). After 15–30 min, when most cells were settled, the medium was renewed.

Freezing medium

60% heat inactivated FCS
30% Schneider Media (GIBCO)
10% DMSO

Heat inactivation was done at 55°C for 10 min.

4.2.1.3. Generation of stable cell lines

L2-4 cells were split the day before transfection and $2*10^6$ cells were seeded. To generate a cell line that stably expresses Sam-S, the X-tremeGENE HP DNA Transfection Reagent was used according to the manufacturer's instructions (Roche).

For selection of transfected cells 150 µg/ml hygromycin B was added. Expression of the Sam-S transgene was induced 24 h before cells were harvested by adding 0.25 µM $CuSO_4$.

4.2.1.4. Knockdown of Sam-S in *Drosophila* Schneider L2-4 cells

Sam-S was knocked down by dsRNA as described in Worby et al. (Worby et al., 2001). A sequence in the gene region of the enzyme was flanked by T7 promotor sites and amplified by PCR. The PCR product was then used for *in vitro* transcription (Ambion MEGAscript T7 kit) to produce dsRNA according to the manufacturer's instructions. $1*10^6$ cells were seeded in 1 ml of serum-free medium and treated with 10 µg dsRNA for 1 h. After this incubation, 2 ml serum-containing medium was added. Knockdown efficiency was tested after five days by qPCR and western blot using the Sam-S antibody (Figure 2.5 A and B).

4.2.1.5. Preparation of whole cell extract

Typically, $5–10*10^6$ L2-4 cells were harvested and washed once with 1x PBS. The cell pellet was resuspended in 1x RIPA buffer, vortexed for 10 s and put on ice for 10 min. This step was repeated three times. Samples were then centrifuged for 30 min at 18000x g at 4°C and the supernatant was used as whole cell extract (also RIPA extract) for further applications.

RIPA buffer	**PBS buffer**
50 mM Tris/HCl, pH 7.5	2.7 mM KCl
150 mM NaCl	136 mM NaCl
1 mM EDTA, pH 8.0	4 mM Na_2HPO_4
1% (w/v) SDS	1.7 mM KH_2PO_4
0.5% (v/v) NP- 40	Adjust pH to 7.4 with HCl

Protease inhibitors and 1 mM DTT were added freshly.

4.2.1.6. Preparation of nuclear extract

L2-4 cells were expanded over 2–3 weeks leading to a total cell density of at least $3*10^9$ cells. Cells were harvested by centrifugation at 1000x g for 20 min at 15°C and washed twice with ice cold 1x PBS. The packed cell volume (PCV) was estimated and the cell pellet was resuspended in 3x PCV of ice cold

hypotonic buffer A. After incubation on ice for 30 min, cells were homogenized using a Dounce homogenizer (B. Braun S fit pestle). In order to increase stabilization of nuclei, the ionic strength was increased by the addition of 1/10 volume of buffer B. The cytosolic fraction was removed by centrifugation for 15 min at 8000x g at 4°C and the packed nuclear pellet volume (PNV) was estimated. The cell pellet was resuspended with the 3x PNV in a mixture of hypotonic buffers A and B in the ratio 9:1. To lyse the nuclear membrane 1/10 sample volume of 4 M $(NH_4)_2SO_4$, pH 7.9 was added and the nuclei suspension was incubated on a rotating wheel for 25 min at 4°C. The sample was then ultracentrifuged for 95 min at 100000x g at 4°C to remove unsoluble nuclear debris. The supernatant was recovered and dissolved proteins were precipitated by slowly adding 0.3 g of solid $(NH_4)_2SO_4$ per ml of nuclear extract under continuous stirring and then left for another for 10-15 min at 4°C. This will slowly increase $(NH_4)_2SO_4$ concentration to ensure efficient precipitation of proteins with a wide range of hydrophobic properties. Precipitated proteins were then pelleted by centrifugation for 35 min at 15000 rpm in a SS34 (Sorvall RC6PLUS) rotor at 4°C. The supernatant was discarded and the protein-containing pellet was dissolved in 0.2–0.5 PCV of buffer C and the nuclear extract was subsequently dialyzed three times against 1 l of buffer C (for 1–2 hs each; Spectra/Pro Dialysis membrane, size 1 (cut off 6–8 kDa)). A final centrifugation was performed for 15 min at 15000 rpm in a SS34 (Sorvall RC6PLUS) rotor at 4°C to remove precipitates from dialysis. The obtained nuclear extract was flash frozen in liquid nitrogen and stored in aliquots at -80 °C for further experiments.

Buffer A	**Buffer B**	**Buffer C**
10 mM HEPES, pH 7.6	50 mM HEPES, pH 7.6	25 mM HEPES, pH 7.6
15 mM KCl	1 M KCl	150 mM KCl
2 mM $MgCl_2$	30 mM $MgCl_2$	12.5 mM $MgCl_2$
0.1 mM EDTA, pH 8.0	0.1 mM EDTA, pH 8.0	0.1 mM EDTA, pH 8.0
		10% (v/v) glycerol

Protease inhibitors and 1 mM DTT were added freshly.

4.2.1.7. Preparation of nuclear and cytosolic fraction

Typically, 5–10*10^6 cells were harvested and washed twice with 1x PBS. The cell pellet was then resuspended in 1x PBS/0.1% Triton and put on ice for 10 min. Samples were centrifuged at 900x g for 10 min at room temperature. The supernatant was recovered as a cytosolic fraction. The precipitated pellet was resuspended in 1x PBS containing 1 µl of benzonase. The samples were then incubated at 37°C for 15–20 min and subsequently boiled in an appropriate volume of SDS sample buffer. Samples

were separated by SDS-PAGE and stained with Coomassie Brilliant Blue G250 or used for western blot analysis.

4.2.1.8. Preparation of Sf21 cell extracts for recombinant protein expression

The polycomb repressive complex 2 was recombinantly expressed using the baculovirus system. A 100–250-ml Sf21 cell culture with a concentration of $1*10^6$ cells/ml was prepared and co-transfected with the designed baculoviruses carrying the gene of interest. The volume of baculovirus solution depends on the concentration of the batch and was titrated. The baculoviruses were slowly added to the expression culture and then incubated in a shaker at 27°C for 2–2.5 days. Subsequently, cells were harvested by centrifugation at room temperature for 10 min at 200x g and the supernatant was discarded. Pelleted cells were washed once with 1x PBS. The obtained cell pellet was carefully resuspended in 5 ml lysis buffer BC 300 per 100-ml expression culture and put on ice for 10 min. Afterwards, the cell suspension was sonicated 4x 10 s, 20–30% amplitude on ice (20 s pause in between) and centrifuged for 30 min at 800x g at 4°C. The supernatant was further used for immunoprecipitation.

Lysis buffer BC 300

25 mM HEPES, pH 7.6
300 mM KCl
1 mM $MgCl_2$
0.5 mM EDTA, pH 8.0
0.5 mM EGTA, pH 8.0
0.1% (v/v) NP-40
10% (v/v) glycerol

Protease inhibitors and 1 mM DTT were added freshly.

4.2.2. Microbiology methods

4.2.2.1. Plasmid transformation

For cloning the *Sam-S* gene into the pMT-FLAG-HA vector (Thomae et al., 2013), the plasmid pMK33-CFH-BD (FMO10208) was purchased from *Drosophila* Genomics Resource Center (DGRC) gold collection. The plasmid was incubated with the DH5α *E.coli*-strain for 45 min on ice. A heat shock was performed at 42°C in a water bath for 90 s and immediately put back on ice for another 2 min. 1 ml LB medium was added and bacteria were incubated at 37°C for 1 h in a shaker at 750 rpm. 100 µl of this bacteria suspension was directly transferred onto a LB agar plate with the appropriate antibiotics for

selection. The remaining cell suspension was centrifuged at 800x g for 3 min at room temperature and the supernatant was removed except for 100 µl for resuspension. The resuspended cells were plated on a separate LB agar plate. Both plates were incubated over night at 37°C.

4.2.2.2. Extraction and purification of plasmid DNA

A single clone was picked from the LB agar plate. LB medium was supplemented with the appropriate antibiotics, inoculated with the picked clone and incubated over night at 37°C in a shaker (Infors Multitron) at 180 rpm. The subsequent extraction of the amplified plasmid DNA was carried out using Qiagen Plasmid Kits according to the manufacturer's instructions.

Luria-Bertani (LB) medium

1.0% (w/v) Bacto-Tryptone
1.0% (w/v) NaCl
0.5% (w/v) Bacto-Yeast extract

The pH was adjusted with NaOH and autoclaved at 120°C for 200 min. Plates were prepared by adding 1.5% (w/v) agar to LB medium.

4.2.3. Molecular biology methods

4.2.3.1. Storage of DNA and RNA

Isolated and purified DNA as well as cDNA was stored at -20°C in TE buffer. Isolated RNA was also stored at -20°C in RNase-free water. All RNA applications were done with RNase-free water, all DNA and RNA experiments were performed in RNase- and DNase-free and low-binding tubes (Biozym).

TE buffer

10 mM Tris-HCl, pH 8.0
1 mM EDTA, pH 8.0

4.2.3.2. DNA and RNA quantitation

For quantitation of DNA and RNA fragments a nanoDrop ND-1000 Spectrophotometer (Peqlab) was used. The absorbance at 260 nm was measured and the ratio of 260/280 absorbances was used to assess the purity of DNA and RNA. A ratio of ~1.8 was considered to be "pure" for DNA, while a ratio of ~2.0 was accepted as "pure" RNA.

4.2.3.3. Agarose gel electrophoresis

To analyze and separate DNA fragments of different sizes after PCR reactions and restriction digests, an agarose gel electrophoresis was performed. Agarose was dissolved in 1x TBE buffer by heating in the microwave and polymerized in a gel chamber. The percentage of the gel was chosen according to the DNA fragments that had to be separated, for smaller fragments a higher percentage of agarose was applied. DNA samples were mixed with 6x gel loading dye (NEB) prior to loading on the gel. A 1-kb DNA ladder (NEB) was used as a marker to distinguish different sizes. The DNA fragments were visualized by ethidium bromide (0.2 µg/µl) which was added to the gel prior to pouring. Subsequently, the presence of DNA fragments of the expected size was determined by UV light (254–366 nm) and documented with the gel documentation system G:BOX. In order to extract a particular DNA fragment the QIAquick® Gel extraction Kit (Qiagen) was used according to the manufacturer's instructions.

1x TBE buffer

90 mM Tris-HCl, pH 8.0
90 mM boric acid
2 mM EDTA, pH 8.0

4.2.3.4. Restriction digest

Enzymes for restriction digests were purchased from New England Biolabs (NEB). Buffer conditions and temperatures were used as suggested by the manufacturer. The required amount of enzyme was calculated according to their unit definition. All reaction products were analyzed by agarose gel electrophoresis and were purified with the QIAquick® PCR purification Kit (Qiagen) according to the manufacturer's instructions.

4.2.3.5. Polymerase chain reaction

DNA was amplified by polymerase chain reaction (PCR) using Phusion® High-Fidelity DNA Polymerase. This enzyme contains a proof reading function. Reaction products were analyzed using agarose gel electrophoresis as described previously and were purified with the QIAquick® PCR purification Kit (Qiagen) according to the manufacturer's instructions. Amplified and purified fragments were then sent to GATC for sequencing.

The following conditions were used for PCR reaction:

Template DNA	10 ng plasmid DNA, 100–500 ng genomic DNA
10x buffer (NEB)	2 µl
Primer fw/rev	0.5 µl each
dNTP mix (10mM each nucleotide, NEB)	1 µl
Phusion® High-Fidelity DNA Polymerase	1 µl
ddH_2O	Add to 50 µl

Reaction	**Temperature [°C]**	**Time [s]**	
Initial denaturation	98	120	
Denaturation	98	15	25–30 cycles
Annealing	Adjusted to primer size	15	
Elongation	72	15–30/kbp	
Final elongation	72	300	

4.2.3.6. Ligation

Sequenced DNA fragments were ligated into the linearized vector backbone pMT-FLAG-HA. The following condition was used:

Insert DNA and vector backbone	Vector and insert were added in a molar ratio of 1:3–1:5
10x T4 Ligase Buffer (NEB)	1 µl
Ligase T4 (NEB)	1 µl
ddH_2O	Add to 10 µl

The reaction was incubated over night at 16°C. Finally, ligation was heat inactivated at 65°C for 10 min.

4.2.3.7. Isolation of genomic DNA from *Drosophila melanogaster*

Two *Drosophila melanogaster* flies were anesthetized with CO_2, transferred into a 1.5-ml Eppendorf tube and put on ice for 5 min. 50 µl of Squish buffer was added, the flies were homogenized by crushing them with a pipet tip against the wall of the tube. The mixture was incubated for 30 min at 37°C for Proteinase K digestion and afterwards heated to 85°C for another 20 min to inactivate the

enzyme. The sample was centrifuged for 10 min at 18000x g. Supernatant was transferred to a new tube and stored at -20°C.

Squish buffer

25 mM NaCl
10 mM Tris-HCl, pH 8.2
1 mM EDTA, pH 8.0

200 µg Proteinase K was added freshly per 1 ml Squish buffer.

4.2.3.8. RNA isolation

RNA was extracted using the RNeasy Kit from Qiagen according to the manufacturer's instructions. RNA quality was checked using the Bioanalyzer (Agilent Technologies).

4.2.3.9. cDNA synthesis

To analyze gene expression in L2-4 cells, isolated RNA was reverse transcribed to complementary DNA (cDNA). 1 µg RNA was used per reaction, which was performed with the DyNAmo cDNA Synthesis Kit according to the manufacturer's instructions. The obtained cDNA was used for qPCR experiments.

4.2.3.10. Microarray analysis

The GeneChip® Drosophila Genome 2.0 Array (Affymetrix) was used for a genome-wide expression profile of *Drosophila melanogaster* transcripts. It provides a comprehensive coverage of the transcribed *Drosophila* genome. It is comprised of 18880 probe sets that analyze over 18500 transcripts. Sequences that were used to design the array were selected from Flybase version 3.1. The microarray readout was performed at the Gene Center, Munich, in the lab of Dr. Dietmar E. Martin. Raw sequencing data were bioinformatically analyzed by Dr. Tobias Straub, Adolf-Butenandt-Institute, LMU, Munich.

4.2.3.11. Quantitative real-time polymerase chain reaction

The quantitative real-time PCR method is used to amplify and simultaneously quantify a targeted DNA molecule. In this study, gene expression and the expression levels of transposons were monitored with the Roche LightCycler® system with 384-well plates. The housekeeping gene tubulin was used as reference gene. A volume of 10 µl/well was prepared with the following protocol, 2 µl of the appropriate cDNA concentration was used:

Reagent	Volume
cDNA template*	2 µl
Fast SYBR Green Master Mix	5 µl
Fw/rev primer mix (3 µM each)	1 µl
H_2O	2 µl

*cDNA was diluted and used in appropriate concentration depending on primer.

All used oligonucleotides were designed with a common annealing temperature with the Primer3 online software. The thermocycling program was performed as follows:

	Temperature	Time	Cycles
Denaturation	95°C	5 min	1x
Denaturation	95°C	10 s	
Annealing	60°C	20 s	45x
Elongation	72°C	10 s	
Melting	95°C	5 s	
	65–97°C	1 min	1x
Cooling	40°C	30 s	1x

For every primer pair the proper conditions and cDNA concentration (standard curves) were tested before the experiment was performed. Technical triplicates were performed and the mean of the triplicates was used for further data analysis.

4.2.4. Protein methods

4.2.4.1. Protein quantitation

To determine the concentration of proteins in solution (e.g. nuclear/whole cell extracts) the Bradford protein assay was performed (Bradford, 1976). Bradford solution (Biorad) was used according to the manufacturer's instructions (microassay procedure). A dilution series of 3–5 dilutions of BSA was prepared as a standard curve. The linear range of this assay for BSA is 1.2–10 µg/ml. The absorbance at 595 nm was measured after 5 min.

4.2.4.2. SDS-polyacrylamide gel electrophoresis

SDS-polyacrylamide gel electrophoresis (SDS-PAGE) is a method to separate proteins by their molecular mass and resulting electrophobic mobility (Laemmli, 1970).

After separation, proteins were either stained by silver nitrate or with Coomassie Brilliant Blue G250 depending on the amount of protein that was loaded on the gel.

4x SDS sample buffer	SDS running buffer
200 mM Tris-HCl, pH 6.8	192 mM glycine
8% (w/v) SDS	25 mM Tris
40% (v/v) glycerol	0.1% (w/v) SDS
4.2% (v/v) β-mercaptoethanol	
0.2% (w/v) bromphenol blue	

4.2.4.3. Protein staining methods

Coomassie staining

After electrophoresis, the separation gel was put in fixation and staining solution and incubated for at least 20 min at room temperature. For visualization of proteins, the gel was afterwards incubated in destaining solution until the unspecific background staining was removed and documented with the gel documentation system G:BOX (Syngene).

For mass spectrometry analysis, gel bands at the expected protein size were cut out with a clean scalpel and stored in 100 µl of HPLC water (Millipore) at -20° C for further analysis.

Fixation and staining solution	Destaining solution
50% (v/v) methanol	10% (v/v) acetic acid
10% (v/v) acetic acid	
0.25% (w/v) Coomassie Brilliant Blue G-250	

Fast Coomassie staining

Following electrophoresis, the polyacrylamide gel was put in 50 ml of suspension buffer, heated for 10–15 s in the microwave and then incubated 5–10 min at room temperature. Gel was transferred to 50 ml of staining solution, supplemented with 500 ml of blue solution and incubated another 10–15 min until proteins were visible. The gel was stored in water and documented with the gel documentation system G:BOX (Syngene).

Suspension solution	Staining solution	Blue solution
50% (v/v) ethanol	5% (v/v) ethanol	96% (v/v) ethanol
10% (v/v) acetic acid	7,5% (v/v) acetic acid	0.25% (w/v) Coomassie Brilliant Blue G-250

Silver staining

Silver nitrate staining of gels was performed as described in Blum et al. (Blum et al., 1987). It was used for sensitive detection of proteins with detection limits from 1–10 ng while Coomassie staining has a detection limit of 50–100 ng (Shevchenko et al., 1996).

4.2.4.4. Western blot analysis

Western blot analysis was performed using a wet blot chamber (Mini-Protean Tetra System, Biorad). First, the nitrocellulose membrane (Protran®, Amersham, GE Healthcare) was shortly incubated in 1x western blot buffer. Proteins were then transferred at 300 mA for 2 h at 4°C also using 1x western blot buffer. After the transfer, the membrane was blocked for 1 h at room temperature in 5% (w/v) milk (Heirler) in 1x PBS on a shaker. Subsequently, the incubation with the primary antibody was performed over night at 4°C on a shaker. The membrane was washed three times with 1x PBS/0.1% (v/v) Tween 20 (Sigma) for 10 min per step before it was incubated with the secondary antibody for 1 h at room temperature. Depending on the protein of interest, the secondary antibody was either coupled to horseradish peroxidase (1:5000 in 1x PBS/0.1% (v/v) Tween 20) for detection with the ECL detection system or was fluorescently labeled (1:10000 in 1x PBS/0.1% (v/v) Tween 20) for detection with the Odyssey® system.

For detection of biotinylated proteins, streptavidin coupled to horseradish peroxidase (Streptavidin-HRP) was used as primary antibody and was directly detected with the ECL method.

Enhanced chemiluminescence detection

After two washing steps in 1x PBS/0.1% (v/v) Tween 20 (10 min each), the membrane was incubated in enhanced chemiluminescence (ECL) solution (Clarity® Western ECL Blotting Substrate, Biorad) for 5 min and signals were visualized with Fuji X-ray films (Röntgen Bender) on an Agfa Curix 60 developer machine

Western blot buffer
25 mM Tris
192 mM glycine
0.02% (w/v) SDS
15% (v/v) methanol

Odyssey® detection

After two washing steps in 1x PBS/0.1% (v/v) Tween 20 (10 min each), the signals were detected, documented and quantified with an Odyssey® system (LI-COR).

4.2.4.5. Immunoprecipitation of PRC2 from Sf21 cell extracts

The polycomb repressive complex 2 was co-immunoprecipitated using the FLAG-tag of the methyltransferase E(z). First, the ANTI-FLAG® M2 affinity gel agarose beads (Sigma) were equilibrated. Therefore, lysis buffer BC300 was added to the beads (10x the volume of the beads) and mixed by gently inverting the tube several times. Beads were then centrifuged for 2 min at room temperature at 300x g. This step was repeated three times and subsequently, lysis buffer BC300 was added to the beads to generate a 1:1-slurry Sf21 cell extract was thawed and added to the slurry (dilution ratio) followed by incubation for 2 h at 4°C on a rotating wheel. Following the incubation, beads were separated from the supernatant and subjected to three washing steps with lysis buffer BC300 for 10 min each. Then, bound proteins were eluted with FLAG peptide (200 ng/ml) in elution buffer BC250 for 1 h at 4°C. Subsequently, beads were centrifuged for 2 min at 4°C at 300x g, the supernatant was aliquoted, flash frozen in liquid nitrogen and stored at -80 °C for further experiments. The purity of the protein was checked by SDS-PAGE followed by Coomassie Brilliant Blue G250 staining.

Elution buffer BC 300	Lysis buffer BC 250
25 mM HEPES, pH 7.6	25 mM HEPES, pH 7.6
300 mM KCl	250 mM KCl
1 mM $MgCl_2$	1 mM $MgCl_2$
0.5 mM EDTA, pH 8.0	0.5 mM EDTA, pH 8.0
0.5 mM EGTA, pH 8.0	0.5 mM EGTA, pH 8.0
0.1% (v/v) NP-40	10% (v/v) glycerol
10% (v/v) glycerol	

Protease inhibitors and 1 mM DTT were added freshly.

4.2.5. Immunofluorescence techniques

4.2.5.1. Immunostaining of *Drosophila* Schneider L2-4 cells

Immunostaining was performed in the *Drosophila* Schneider L2-4 cell line that stably expresses a FLAG-HA-tagged version of Sam-S. Expression was induced with copper 24 h before cells were used for staining experiments. Cells were detached from the flask and 100 µl of the cell suspension (~$3*10^6$ cells/ml) was pipetted on a poly-L-lysine-coated slide (Sigma). Cells were allowed to settle for 30 min

before the slide was washed twice with 1x PBS in a Coplin Jar for 5–10 min. Cells were then fixed with 1x PBS/3.7% (v/v) formaldehyde for exactly 10 min at room temperature and immediately washed twice with 1x PBS for 5–10 min. Subsequent permeabilization of the cells was done for precisely 6 min on ice with 1x PBS/0.25% (v/v) Triton X-100 and they were immediately washed twice as before. Cells were blocked with Image-iT® FX signal enhancer (Invitrogen) for 45 min at room temperature. Primary antibodies were diluted in 1x PBS/5 % (v/v) normal goat serum (NGS) (Dianova), covered with parafilm and incubated in a wet chamber over night at 4°C. The day after, slides were washed again twice with 1x PBS/0.1% (v/v) Triton and incubated with the secondary antibodies, which were coupled to a fluorophore (indirect staining). Secondary antibodies diluted in 1x PBS/5% (v/v) NGS were added to the cells and sample slides were incubated for 1 h at room temperature. Cells were washed twice with 1x PBS/0.1% (v/v) Triton and mounted with 7 µl Vectashield® DAPI (Vector Laboratories), covered with a coverslip and sealed with nail polish.

Axiovert 200 M epifluorescence microscopy

Images for antibody testing were acquired with a 60x zoom objective and were saved using the Axiovision 4.7 software (Zeiss). Subsequent analysis of images was carried out with Adobe CS5 Photoshop and Illustrator.

Leica TCS SP5 II confocal microscopy

Images for Sam-S localization were acquired with a 63x glycerol immersion objective (NA=1.3). Z-stacks were deconvolved using the Huygens Essential software (SVI) and further analyzed with ImageJ software.

4.2.5.2. Flow cytometry - Fluorescence-activated cell sorting

L2-4 cells were treated with dsRNA against Sam-S and GST, respectively, as described in chapter 4.2.1.4. After five days, approximately $5*10^6$ cells were harvested, washed with 1x PBS and fixed in 70% methanol/30% PBS. Fixed cell pellets were kept at -20°C for at least 1 h (maximum for one week). For fluorescence-activated cell sorting (FACS) analysis, cell pellets were washed twice with 1x PBS, resuspended in 200 µl 1x PBS supplemented with RNase A (100 µg/ml) and incubated for 10 min on ice. 10 µl propidium iodide (1 mg/ml, Sigma) and 2 µl 0.5 M EDTA, pH 8.0, were added and the samples directly analyzed on the FACSCanto device (BD Biosciences). Cell appearance was measured with forward and side scatter (FSC/SSC) indicating cell size and granularity, respectively. Propidium iodide

was measured in the PE channel (Phycoerythrin). Per condition, 100000 cell events were measured. Results were analyzed using the FlowJo software.

4.2.6. Mass spectrometry methods

4.2.6.1. Proteomics – Sam-S interactors

Co-Immunoprecipitation of endogenous Sam-S

Endogenous Sam-S was co-immunoprecipitated from nuclear extract of L2-4 cells using the Sam-S antibody 4A2. The antibody was coupled to a mixture of Protein A and G Sepharose beads. First, beads were equilibrated three times in buffer C (10x the volume of the beads) and mixed by gently inverting the tube several times. Beads were centrifuged for 2 min at 300x g at room temperature. A 1:1-slurry of beads and buffer C was generated and added to the nuclear extract. The suspension was incubated for 2 h at 4°C on a rotating wheel. Beads were recovered by centrifugation and subsequently washed three times for 10 min with buffer C. Purified proteins were eluted from the beads by boiling in SDS sample buffer. SDS-PAGE was performed to separate isolated proteins according to protein size. Following electrophoresis, gels were stained with Coomassie Brilliant Blue G250, tryptic in-gel digested (chapter 4.2.6.2.) and subjected to LC-MS/MS analysis.

Buffer C

25 mM HEPES pH 7.6
150 mM KCl
12.5 mM $MgCl_2$
EDTA pH 8.0
10% glycerol

Protease inhibitors were added freshly.

LC/MS-MS method (LTQ Orbitrap XL™)

For mass spectrometry analysis, samples were desalted on-line by a C18 micro trap column (5 mm x 300 µm inner diameter, packed with C18 PepMapTM, 5 µm, 100 Å; Thermo Fisher Scientific) before conducting nano-reversed phase HPLC separation. Tryptic peptide mixtures were separated on a C18 analytical column (10 cm x 75 µm, packed in house with C18 PepMapTM, 3 µm, 100 Å, Thermo Fisher Scientific) using a gradient from 5%–60% (v/v) ACN in 0.1% (v/v) FA over 40 min, flow rate 300 nl/min. Peptides eluting from the RP-HPLC column were introduced into the mass spectrometer via a nano-electrospray ion source (nESI, Proxeon). To further analyze the nature of the eluting peptides, the MS was operated in the data-dependent acquisition mode to automatically switch between full scan MS

and MS/MS acquisition. Survey full scan MS1 spectra (m/z 250–1800) were acquired in the Orbitrap with resolution R = 60.000 at m/z 400. The six most intense peptide signals with charge states between two and five were sequentially isolated applying a 2-Dalton (Da) window centered around the most abundant isotope to a target value of 10000 and fragmented in the linear ion trap by collision-induced dissociation (CID). Fragment ion spectra were recorded by the detector of the linear trap. For all measurements with the Orbitrap detector, three lock-mass ions (siloxanes) from ambient air (m/z=371.10123, 445.12002, 519.13882) were applied for internal calibration as described (Olsen et al., 2005).

For ionization, the spray voltage was set to 1.4 kV and the capillary temperature to 200°C. Peptides were fragmented applying an activation time of 30 ms and a normalized collision energy of 35% for CID in the linear ion trap.

MaxQuant quantitation

Raw data were analyzed using the MaxQuant (Version 1.2.2.5) software (Cox and Mann, 2008). Datafiles resulting from analysis of individual gel slices were grouped as sample fractions for each biological replicate. Biological replicates of different experimental conditions were not grouped together. For protein identification, the following settings in MaxQuant were applied: Database: Swissprot 57.10; Taxonomy: *Drosophila melanogaster*; MS tol: 10 ppm; MS/MS tol: 0.5 Da; Peptide FDR: 0.01; Protein FDR: 0.01; minimal peptide length: 6; Variable modifications: Oxidation (M), Acetylation (K, Nterminus); Fixed modifications: Carbamidomethyl (C). For quantitation of protein, extracted peptide signal intensities were converted into intensity based absolute quantitation (iBAQ) intensities (Schwanhausser et al., 2011), thereby normalizing the quantitation to the number of detectable peptides. The generated proteingroups.txt file was filtered for "contaminants", "reverse hits" and "only identified by site". Obtained iBAQ intensitities of protein hits were logarithmically (base 2) transformed and subsequently the specific enrichment factors were calculated and a threshold of 2 was set.

4.2.6.2. Capture Compound™ Mass Spectrometry

Capture Compound™ Mass Spectrometry – proof of principle

For capturing SAH-binding proteins, 1.5 µg of recombinant protein was used and 5 µM of SAH-Capture Compound™ was added. The capture reaction was incubated for 2 h at 4°C and irradiated with UV light for 5 min. Beads were then boiled in SDS sample buffer, separated by SDS-PAGE and analyzed by protein staining or western blot.

Comparison between in-gel and in-solution digestion

In order to get an idea which digestion gives the highest number of protein identifications, an in-gel digestion was compared to an in-solution digestion. A Capture Compound™ Mass Spectrometry experiment was performed as described above. Three mg of nuclear extract of L2-4 cells were used in two independent experiments, one sample without SAH-CC_{aa} served as a negative control. Concentration of SAH-CC_{aa} was 15 µM in each sample.

After irradiation, beads were washed and split into two parts: 50% of the beads were boiled in SDS sample buffer, separated by SDS-PAGE and an in gel-digestion was performed. The other 50% of the beads were used for an in-solution digestion.

In-solution digestion

Beads were resuspended in 50 µl 6 M Urea/2 M Thiourea/50 mM dithiothreitol (DTT) and incubated for 2 h at 20°C. In this step, proteins are denaturated and disulfide bonds are reduced by DTT. To alkylate reduced disulfide bonds, iodacetamide (IAA) was added to a final concentration of 25 mM. The sample was incubated for 30 min at 20°C in the dark since IAA is light sensitive. To quench alkylation, DTT was added to a final concentration of 50 mM and the mixture was incubated for another 30 min at 20°C. Afterwards, the sample was diluted with 50 mM ammonium bicarbonate (NH_4HCO_3) to reach a urea concentration below 1 M. Trypsin was then added in a ratio of trypsin/protein ~1:200 and incubated at 20°C for 3 h. After this pre-incubation, the sample was centrifuged for 2 min at 300x g, beads discarded and the same amount of trypsin as before was added. The sample was then incubated over night at 20°C. The day after, tryptic digest was stopped by adding trifluoric acid (TFA) to a final concentration of 1%. The sample was then centrifuged at maximum speed for 30 min and the supernatant was used for C18 peptide purification and desalting. C18 STAGE tips were prepared as described in Rappsilber et. al. (Rappsilber et. al, 2007) and equilibrated twice with 100 µl methanol, 100 µl with 80% acetonitrile (ACN)/0.1% TFA and finally three times with 100 µl 0.1% TFA. All equilibration steps were performed in a table top centrifuge (Eppendorf) at 1500 rpm at room temperature. The sample was then transferred on top of the C18 STAGE tip discs and centrifuged at the lowest speed (800 rpm) until the sample was almost completely filtered. This step was then repeated once. The C18 STAGEtip was washed twice with 150 µl 0.1% TFA before peptides were eluted twice with 60 µl 80% ACN/0.25% TFA. Eluents were pooled and dried in a speedvac dryer. For subsequent analysis in a LTQ Orbitrap XL mass spectrometer (Thermo Fisher Scientific), the sample was resuspended in an appropriate volume of 0.1% formic acid (FA).

In-gel digestion

After SDS-PAGE, the gel was stained with Coomassie Brilliant Blue G250 and bands were excised manually with a scalpel into 8 strips (Figure 4.1 A). Gel pieces were transferred into 8-stripes tubes and covered with 200 µl of HPLC grade water. All steps were performed at room temperature. Gel pieces were washed twice with 100 µl HPLC grade water, three times with 100 µl NH_4HCO_3 and destained with 50% 25 mM NH_4HCO_3/50% ACN. After gel pieces were completely destained, they were dehydrated three times with 100% ACN. Reduction of disulfide bonds was then performed in 50 µl 10 mM DTT in 25 mM NH_4HCO_3 for 1 h. This step was followed by alkylation with 50 µl 55 mM IAA in 25 mM NH_4HCO_3 for 30 min in the dark. Gel pieces were washed once with 100 µl 25 mM NH_4HCO_3 and dehydrated again three times with 100 µl ACN. 20 µl of trypsin (25 ng/µl) dissolved in 25 mM NH_4HCO_3 was added to each sample and incubated for 45 min at 4°C. The non-absorbed trypsin solution was removed and gel pieces were covered with 25 mM NH_4HCO_3 and digested for 12–16 h at 37°C. For acid extraction of peptides, gel pieces were incubated twice with 50 µl 60% ACN/0.25% TFA and twice with 50 µl 100% ACN for 10 min each. The extraction solutions were pooled and dried in a speedvac dryer (Scanvac). For subsequent analysis in a LTQ Orbitrap XL mass spectrometer (Thermo Fisher Scientific), the sample was resuspended in an appropriate volume of 0.1% FA.

For mass spectrometry, analysis settings as described in chapter 4.2.6.1. were used. In-gel digestion gave higher numbers of identified proteins than in-solution digestion, even if the total number of identified proteins was low in both experiments (Figure 4.1 C, Table 2). Therefore, in-gel digestion was the method of choice and was used in the following experiments.

Table 2: Comparison of in-gel digestion versus in-solution digestion:
Shown are the total numbers of proteins identified with the two different digestion methods, in-gel versus in-solution. Each technique was performed in three independent samples.

In-gel			**In-solution**		
Xlink SAH-CC_{aa}	-xlink	-SAH-CC_{aa}	Xlink SAH-CC_{aa}	-xlink	-SAH-CC_{aa}
963	708	673	627	419	437

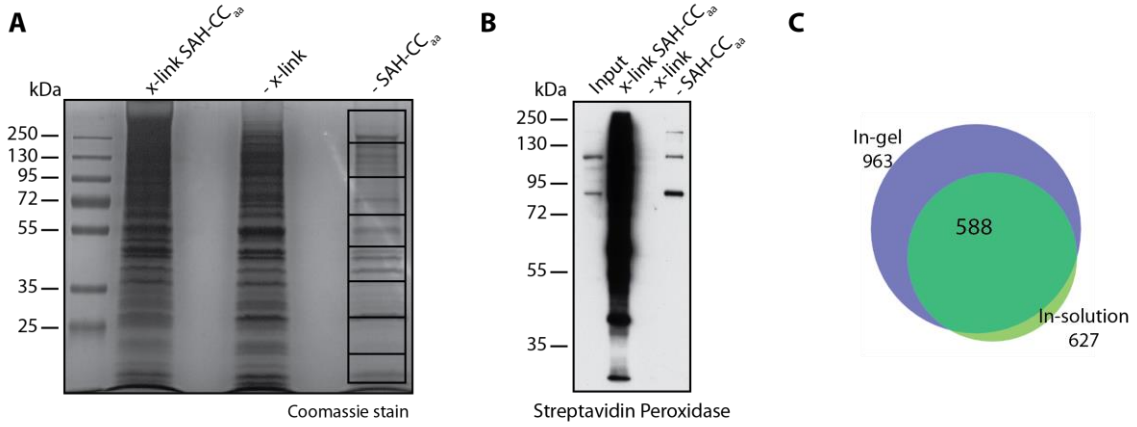

Figure 4.1: Comparison between in-gel and in-solution digestion
(A) SAH-binding proteins were purified from nuclear extract of L2-4 cells using SAH-Capture Compound™ (SAH-CC_{aa}). One sample without SAH-CC_{aa} served as a control. After irradiation (x-link) samples were divided in two parts. One part was subjected to in-solution tryptic digestion and analyzed by LC-MS/MS. The other part was boiled in SDS buffer, samples were separated by 12% SDS-PAGE and stained with Coomassie Brilliant Blue G250. Subsequently, lanes were excised in eight fractions. Each fraction was subjected to in-gel tryptic digestion and individually analyzed by LC-MS/MS. **(B)** Western blot using the indicated antibody to show protein biotinylation via the biotin-tag of SAH-CC_{aa} after cross-link. **(C)** Venn diagram gives proportions and total numbers of all identified proteins and their overlap in different digestion method. Diagram was created with BioVenn (http://cmbi.ru.nl/cdd/biovenn/).

Capture Compound™ Mass Spectrometry – profiling of methyltransferases

For capturing methyltransferases, 200 µl (10 µg/µl) nuclear extract from L2-4 cells was used and 45 µM SAH-Capture Compound™ was added with either fluorinated aryl azide (SAH-CC_{aa}) or benzophenone (SAH-CC_{bp}) as photo crosslinker. In addition, 10 µM DZnep, an inhibitor for adenosylhomocysteinase, was added to prevent metabolism of SAH-CC. Capture reactions were incubated for 2 h at 4°C and then irradiated for 5 min at 315 nm for SAH-CC_{aa} and 90 min at 350 nm for SAH-CC_{bp}. To isolate the SAH-CC-protein complex, 50 µl (per 5 µM SAH-CC) Streptavidin My one C1 beads were added and incubated for 1 h at 4°C. The beads were then washed four times with buffer C/0.1% NP40 and twice with buffer C. For subsequent LC-MS/MS analysis, beads were boiled in 2x SDS sample buffer, pre-separated by SDS-PAGE and an in-gel digestion was performed (see above).

Buffer C

25 mM HEPES pH 7.6
150 mM KCl
12.5 mM $MgCl_2$
EDTA pH 8.0
10% glycerol

Protease inhibitors were added freshly

Mass spectrometry analysis (Triple TOF)

Peptides recovered from in-gel digestion were sequentially eluted from a 12-cm in house-poured C18 column using a Ultimate3000 UHPLC system (Thermo-Fisher, San Jose) at a flow rate of 0.3 µl/min. A linear gradient from 5% B (80% ACN, 0.1% FA in H2O) to 45% B was established to separate peptides according to their hydrophobicity. Peptides were on-line detected and analyzed on a 5600 TripleTOF mass spectrometer (Sciex, USA). A data-dependent acquisition mode was selected which detected eluting peptides in a mass range from 300–1250 m/z in a survey scan and enabled fragmentation of up to 30 selected peptide ions with charge states 2–5 and intensity of more than 100 cps (counts per second). Options for background calibration and dynamic background subtraction were disabled. The instrument was calibrated by standard runs which were interspersed between sample runs. Peptide ions were fragmented using the rolling collision energy option and resulting peptide fragments were detected from 150 to 1800 m/z. Scan times were set to 200 ms for the MS survey scan and 150 ms per MS/MS scan. Previously selected peptide ions were excluded from reanalysis for 10 s by applying a 50-ppm mass window centered around the observed precursor mass.

Data analysis – MaxQuant

All datafiles were searched in parallel using the Andromeda search algorithm within the MaxQuant software (version 1.5.1.2). Datafiles resulting from analysis of individual gel slices were grouped as sample fractions to each biological replicate. Biological replicates of different experimental conditions were not grouped together.

Data were searched against a *Drosophila melanogaster* translation database from Flybase (vs. 5.24) applying a precursor mass error of 20 ppm and a fragment mass error of 80 ppm. Protein N-terminal-acetylation and methionine oxidation were allowed as variable modifications; cysteine carbamidomethylation was set as a fixed modification. Results were filtered for a false discovery rate of 1% on Peptide spectrum match and protein level and proteins required at least one razor peptide with >7 amino acids to be identified.

Proteins with 2 or more identified razor peptide hits were quantified using the label-free quantitation algorithm in MaxQuant.

Data analysis – Python script

A list of putative methyltransferases was compiled from the Pfam and the Superfamily databases. Proteins listed in a Pfam methyltransferase family with an E-value < 1.0 were merged with proteins

listed in a Superfamily methyltransferase category; redundant hits were discarded. To check if identifications of the LC-MS/MS experiments were present in the above list of methyltransferases, Victor Solis wrote a Python script that performed the intersection of IDs between both sets and annotated the putative methyltransferase family of the LC-MS/MS identifications. The script was similarly used to check the methyltransferases found in RNA-Seq datasets from modENCODE projects (namely from cell lines S2DRSC, S2Rplus and Sg4). A list of methyltransferases previously identified by Weinmann et al. in a yeast-two-hybrid assay in human cell lines (Weimann et al., 2013) was downloaded from the supplementary file of the publication and mapped to their corresponding fly orthologues using Ensembl-Biomart. This list was used as an additional source to corroborate the presence of putative methyltransferases in the experimental datasets.

4.2.6.3. Histone modification analysis

Histone extraction

Typically, 5–10*10^6 cells were harvested and washed once with 1x PBS. The cell pellet was then resuspended in 1x PBS/ 0.1% Triton/ protein inhibitors and put on ice for 10 min. Samples were centrifuged at 900x g for 10 min at room temperature. The supernatant was discarded, the cell pellet resuspended in 1x PBS/ protein inhibitors and 1 µl of benzonase was added. The samples were then incubated at 37° C for 15–20 min and afterwards boiled in 2x SDS sample buffer and separated by 15–18% SDS-PAGE. After electrophoresis, gels were stained with Coomassie Brilliant Blue G250 and bands corresponding to H2A, H2B, H3 and H4 were excised (between 11 and 17 kDa). Gel bands were destained, acylated and digested with trypsin as previously described (Villar-Garea et al., 2008).

LC/MS-MS method for H3 and H4 (LTQ Orbitrap XL™)

For the analysis of H3 and H4 peptides an internal standard was added to the tryptic digest. The internal standard comprised a mix of different heavily labeled synthetic peptides (SpikeTides™) added from a stock solution of 200 fmol/µl such that eventually 200 fmol of SpikeTides™ (JPT) were applied onto the column. To get high sequence coverage, histone peptides were desalted using Carbon ZipTips (Glygen) according to the manufacturer's instructions. The desalted peptides were dried in a vacuum concentrator, resuspended in an appropriate volume of 0.1% TFA and directly loaded onto an Ultimate 3000 HPLC system (Thermo Fisher Scientific) without the use of a trap column. For mass spectrometry analysis settings as described in chapter 4.2.6.1. were used.

Quantitation of histone post-translational modifications

Masses of expected modified peptides can be calculated using the GPMAW software (http://www.gpmaw.com/). Those masses were then used to search for the corresponding m/z value in the acquired mass spectrum (MS1) using the XCalibur Qual Browser software (Thermo scientific), by that means obtaining extracted ion chromatograms (XICs). The area under the curve of an XIC displays the intensity of a peptide versus its retention time and therefore reflects its abundance (Figure 4.2). The QualBrowser software automatically integrates this area under the curve and the extracted number was exported to an excel file (Epigenesys protocols, Forné and Barth). The identity of the peptide ions that were quantified was confirmed by analyzing the MS/MS spectra. For relative quantitation, all detected modification states were summed up to 100%. Percentages of the appropriately modified peptides were calculated and then compared between the knockdown and control cells.

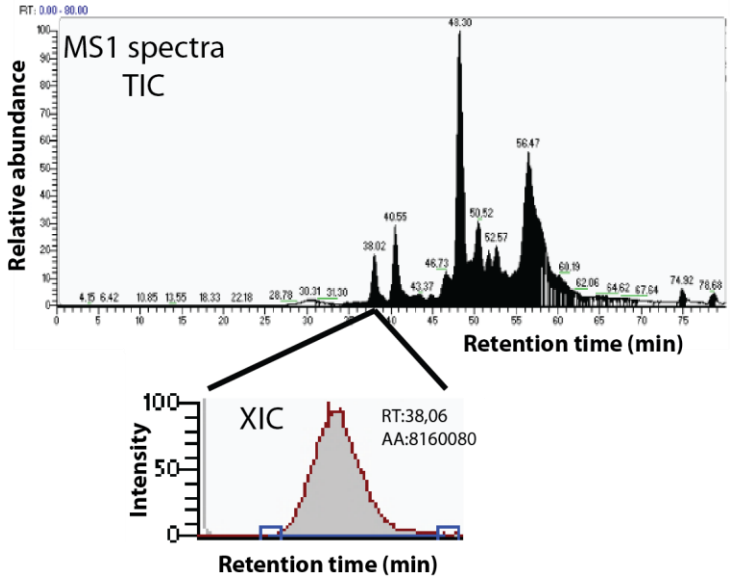

Figure 4.2: Quantitation of histone modifications using mass spectrometry
Theoretical calculated masses of histone peptides carrying a distinct PTM were used to search for the corresponding m/z value in the acquired mass spectrum (MS1). Extracted ion chromatograms (XICs) were obtained using the XCalibur Qual Browser software (Thermo scientific). The area under the curve of an XIC displays the intensity of a peptide versus its retention time and therefore reflects its abundance. TIC: total ion count

Mass spectrometry analysis for H2B (MALDI-TOF)

For H2B, the peptides were desalted with ZipTip µ-C18 (Millipore) according to the manufacturer's instructions, mixed with a saturated α-cyano-hydroxycinnamic acid (Sigma) in 50% ACN/0.3% TFA solution and immediately spotted onto a stainless steel target plate. Spectra were acquired on a Voyager DE STR workstation (MALDI-TOF). Typically 100 shots per spectrum were acquired, shooting 5

times in the same position. In all the experiments, the acquisition was performed the same way for all samples. Spectra were acquired using the reflector mode.

Typical reflector mode conditions were: accelerating voltage 20 kV, grid voltage 66%, mirror voltage ratio 1.12, delayed extraction with 100 ns delay time, guide wire 0.1%, 100 shots/spectrum, laser repetition 20 Hz, low mass gate 500.

4.2.6.4. Quantitative analysis of the metabolites SAM and SAH

In order to determine the concentration of endogenous SAM and SAH in L2-4 cells, a quantitative mass spectrometry method was established and validated after Burren et al. (Burren et al., 2006).

Isolation of S-Adenosylmethionine and S-Adenosylhomocysteine from L2-4 cells

For quantitative determination of SAM and SAH, cells of interest were harvested and washed twice with 1x PBS. Cell pellets were either flash frozen and stored at -80°C or directly used for further analysis. $2*10^6$ cells were then resuspended in 40 µl (injection volume) of ice cold buffer A (see below) and lysed 4x for 10 s in an ultrasonic cleaner. Cells were then heated to 80°C for 5 min and put immediately on ice for 2 min. Afterwards, cells were centrifuged for 15 min at 4°C at 12000x g. As an internal standard, 1 µM [$^2H_3$]-SAM was added.

LC/MS-MS method for SAM and SAH (4000 QTRAP)

Prior to analysis by mass spectrometry, the metabolites SAM (and [$^2H_3$]-SAM) and SAH were separated on a pentafluorophenylpropyl (PFPP)-bonded silica column (Discovery HS F5; 50 mm x 2.1 mm (i.d.); 5 µm bead size; Supelco, Sigma-Aldrich) using a liquid chromatography (LC) system (Shimadzu). The injection volume was 40 µl, flow rate 0.5 ml/min. The LC protocol was as follows: the column was equilibrated for 2 min with 40% A:60% B before a gradient from 60%–90% A over 4 min was run. The column was then washed with 100% A for 3 min, and for 2 min with 100% B before re-equilibration for 2 min was started. All gradient changes were set within 1 min. The metabolites were then injected into a 4000 QTRAP mass spectrometer (AB Sciex) via a Turbo Spray ion source. The MS instrument was operated in the positive-ion mode using the following settings after a compound optimization run was performed for each metabolite: source temperature (TEM) 600 °C, ion spray voltage (IS) 5500 V, curtain gas (CUR) 20 ml/min, 60 psi and collision energy (CAD) 5 V. The MRM mode was used for quantitation and data were acquired and processed using the analyst 1.5.1 software (AB Sciex).

Buffer A	Buffer B
4 mM ammonium acetate 0.1% (v/v) formic acid 0.1% (v/v) heptafluorobutyric acid	100 % methanol

4.2.6.5. Heavy methyl SILAC

Heavy methyl SILAC labeling

For metabolic labeling, L2-4 cells were cultured in Sf4 Baculo Express Insect Culture Medium (ICM) without L-Methionine (BIO&SELL) at 26°C. Media was supplemented with 10% dialyzed FCS (Sigma), Pen/Strep (100 U/ml Pen G; 0.1 mg/ml Strep), L-Glutamine (1.8 g/l; Sigma) and either a light (Met-0) or heavy (Met-4) version of L-Methionine (1 g/l). Amino acids were dissolved in the medium. Before cells were heavily labeled, they were passaged at least four times for adjustment to the new medium. After Met-4 was added, cells were passaged at least nine times before they were harvested to reach a high incorporation rate (higher than 95%).

Subcellular fractionation of hmSILAC-labeled L2-4 cells

Heavy and light cells were mixed in a 1:1 ratio and subcellular fractionation was performed. $50*10^6$ cells were harvested and washed twice with 1x PBS. The packed cell volume (PCV) was estimated and the cell pellet was resuspended in 5x PCV of ice cold hypotonic buffer A and incubated for 10 min on ice. Cells were centrifuged for 5 min at 400x g at 4°C and resuspended in 2x PCV of buffer A and 0.2% NP-40 (cell volume should have increased due to osmotic uptake of liquid by the cells). Cell suspension was then transferred to a Dounce Homogenisator (B. Braun S fit pestle) and treated with 20 strokes on ice. The cytosolic fraction was removed by centrifugation for 15 min at 8000x g at 4°C and the nuclear pellet was washed twice with 1x PBS. The nuclear pellet volume (PNV) was estimated and resuspended in 2x PNV of buffer C. This step was carried out to strip off non-histone nucleosome binding proteins from chromatin, leaving the histones and nuclear matrix in the pellet. The nuclei were rotated for 1 h at 4°C. Afterwards, cytosolic and nuclear fractions were ultra-centrifuged for 1 h at 60000x g at 4°C. Supernatants were collected, glycerol (10% final concentration) and NaCl (150 mM final concentration) were added to the cytoplasmic fraction. Aliquots were flash frozen in liquid nitrogen and stored at -80 °C for further experiments.

Buffer A	Buffer C
10 mM HEPES, pH 7.6	20 mM HEPES, pH 7.6
10 mM KCl	450 mM KCl
1.5 mM $MgCl_2$	2 mM $MgCl_2$
	0.2 mM EDTA, pH 8.0
	20% glycerol

Protease inhibitors and 1 mM DTT were added freshly.

LC-MS/MS analysis (Orbitrap instruments)

LC-MS/MS analysis was performed as described in Bremang et al.(Bremang et al., 2013).

Data analysis

Raw data were analysed using the MaxQuant software (v1.3.0.5) and searched against a *Drosophila melanogaster* proteome, derived from the UniProt database (14/06). Three searches were performed in parallel, using the following sets of variable modifications: First, monomethyl (K/R), monomethyl-4 (K/R), Met-4 (M), Oxidation (M), Met-4 Oxidation (M). Second, dimethyl (K/R), dimethyl-4 (K/R), Met-4 (M), Oxidation (M), Met-4 Oxidation (M) and third, trimethyl (K), trimethyl-4 (K), Met-4 (M), Oxidation (M), Met-4 Oxidation (M). Output from the MaxQuant searches were post-processed using a pipeline developed in-house for detecting hmSILAC pairs (Perl) (Bremang et al., 2013).

Confident identifications required the identification of sequenced peptides, in both heavy and light forms. Modified sites with localization probabilities <0.75 (a widely-used threshold for MaxQuant-based posttranslational modification studies) were classed as ambiguous. Those with localization >0.75 are counted in the methylome. Sites identified on peptides with an identified hmSILAC pair were assigned to Class A. Those with a peptide Score >62 were classed as A1. Those with Score <63 were classed as A2. This score threshold is derived from the HeLa study (Bremang et al., 2013) and can be considered as an approximate indicator of high confidence identification, noting that the presence of the hmSILAC doublet increases confidence in the identification.

Abbreviations

ACN	Acetonitrile
ATP	Adenosine triphosphate
°C	Degree Celsius
bp	Basepair(s)
$CuSO_4$	Copper sulfate
cDNA	Complementary DNA
CoA	Coenzyme A
Da	Dalton
DAPI	4', 6-diamidino-2-phenylindole
DMSO	Dimethyl sulfoxide
DNA	Deoxyribonucleic acid
DTT	Dithiothreitol
dsRNA	Double stranded RNA
DZNep	3-deazaneplanocin A
EDTA	Ethylenediaminetetraacetic acid
EGTA	Ethylene glycol-bis(β-aminoethyl ether)-N,N,N',N'-tetraacetic acid
ESI	Electrospray ionization
EtOH	Ethanol
e.g.	Exempli gratia (for example)
FA	Formic acid
FACS	Fluorescence-activated cell sorting
FAD	Flavin adenine dinucleotide
FCS	Fetal calf serum
fw	Forward
g	Standard gravity
h	Hour
H1/H2A/H2B/H3/H4	Histone 1/2A/2B/3/4
HCl	Hydrochloric acid
HEPES buffer	4-(2-hydroxyethyl)-1-piperazineethanesulfonic acid
HRP	Horseradish peroxidase
IAA	Iodoacetamide

IF	Immunofluorescence
IP	Immunoprecipitation
iBAQ	Intensity based absolute quantitation
k	Kilo
LC-MS/MS	Liquid chromatography tandem mass spectrometry
min	Minutes
ml	Milliliter
mRNA	Messenger RNA
MT	Methyltransferase
m/z	Mass-to-charge
µl/µg	Microliter/microgram
NaCl	Sodium chloride
NaOH	Sodium hydroxide
ng	Nanogram
ncRNA	Non-coding RNA
PAGE	Polyacrylamide gel electrophoresis
PCR	Polymerase chain reaction
PBS	Phosphate-bufferd saline
pH	Potential Hydrogenii
pI	Isoelectric point
PMSF	Phenylmethylsulfonyl fluoride
pMT	Metallothionein promotor
ppm	Parts per million
PTM	Posttranslational modification
PVDF	Polyvinylidene difluoride
qPCR	Quantitative real-time PCR
rev	Reverse
RIPA buffer	Radioimmunoprecipitation assay buffer
RNA	Ribonucleic acid
RNAi	RNA interference
rpm	Rounds per minute
rRNA	Ribosomal RNA

s	Seconds
SAH	S-adenosylhomocysteine
SAM	S-adenosylmethionine
SDS	Sodiumdodecylsulfate
TBE buffer	Tris/borate/EDTA buffer
TE	Transposable elements
TE buffer	Tris/EDTA buffer
TFA	Triflouric acid
Tris	Trishydroxymethylaminomethane
tRNA	Transfer RNA
UV	Ultraviolet
v/v	Volume per volume
w/v	Weight per volume

References

Ahmad, K., and Henikoff, S. (2002). Histone H3 variants specify modes of chromatin assembly. Proc Natl Acad Sci U S A *99 Suppl 4*, 16477-16484.

Allfrey, V.G., and Mirsky, A.E. (1964). Structural Modifications of Histones and their Possible Role in the Regulation of RNA Synthesis. Science *144*, 559.

Allis, C.D., Berger, S.L., Cote, J., Dent, S., Jenuwien, T., Kouzarides, T., Pillus, L., Reinberg, D., Shi, Y., Shiekhattar, R., *et al.* (2007). New nomenclature for chromatin-modifying enzymes. Cell *131*, 633-636.

Ambler, R.P., and Rees, M.W. (1959). Epsilon-N-Methyl-lysine in bacterial flagellar protein. Nature *184*, 56-57.

Bannister, A.J., Zegerman, P., Partridge, J.F., Miska, E.A., Thomas, J.O., Allshire, R.C., and Kouzarides, T. (2001). Selective recognition of methylated lysine 9 on histone H3 by the HP1 chromo domain. Nature *410*, 120-124.

Barski, A., Cuddapah, S., Cui, K., Roh, T.Y., Schones, D.E., Wang, Z., Wei, G., Chepelev, I., and Zhao, K. (2007). High-resolution profiling of histone methylations in the human genome. Cell *129*, 823-837.

Barth, T.K., and Imhof, A. (2010). Fast signals and slow marks: the dynamics of histone modifications. Trends Biochem Sci *35*, 618-626.

Becker, P.B., and Horz, W. (2002). ATP-dependent nucleosome remodeling. Annu Rev Biochem *71*, 247-273.

Bell, J.T., and Spector, T.D. (2011). A twin approach to unraveling epigenetics. Trends Genet *27*, 116-125.

Bell, O., Conrad, T., Kind, J., Wirbelauer, C., Akhtar, A., and Schubeler, D. (2008). Transcription-coupled methylation of histone H3 at lysine 36 regulates dosage compensation by enhancing recruitment of the MSL complex in Drosophila melanogaster. Molecular and cellular biology *28*, 3401-3409.

Biggar, K.K., and Li, S.S. (2015). Non-histone protein methylation as a regulator of cellular signalling and function. Nat Rev Mol Cell Biol *16*, 5-17.

Biterge, B., and Schneider, R. (2014). Histone variants: key players of chromatin. Cell Tissue Res *356*, 457-466.

Black, J.C., Van Rechem, C., and Whetstine, J.R. (2012). Histone lysine methylation dynamics: establishment, regulation, and biological impact. Molecular cell *48*, 491-507.

Blum, H., Beier, H., and Gross, H.J. (1987). Improved silver staining of plant proteins, RNA and DNA in polyacrylamide gels ELECTROPHORESIS Volume 8, Issue 2. In Electrophoresis, pp. 93-99.

Bonisch, C., Nieratschker, S.M., Orfanos, N.K., and Hake, S.B. (2008). Chromatin proteomics and epigenetic regulatory circuits. Expert Rev Proteomics *5*, 105-119.

Boriack-Sjodin, P.A., and Swinger, K.K. (2016). Protein Methyltransferases: A Distinct, Diverse, and Dynamic Family of Enzymes. Biochemistry *55*, 1557-1569.

Bradford, M.M. (1976). A rapid and sensitive method for the quantitation of microgram quantities of protein utilizing the principle of protein-dye binding. Anal Biochem *72*, 248-254.

Bremang, M., Cuomo, A., Agresta, A.M., Stugiewicz, M., Spadotto, V., and Bonaldi, T. (2013). Mass spectrometry-based identification and characterisation of lysine and arginine methylation in the human proteome. Mol Biosyst *9*, 2231-2247.

Brosnan, J.T., and Brosnan, M.E. (2006). Branched-chain amino acids: enzyme and substrate regulation. J Nutr *136*, 207S-211S.

Brown, L.J., Baranowski, M., Wang, Y., Schrey, A.K., Lenz, T., Taverna, S.D., Cole, P.A., and Sefkow, M. (2014). Using S-adenosyl-L-homocysteine capture compounds to characterize S-adenosyl-L-methionine and S-adenosyl-L-homocysteine binding proteins. Anal Biochem *467*, 14-21.

Bruneau, B.G. (2010). Epigenetic regulation of the cardiovascular system: introduction to a review series.Circ Res 107, 324-326.

Burren, K.A., Mills, K., Copp, A.J., and Greene, N.D. (2006). Quantitative analysis of s-adenosylmethionine and s-adenosylhomocysteine in neurulation-stage mouse embryos by liquid chromatography tandem mass spectrometry. J Chromatogr B Analyt Technol Biomed Life Sci *844*, 112-118.

Caggese, C., Ragone, G., Barsanti, P., Moschetti, R., Messina, A., Massari, S., and Caizzi, R. (1997). The S-adenosyl-L-homocysteine hydrolase of Drosophila melanogaster: identification, deduced amino acid sequence and cytological localization of the structural gene. Molecular & general genetics : MGG *253*, 492-498.

Cantoni, G.L. (1951). Activation of methionine for transmethylation. The Journal of biological chemistry *189*, 745-754.

Cantoni, G.L. (1975). Biological methylation: selected aspects. Annu Rev Biochem *44*, 435-451.

Cantoni, G.L. (1985). The role of S-adenosylhomocysteine in the biological utilization of S-adenosylmethionine. Prog Clin Biol Res *198*, 47-65.

Cao, X.J., Arnaudo, A.M., and Garcia, B.A. (2013). Large-scale global identification of protein lysine methylation in vivo. Epigenetics *8*, 477-485.

Capuano, F., Mulleder, M., Kok, R., Blom, H.J., and Ralser, M. (2014). Cytosine DNA methylation is found in Drosophila melanogaster but absent in Saccharomyces cerevisiae, Schizosaccharomyces pombe, and other yeast species. Anal Chem *86*, 3697-3702.

Caudill, M.A., Wang, J.C., Melnyk, S., Pogribny, I.P., Jernigan, S., Collins, M.D., Santos-Guzman, J., Swendseid, M.E., Cogger, E.A., and James, S.J. (2001). Intracellular S-adenosylhomocysteine concentrations predict global DNA hypomethylation in tissues of methyl-deficient cystathionine beta-synthase heterozygous mice. J Nutr *131*, 2811-2818.

Chang, B., Chen, Y., Zhao, Y., and Bruick, R.K. (2007). JMJD6 is a histone arginine demethylase. Science *318*, 444-447.

Cherbas, L., and Gong, L. (2014). Cell lines. Methods *68*, 74-81.

Chiacchiera, F., Piunti, A., and Pasini, D. (2013). Epigenetic methylations and their connections with metabolism. Cell Mol Life Sci *70*, 1495-1508.

Chiang, P.K. (1998). Biological effects of inhibitors of S-adenosylhomocysteine hydrolase. Pharmacol Ther *77*, 115-134.

Chuikov, S., Kurash, J.K., Wilson, J.R., Xiao, B., Justin, N., Ivanov, G.S., McKinney, K., Tempst, P., Prives, C., Gamblin, S.J., *et al.* (2004). Regulation of p53 activity through lysine methylation. Nature *432*, 353-360.

Clarke, S.G. (2013). Protein methylation at the surface and buried deep: thinking outside the histone box. Trends Biochem Sci *38*, 243-252.

Cloos, P.A., Christensen, J., Agger, K., Maiolica, A., Rappsilber, J., Antal, T., Hansen, K.H., and Helin, K. (2006). The putative oncogene GASC1 demethylates tri- and dimethylated lysine 9 on histone H3. Nature *442*, 307-311.

Copeland, R.A., Solomon, M.E., and Richon, V.M. (2009). Protein methyltransferases as a target class for drug discovery. Nat Rev Drug Discov *8*, 724-732.

Cox, J., and Mann, M. (2008). MaxQuant enables high peptide identification rates, individualized p.p.b.-range mass accuracies and proteome-wide protein quantification. Nat Biotechnol *26*, 1367-1372.

Cremer, T., Cremer, M., Hubner, B., Strickfaden, H., Smeets, D., Popken, J., Sterr, M., Markaki, Y., Rippe, K., and Cremer, C. (2015). The 4D nucleome: Evidence for a dynamic nuclear landscape based on co-aligned active and inactive nuclear compartments. FEBS letters *589*, 2931-2943.

Crona, F., Dahlberg, O., Lundberg, L.E., Larsson, J., and Mannervik, M. (2013). Gene regulation by the lysine demethylase KDM4A in Drosophila. Dev Biol *373*, 453-463.

Dalhoff, C., Huben, M., Lenz, T., Poot, P., Nordhoff, E., Koster, H., and Weinhold, E. (2010). Synthesis of S-adenosyl-L-homocysteine capture compounds for selective photoinduced isolation of methyltransferases. Chembiochem *11*, 256-265.

Delatte, B., Wang, F., Ngoc, L.V., Collignon, E., Bonvin, E., Deplus, R., Calonne, E., Hassabi, B., Putmans, P., Awe, S., *et al.* (2016). RNA biochemistry. Transcriptome-wide distribution and function of RNA hydroxymethylcytosine. Science *351*, 282-285.

Desrosiers, R., and Tanguay, R.M. (1988). Methylation of Drosophila histones at proline, lysine, and arginine residues during heat shock. The Journal of biological chemistry *263*, 4686-4692.

Di Lorenzo, A., and Bedford, M.T. (2011). Histone arginine methylation. FEBS letters *585*, 2024-2031.

Di Stefano, L., Ji, J.Y., Moon, N.S., Herr, A., and Dyson, N. (2007). Mutation of Drosophila Lsd1 disrupts H3-K4 methylation, resulting in tissue-specific defects during development. Curr Biol *17*, 808-812.

Dillon, M.B., Rust, H.L., Thompson, P.R., and Mowen, K.A. (2013). Automethylation of protein arginine methyltransferase 8 (PRMT8) regulates activity by impeding S-adenosylmethionine sensitivity. The Journal of biological chemistry *288*, 27872-27880.

Dorman, G., and Prestwich, G.D. (1994). Benzophenone photophores in biochemistry. Biochemistry *33*, 5661-5673.

Dulac, C. (2010). Brain function and chromatin plasticity. Nature 465, 728-735.

Dunwell, T.L., and Pfeifer, G.P. (2014). Drosophila genomic methylation: new evidence and new questions. Epigenomics *6*, 459-461.

Ebert, A., Schotta, G., Lein, S., Kubicek, S., Krauss, V., Jenuwein, T., and Reuter, G. (2004). Su(var) genes regulate the balance between euchromatin and heterochromatin in Drosophila. Genes Dev *18*, 2973-2983.

Elgin, S.C., and Grewal, S.I. (2003). Heterochromatin: silence is golden. Curr Biol *13*, R895-898.

Eskeland, R., Czermin, B., Boeke, J., Bonaldi, T., Regula, J.T., and Imhof, A. (2004). The N-terminus of Drosophila SU(VAR)3-9 mediates dimerization and regulates its methyltransferase activity. Biochemistry *43*, 3740-3749.

Feller, C., Forne, I., Imhof, A., and Becker, P.B. (2015). Global and specific responses of the histone acetylome to systematic perturbation. Molecular cell *57*, 559-571.

Flaus, A., and Owen-Hughes, T. (2011). Mechanisms for ATP-dependent chromatin remodelling: the means to the end. FEBS J *278*, 3579-3595.

Fontecave, M., Atta, M., and Mulliez, E. (2004). S-adenosylmethionine: nothing goes to waste. Trends Biochem Sci *29*, 243-249.

Foss, E.J., Radulovic, D., Shaffer, S.A., Ruderfer, D.M., Bedalov, A., Goodlett, D.R., and Kruglyak, L. (2007). Genetic basis of proteome variation in yeast. Nature genetics *39*, 1369-1375.

Frezza, C., Pollard, P.J., and Gottlieb, E. (2011). Inborn and acquired metabolic defects in cancer. J Mol Med (Berl) *89*, 213-220.

Gardner, L.A., Desiderio, D.M., Groover, C.J., Hartzes, A., Yates, C.R., Zucker-Levin, A.R., Bloom, L., and Levin, M.C. (2013). LC-MS/MS identification of the one-carbon cycle metabolites in human plasma. Electrophoresis *34*, 1710-1716.

Gellekink, H., van Oppenraaij-Emmerzaal, D., van Rooij, A., Struys, E.A., den Heijer, M., and Blom, H.J. (2005). Stable-isotope dilution liquid chromatography-electrospray injection tandem mass spectrometry method for fast, selective measurement of S-adenosylmethionine and S-adenosylhomocysteine in plasma. Clin Chem *51*, 1487-1492.

Ghazalpour, A., Bennett, B., Petyuk, V.A., Orozco, L., Hagopian, R., Mungrue, I.N., Farber, C.R., Sinsheimer, J., Kang, H.M., Furlotte, N., *et al.* (2011). Comparative analysis of proteome and transcriptome variation in mouse. PLoS genetics *7*, e1001393.

Ghildiyal, M., Seitz, H., Horwich, M.D., Li, C., Du, T., Lee, S., Xu, J., Kittler, E.L., Zapp, M.L., Weng, Z., *et al.* (2008). Endogenous siRNAs derived from transposons and mRNAs in Drosophila somatic cells. Science *320*, 1077-1081.

Gillette, T.G., and Hill, J.A. (2015). Readers, writers, and erasers: chromatin as the whiteboard of heart disease. Circ Res *116*, 1245-1253.

Glazer, R.I., Hartman, K.D., Knode, M.C., Richard, M.M., Chiang, P.K., Tseng, C.K., and Marquez, V.E. (1986). 3-Deazaneplanocin: a new and potent inhibitor of S-adenosylhomocysteine hydrolase and its effects on human promyelocytic leukemia cell line HL-60. Biochem Biophys Res Commun *135*, 688-694.
Goll, M.G., Kirpekar, F., Maggert, K.A., Yoder, J.A., Hsieh, C.L., Zhang, X., Golic, K.G., Jacobsen, S.E., and Bestor, T.H. (2006). Methylation of tRNAAsp by the DNA methyltransferase homolog Dnmt2. Science *311*, 395-398.

Guruharsha, K.G., Rual, J.F., Zhai, B., Mintseris, J., Vaidya, P., Vaidya, N., Beekman, C., Wong, C., Rhee, D.Y., Cenaj, O., *et al.* (2011). A protein complex network of Drosophila melanogaster. Cell *147*, 690-703.

Heitz, E. (1928). Das Heterochromatin der Moose. Jahrbuch wissenschaftliche Botanik *1*, 762-818.

Herz, H.M., Garruss, A., and Shilatifard, A. (2013). SET for life: biochemical activities and biological functions of SET domain-containing proteins. Trends Biochem Sci *38*, 621-639.

Heyn, H., and Esteller, M. (2015). An Adenine Code for DNA: A Second Life for N6-Methyladenine. Cell *161*, 710-713.

Holowatyj, A., Yang, Z.Q., and Pile, L.A. (2015). Histone lysine demethylases in Drosophila melanogaster. Fly (Austin) *9*, 36-44.

Horiuchi, K.Y., Eason, M.M., Ferry, J.J., Planck, J.L., Walsh, C.P., Smith, R.F., Howitz, K.T., and Ma, H. (2013). Assay development for histone methyltransferases. Assay Drug Dev Technol *11*, 227-236.

Horne, D.W., Holloway, R.S., and Wagner, C. (1997). Transport of S-adenosylmethionine in isolated rat liver mitochondria. Arch Biochem Biophys *343*, 201-206.

Huang, D.W., Sherman, B.T., Tan, Q., Collins, J.R., Alvord, W.G., Roayaei, J., Stephens, R., Baseler, M.W., Lane, H.C., and Lempicki, R.A. (2007a). The DAVID Gene Functional Classification Tool: a novel biological module-centric algorithm to functionally analyze large gene lists. Genome biology *8*, R183.

Huang, J., Sengupta, R., Espejo, A.B., Lee, M.G., Dorsey, J.A., Richter, M., Opravil, S., Shiekhattar, R., Bedford, M.T., Jenuwein, T., *et al.* (2007b). p53 is regulated by the lysine demethylase LSD1. Nature *449*, 105-108.

Iberg, A.N., Espejo, A., Cheng, D., Kim, D., Michaud-Levesque, J., Richard, S., and Bedford, M.T. (2008). Arginine methylation of the histone H3 tail impedes effector binding. The Journal of biological chemistry *283*, 3006-3010.

Ito, S., Shen, L., Dai, Q., Wu, S.C., Collins, L.B., Swenberg, J.A., He, C., and Zhang, Y. (2011). Tet proteins can convert 5-methylcytosine to 5-formylcytosine and 5-carboxylcytosine. Science *333*, 1300-1303.

Kalantari, R., Hicks, J.A., Li, L., Gagnon, K.T., Sridhara, V., Lemoff, A., Mirzaei, H., and Corey, D.R. (2016). Stable association of RNAi machinery is conserved between the cytoplasm and nucleus of human cells. RNA *22*, 1085-1098.

Kalisch, W.E., and Rasmuson, B. (1974). Changes of zeste phenotype induced by autosomal mutations in Drosophila melanogaster. Hereditas *78*, 97-104.

Katada, S., Imhof, A., and Sassone-Corsi, P. (2012). Connecting threads: epigenetics and metabolism. Cell *148*, 24-28.

Katoh, Y., Ikura, T., Hoshikawa, Y., Tashiro, S., Ito, T., Ohta, M., Kera, Y., Noda, T., and Igarashi, K. (2011). Methionine adenosyltransferase II serves as a transcriptional corepressor of Maf oncoprotein. Molecular cell *41*, 554-566.
Kebede, A.F., Schneider, R., and Daujat, S. (2015). Novel types and sites of histone modifications emerge as players in the transcriptional regulation contest. FEBS J *282*, 1658-1674.

Kera, Y., Katoh, Y., Ohta, M., Matsumoto, M., Takano-Yamamoto, T., and Igarashi, K. (2013). Methionine adenosyltransferase II-dependent histone H3K9 methylation at the COX-2 gene locus. The Journal of biological chemistry *288*, 13592-13601.

Kharchenko, P.V., Alekseyenko, A.A., Schwartz, Y.B., Minoda, A., Riddle, N.C., Ernst, J., Sabo, P.J., Larschan, E., Gorchakov, A.A., Gu, T., *et al.* (2011). Comprehensive analysis of the chromatin landscape in Drosophila melanogaster. Nature *471*, 480-485.

Kitteringham, N.R., Jenkins, R.E., Lane, C.S., Elliott, V.L., and Park, B.K. (2009). Multiple reaction monitoring for quantitative biomarker analysis in proteomics and metabolomics. J Chromatogr B Analyt Technol Biomed Life Sci *877*, 1229-1239.

Klenov, M.S., Lavrov, S.A., Stolyarenko, A.D., Ryazansky, S.S., Aravin, A.A., Tuschl, T., and Gvozdev, V.A. (2007). Repeat-associated siRNAs cause chromatin silencing of retrotransposons in the Drosophila melanogaster germline. Nucleic Acids Res *35*, 5430-5438.

Klose, R.J., and Bird, A.P. (2006). Genomic DNA methylation: the mark and its mediators. Trends Biochem Sci *31*, 89-97.

Klose, R.J., Yamane, K., Bae, Y., Zhang, D., Erdjument-Bromage, H., Tempst, P., Wong, J., and Zhang, Y. (2006). The transcriptional repressor JHDM3A demethylates trimethyl histone H3 lysine 9 and lysine 36. Nature *442*, 312-316.

Kornberg, R.D., and Thomas, J.O. (1974). Chromatin structure; oligomers of the histones. Science *184*, 865-868.

Koster, H., Little, D.P., Luan, P., Muller, R., Siddiqi, S.M., Marappan, S., and Yip, P. (2007). Capture compound mass spectrometry: a technology for the investigation of small molecule protein interactions. Assay Drug Dev Technol *5*, 381-390.

Kotb, M., Mudd, S.H., Mato, J.M., Geller, A.M., Kredich, N.M., Chou, J.Y., and Cantoni, G.L. (1997). Consensus nomenclature for the mammalian methionine adenosyltransferase genes and gene products. Trends Genet *13*, 51-52.

Kouzarides, T. (2007). Chromatin modifications and their function. Cell *128*, 693-705.

Kramer, A., Ludwig, Y., Shahin, V., and Oberleithner, H. (2007). A pathway separate from the central channel through the nuclear pore complex for inorganic ions and small macromolecules. The Journal of biological chemistry *282*, 31437-31443.

Krauss, V., and Reuter, G. (2011). DNA methylation in Drosophila--a critical evaluation. Prog Mol Biol Transl Sci *101*, 177-191.

Krijt, J., Duta, A., and Kozich, V. (2009). Determination of S-Adenosylmethionine and S-Adenosylhomocysteine by LC-MS/MS and evaluation of their stability in mice tissues. J Chromatogr B Analyt Technol Biomed Life Sci *877*, 2061-2066.

Kucharski, R., Maleszka, J., Foret, S., and Maleszka, R. (2008). Nutritional control of reproductive status in honeybees via DNA methylation. Science *319*, 1827-1830.
Kunert, N., Marhold, J., Stanke, J., Stach, D., and Lyko, F. (2003). A Dnmt2-like protein mediates DNA methylation in Drosophila. Development *130*, 5083-5090.

Lachner, M., O'Sullivan, R.J., and Jenuwein, T. (2003). An epigenetic road map for histone lysine methylation. J Cell Sci *116*, 2117-2124.

Laemmli, U.K. (1970). Cleavage of structural proteins during the assembly of the head of bacteriophage T4. Nature *227*, 680-685.

Lanctot, C., Cheutin, T., Cremer, M., Cavalli, G., and Cremer, T. (2007). Dynamic genome architecture in the nuclear space: regulation of gene expression in three dimensions. Nature reviews Genetics *8*, 104-115.

Larsson, J., and Rasmuson-Lestander, A. (1998). Somatic and germline clone analysis in mutants of the S-adenosylmethionine synthetase encoding gene in Drosophila melanogaster. FEBS letters *427*, 119-123.

Larsson, J., Zhang, J., and Rasmuson-Lestander, A. (1996). Mutations in the Drosophila melanogaster gene encoding S-adenosylmethionine synthetase [corrected] suppress position-effect variegation. Genetics *143*, 887-896.

Lenz, T., Poot, P., Grabner, O., Glinski, M., Weinhold, E., Dreger, M., and Koster, H. (2010). Profiling of methyltransferases and other S-adenosyl-L-homocysteine-binding Proteins by Capture Compound Mass Spectrometry (CCMS). J Vis Exp.

Li, W., Han, Y., Tao, F., and Chong, K. (2011). Knockdown of SAMS genes encoding S-adenosyl-l-methionine synthetases causes methylation alterations of DNAs and histones and leads to late flowering in rice. J Plant Physiol *168*, 1837-1843.

Lin, C.H., Li, B., Swanson, S., Zhang, Y., Florens, L., Washburn, M.P., Abmayr, S.M., and Workman, J.L. (2008). Heterochromatin protein 1a stimulates histone H3 lysine 36 demethylation by the Drosophila KDM4A demethylase. Molecular cell *32*, 696-706.

Lin, C.H., Paulson, A., Abmayr, S.M., and Workman, J.L. (2012). HP1a targets the Drosophila KDM4A demethylase to a subset of heterochromatic genes to regulate H3K36me3 levels. PLoS One *7*, e39758.

Lin, D.W., Chung, B.P., and Kaiser, P. (2014). S-adenosylmethionine limitation induces p38 mitogen-activated protein kinase and triggers cell cycle arrest in G1. J Cell Sci *127*, 50-59.

Liu, M., Barnes, V.L., and Pile, L.A. (2016). Disruption of Methionine Metabolism in Drosophila melanogaster Impacts Histone Methylation and Results in Loss of Viability. G3 (Bethesda) *6*, 121-132.

Lloret-Llinares, M., Carre, C., Vaquero, A., de Olano, N., and Azorin, F. (2008). Characterization of Drosophila melanogaster JmjC+N histone demethylases. Nucleic Acids Res *36*, 2852-2863.

Lorbeck, M.T., Singh, N., Zervos, A., Dhatta, M., Lapchenko, M., Yang, C., and Elefant, F. (2010). The histone demethylase Dmel\Kdm4A controls genes required for life span and male-specific sex determination in Drosophila. Gene *450*, 8-17.

Lu, S.C. (2000). S-Adenosylmethionine. Int J Biochem Cell Biol *32*, 391-395.
Lu, S.C., and Mato, J.M. (2012). S-adenosylmethionine in liver health, injury, and cancer. Physiol Rev *92*, 1515-1542.
Luger, K., Mader, A.W., Richmond, R.K., Sargent, D.F., and Richmond, T.J. (1997). Crystal structure of the nucleosome core particle at 2.8 A resolution. Nature *389*, 251-260.

Luka, Z., Mudd, S.H., and Wagner, C. (2009). Glycine N-methyltransferase and regulation of S-adenosylmethionine levels. The Journal of biological chemistry *284*, 22507-22511.

Lyko, F., Ramsahoye, B.H., and Jaenisch, R. (2000). DNA methylation in Drosophila melanogaster. Nature *408*, 538-540.

Maenner, S., Muller, M., and Becker, P.B. (2012). Roles of long, non-coding RNA in chromosome-wide transcription regulation: lessons from two dosage compensation systems. Biochimie *94*, 1490-1498.

Maleszka, R. (2008). Epigenetic integration of environmental and genomic signals in honey bees: the critical interplay of nutritional, brain and reproductive networks. Epigenetics *3*, 188-192.

Malkowska, M., Kokoszynska, K., Rychlewski, L., and Wyrwicz, L. (2013). Structural bioinformatics of the general transcription factor TFIID. Biochimie *95*, 680-691.

Martinez-Balbas, M.A., Tsukiyama, T., Gdula, D., and Wu, C. (1998). Drosophila NURF-55, a WD repeat protein involved in histone metabolism. Proc Natl Acad Sci U S A *95*, 132-137.

Matthews, R.G., Koutmos, M., and Datta, S. (2008). Cobalamin-dependent and cobamide-dependent methyltransferases. Curr Opin Struct Biol *18*, 658-666.

Meier, J.L. (2013). Metabolic mechanisms of epigenetic regulation. ACS Chem Biol *8*, 2607-2621.

Mentch, S.J., Mehrmohamadi, M., Huang, L., Liu, X., Gupta, D., Mattocks, D., Gomez Padilla, P., Ables, G., Bamman, M.M., Thalacker-Mercer, A.E., *et al.* (2015). Histone Methylation Dynamics and Gene Regulation Occur through the Sensing of One-Carbon Metabolism. Cell Metab *22*, 861-873.

Metzger, E., Wissmann, M., Yin, N., Muller, J.M., Schneider, R., Peters, A.H., Gunther, T., Buettner, R., and Schule, R. (2005). LSD1 demethylates repressive histone marks to promote androgen-receptor-dependent transcription. Nature *437*, 436-439.

Mohan, M., Herz, H.M., Smith, E.R., Zhang, Y., Jackson, J., Washburn, M.P., Florens, L., Eissenberg, J.C., and Shilatifard, A. (2011). The COMPASS family of H3K4 methylases in Drosophila. Molecular and cellular biology *31*, 4310-4318.

Motorin, Y., and Helm, M. (2011). RNA nucleotide methylation. Wiley Interdiscip Rev RNA *2*, 611-631.

Murray, K. (1964). The Occurrence of Epsilon-N-Methyl Lysine in Histones. Biochemistry *3*, 10-15.

Obata, F., Kuranaga, E., Tomioka, K., Ming, M., Takeishi, A., Chen, C.H., Soga, T., and Miura, M. (2014). Necrosis-driven systemic immune response alters SAM metabolism through the FOXO-GNMT axis. Cell Rep *7*, 821-833.

Obata, F., and Miura, M. (2015). Enhancing S-adenosyl-methionine catabolism extends Drosophila lifespan. Nat Commun *6*, 8332.

Oermann, E.K., Wu, J., Guan, K.L., and Xiong, Y. (2012). Alterations of metabolic genes and metabolites in cancer. Semin Cell Dev Biol *23*, 370-380.

Okada, Y., Feng, Q., Lin, Y., Jiang, Q., Li, Y., Coffield, V.M., Su, L., Xu, G., and Zhang, Y. (2005). hDOT1L links histone methylation to leukemogenesis. Cell *121*, 167-178.

Olsen, J.V., de Godoy, L.M., Li, G., Macek, B., Mortensen, P., Pesch, R., Makarov, A., Lange, O., Horning, S., and Mann, M. (2005). Parts per million mass accuracy on an Orbitrap mass spectrometer via lock mass injection into a C-trap. Mol Cell Proteomics *4*, 2010-2021.

Ong, S.E., Mittler, G., and Mann, M. (2004). Identifying and quantifying in vivo methylation sites by heavy methyl SILAC. Nat Methods *1*, 119-126.

Padeken, J., Mendiburo, M.J., Chlamydas, S., Schwarz, H.J., Kremmer, E., and Heun, P. (2013). The nucleoplasmin homolog NLP mediates centromere clustering and anchoring to the nucleolus. Molecular cell *50*, 236-249.

Patnaik, D., Chin, H.G., Esteve, P.O., Benner, J., Jacobsen, S.E., and Pradhan, S. (2004). Substrate specificity and kinetic mechanism of mammalian G9a histone H3 methyltransferase. The Journal of biological chemistry *279*, 53248-53258.

Pedersen, M.T., and Helin, K. (2010). Histone demethylases in development and disease. Trends Cell Biol *20*, 662-671.

Phalke, S., Nickel, O., Walluscheck, D., Hortig, F., Onorati, M.C., and Reuter, G. (2009). Retrotransposon silencing and telomere integrity in somatic cells of Drosophila depends on the cytosine-5 methyltransferase DNMT2. Nature genetics *41*, 696-702.

Raddatz, G., Guzzardo, P.M., Olova, N., Fantappie, M.R., Rampp, M., Schaefer, M., Reik, W., Hannon, G.J., and Lyko, F. (2013). Dnmt2-dependent methylomes lack defined DNA methylation patterns. Proc Natl Acad Sci U S A *110*, 8627-8631.

Reik, W. (2007). Stability and flexibility of epigenetic gene regulation in mammalian development. Nature *447*, 425-432.

Reinhardt, H.C., and Yaffe, M.B. (2009). Kinases that control the cell cycle in response to DNA damage: Chk1, Chk2, and MK2. Curr Opin Cell Biol *21*, 245-255.

Reytor, E., Perez-Miguelsanz, J., Alvarez, L., Perez-Sala, D., and Pajares, M.A. (2009). Conformational signals in the C-terminal domain of methionine adenosyltransferase I/III determine its nucleocytoplasmic distribution. FASEB J *23*, 3347-3360.

Rinn, J.L., and Chang, H.Y. (2012). Genome regulation by long noncoding RNAs. Annu Rev Biochem *81*, 145-166.

Sakata, S.F., Okumura, S., Matsuda, K., Horikawa, Y., Maeda, M., Kawasaki, K., Chou, J.Y., and Tamaki, N. (2005). Effect of fasting on methionine adenosyltransferase expression and the methionine cycle in the mouse liver. J Nutr Sci Vitaminol (Tokyo) *51*, 118-123.

Saksouk, N., Simboeck, E., and Dejardin, J. (2015). Constitutive heterochromatin formation and transcription in mammals. Epigenetics Chromatin *8*, 3.

Schneider, I. (1972). Cell lines derived from late embryonic stages of Drosophila melanogaster. Journal of embryology and experimental morphology *27*, 353-365.
Schotta, G., Lachner, M., Sarma, K., Ebert, A., Sengupta, R., Reuter, G., Reinberg, D., and Jenuwein, T. (2004). A silencing pathway to induce H3-K9 and H4-K20 trimethylation at constitutive heterochromatin. Genes Dev *18*, 1251-1262.

Schubert, H.L., Blumenthal, R.M., and Cheng, X. (2003). Many paths to methyltransfer: a chronicle of convergence. Trends Biochem Sci *28*, 329-335.

Schwanhausser, B., Busse, D., Li, N., Dittmar, G., Schuchhardt, J., Wolf, J., Chen, W., and Selbach, M. (2011). Global quantification of mammalian gene expression control. Nature *473*, 337-342.

Scott, J.M. (1999). Folate and vitamin B12. Proc Nutr Soc *58*, 441-448.

Shevchenko, A., Wilm, M., Vorm, O., and Mann, M. (1996). Mass spectrometric sequencing of proteins silver-stained polyacrylamide gels. Anal Chem *68*, 850-858.

Shi, Y., Lan, F., Matson, C., Mulligan, P., Whetstine, J.R., Cole, P.A., Casero, R.A., and Shi, Y. (2004). Histone demethylation mediated by the nuclear amine oxidase homolog LSD1. Cell *119*, 941-953.

Shyh-Chang, N., Locasale, J.W., Lyssiotis, C.A., Zheng, Y., Teo, R.Y., Ratanasirintrawoot, S., Zhang, J., Onder, T., Unternaehrer, J.J., Zhu, H., *et al.* (2013). Influence of threonine metabolism on S-adenosylmethionine and histone methylation. Science *339*, 222-226.

Silverstein, R.A., and Ekwall, K. (2005). Sin3: a flexible regulator of global gene expression and genome stability. Curr Genet *47*, 1-17.

Simon, J.A., and Kingston, R.E. (2009). Mechanisms of polycomb gene silencing: knowns and unknowns. Nat Rev Mol Cell Biol *10*, 697-708.

Smith, E., and Collins, I. (2015). Photoaffinity labeling in target- and binding-site identification. Future Med Chem *7*, 159-183.

Smith, E., and Shilatifard, A. (2010). The chromatin signaling pathway: diverse mechanisms of recruitment of histone-modifying enzymes and varied biological outcomes. Molecular cell *40*, 689-701.

Staros, J.V., Bayley, H., Standring, D.N., and Knowles, J.R. (1978). Reduction of aryl azides by thiols: implications for the use of photoaffinity reagents. Biochem Biophys Res Commun *80*, 568-572.

Strahl, B.D., and Allis, C.D. (2000). The language of covalent histone modifications. Nature *403*, 41-45.

Struck, A.W., Thompson, M.L., Wong, L.S., and Micklefield, J. (2012). S-adenosyl-methionine-dependent methyltransferases: highly versatile enzymes in biocatalysis, biosynthesis and other biotechnological applications. Chembiochem *13*, 2642-2655.

Struys, E.A., Jansen, E.E., de Meer, K., and Jakobs, C. (2000). Determination of S-adenosylmethionine and S-adenosylhomocysteine in plasma and cerebrospinal fluid by stable-isotope dilution tandem mass spectrometry. Clin Chem *46*, 1650-1656.

Tahiliani, M., Koh, K.P., Shen, Y., Pastor, W.A., Bandukwala, H., Brudno, Y., Agarwal, S., Iyer, L.M., Liu, D.R., Aravind, L., *et al.* (2009). Conversion of 5-methylcytosine to 5-hydroxymethylcytosine in mammalian DNA by MLL partner TET1. Science *324*, 930-935.

Takayama, S., Dhahbi, J., Roberts, A., Mao, G., Heo, S.J., Pachter, L., Martin, D.I., and Boffelli, D. (2014). Genome methylation in D. melanogaster is found at specific short motifs and is independent of DNMT2 activity. Genome Res *24*, 821-830.

Tessarz, P., Santos-Rosa, H., Robson, S.C., Sylvestersen, K.B., Nelson, C.J., Nielsen, M.L., and Kouzarides, T. (2014). Glutamine methylation in histone H2A is an RNA-polymerase-I-dedicated modification. Nature *505*, 564-568.

Thoma, F., and Koller, T. (1977). Influence of histone H1 on chromatin structure. Cell *12*, 101-107.

Thomae, A.W., Schade, G.O., Padeken, J., Borath, M., Vetter, I., Kremmer, E., Heun, P., and Imhof, A. (2013). A pair of centromeric proteins mediates reproductive isolation in Drosophila species. Dev Cell *27*, 412-424.

Trojer, P., and Reinberg, D. (2007). Facultative heterochromatin: is there a distinctive molecular signature? Molecular cell *28*, 1-13.

Ulanovskaya, O.A., Zuhl, A.M., and Cravatt, B.F. (2013). NNMT promotes epigenetic remodeling in cancer by creating a metabolic methylation sink. Nat Chem Biol *9*, 300-306.

Varambally, S., Dhanasekaran, S.M., Zhou, M., Barrette, T.R., Kumar-Sinha, C., Sanda, M.G., Ghosh, D., Pienta, K.J., Sewalt, R.G., Otte, A.P., *et al.* (2002). The polycomb group protein EZH2 is involved in progression of prostate cancer. Nature *419*, 624-629.

Vaughn, J.L., Goodwin, R.H., Tompkins, G.J., and McCawley, P. (1977). The establishment of two cell lines from the insect Spodoptera frugiperda (Lepidoptera; Noctuidae). In vitro *13*, 213-217.

Vermeulen, M., Mulder, K.W., Denissov, S., Pijnappel, W.W., van Schaik, F.M., Varier, R.A., Baltissen, M.P., Stunnenberg, H.G., Mann, M., and Timmers, H.T. (2007). Selective anchoring of TFIID to nucleosomes by trimethylation of histone H3 lysine 4. Cell *131*, 58-69.

Villar-Garea, A., Forne, I., Vetter, I., Kremmer, E., Thomae, A., and Imhof, A. (2012). Developmental regulation of N-terminal H2B methylation in Drosophila melanogaster. Nucleic Acids Res *40*, 1536-1549.

Villar-Garea, A., Israel, L., and Imhof, A. (2008). Analysis of histone modifications by mass spectrometry. Curr Protoc Protein Sci *Chapter 14*, Unit 14 10.

Wang, H., Huang, Z.Q., Xia, L., Feng, Q., Erdjument-Bromage, H., Strahl, B.D., Briggs, S.D., Allis, C.D., Wong, J., Tempst, P., *et al.* (2001). Methylation of histone H4 at arginine 3 facilitating transcriptional activation by nuclear hormone receptor. Science *293*, 853-857.

Wang, Z., Zang, C., Rosenfeld, J.A., Schones, D.E., Barski, A., Cuddapah, S., Cui, K., Roh, T.Y., Peng, W., Zhang, M.Q., *et al.* (2008). Combinatorial patterns of histone acetylations and methylations in the human genome. Nature genetics *40*, 897-903.

Webby, C.J., Wolf, A., Gromak, N., Dreger, M., Kramer, H., Kessler, B., Nielsen, M.L., Schmitz, C., Butler, D.S., Yates, J.R., 3rd, *et al.* (2009). Jmjd6 catalyses lysyl-hydroxylation of U2AF65, a protein associated with RNA splicing. Science *325*, 90-93.

Weimann, M., Grossmann, A., Woodsmith, J., Ozkan, Z., Birth, P., Meierhofer, D., Benlasfer, N., Valovka, T., Timmermann, B., Wanker, E.E., *et al.* (2013). A Y2H-seq approach defines the human protein methyltransferase interactome. Nat Methods *10*, 339-342.

Wellen, K.E., Hatzivassiliou, G., Sachdeva, U.M., Bui, T.V., Cross, J.R., and Thompson, C.B. (2009). ATP-citrate lyase links cellular metabolism to histone acetylation. Science *324*, 1076-1080.

Wise, D.R., Ward, P.S., Shay, J.E., Cross, J.R., Gruber, J.J., Sachdeva, U.M., Platt, J.M., DeMatteo, R.G., Simon, M.C., and Thompson, C.B. (2011). Hypoxia promotes isocitrate dehydrogenase-dependent carboxylation of alpha-ketoglutarate to citrate to support cell growth and viability. Proc Natl Acad Sci U S A *108*, 19611-19616.

Worby, C.A., Simonson-Leff, N., and Dixon, J.E. (2001). RNA interference of gene expression (RNAi) in cultured Drosophila cells. Sci STKE *2001*, pl1.

Xia, M., Chen, Y., Wang, L.C., Zandi, E., Yang, H., Bemanian, S., Martinez-Chantar, M.L., Mato, J.M., and Lu, S.C. (2010). Novel function and intracellular localization of methionine adenosyltransferase 2beta splicing variants. The Journal of biological chemistry *285*, 20015-20021.

Xiao, B., Jing, C., Wilson, J.R., Walker, P.A., Vasisht, N., Kelly, G., Howell, S., Taylor, I.A., Blackburn, G.M., and Gamblin, S.J. (2003). Structure and catalytic mechanism of the human histone methyltransferase SET7/9. Nature *421*, 652-656.

Xu, Y.Z., Kanagaratham, C. and Radzioch, D. (2013). Chromatin Remodelling during host-bacterial pathogen interaction. Chromatin Remodelling, Dr. Danuta Radzioch (Ed.), ISBN: 978-953-51-1087-3.

Yun, M., Wu, J., Workman, J.L., and Li, B. (2011). Readers of histone modifications. Cell Res *21*, 564-578.

Zhang, G., Huang, H., Liu, D., Cheng, Y., Liu, X., Zhang, W., Yin, R., Zhang, D., Zhang, P., Liu, J., *et al.* (2015). N6-methyladenine DNA modification in Drosophila. Cell *161*, 893-906.

Zhang, T., Berrocal, J.G., Frizzell, K.M., Gamble, M.J., DuMond, M.E., Krishnakumar, R., Yang, T., Sauve, A.A., and Kraus, W.L. (2009). Enzymes in the NAD+ salvage pathway regulate SIRT1 activity at target gene promoters. The Journal of biological chemistry *284*, 20408-20417.

Zhang, X., Wen, H., and Shi, X. (2012). Lysine methylation: beyond histones. Acta Biochim Biophys Sin (Shanghai) *44*, 14-27.

Zhao, Y., and Garcia, B.A. (2015). Comprehensive Catalog of Currently Documented Histone Modifications. Cold Spring Harb Perspect Biol *7*, a025064.

Appendix

List 1: Sam-S interactors

Potential interaction partners with a $\log_2$ fold enrichment factor > 2 are listed:

Flybase ID	Name	$\log_2$ IP (Sam-S/Control)	Flybase ID	Name	$\log_2$ IP (Sam-S/Control)
FBgn0005278	Sam-S	28.0	FBgn0005617	msl-1	15.2
FBgn0036974	eRF1	27.8	FBgn0264089	sli	15.2
FBgn0004399	psq	26.3	FBgn0030342	CG10347	15.1
FBgn0028969	deltaCOP	26.1	FBgn0051158	Efa6	15.1
FBgn0032822	CG10466	26.0	FBgn0003575	su(s)	14.9
FBgn0039210	CG13625	25.2	FBgn0085413	CG34384	14.9
FBgn0010356	Taf5	23.8	FBgn0002783	mor	14.9
FBgn0035854	CG8005	23.7	FBgn0042111	CG18766	14.7
FBgn0035107	mri	23.2	FBgn0034763	RYBP	14.5
FBgn0010280	Taf4	23.1	FBgn0038047	CG5245	14.5
FBgn0000617	e(y)1	23.0	FBgn0013955	PR2	14.4
FBgn0022984	qkr58E-3	22.7	FBgn0039488	CG6066	14.4
FBgn0033051	dream	22.4	FBgn0002973	numb	14.4
FBgn0026083	CG4857	22.4	FBgn0031006	rictor	14.3
FBgn0086690	cp309	22.2	FBgn0053196	dp	14.3
FBgn0024909	Taf7	22.1	FBgn0261274	Ero1L	14.2
FBgn0037379	CG10979	22.1	FBgn0031678	CG31918	14.2
FBgn0022724	Taf8	21.5	FBgn0010342	Map60	14.2
FBgn0011290	Taf12	21.1	FBgn0259165	CG42270	14.1
FBgn0029775	Vsx1	21.1	FBgn0024977	CG2709	13.9
FBgn0011836	Taf2	21.1	FBgn0261836	Msp300	13.6
FBgn0039175	CG5706	21.0	FBgn0000212	brm	13.5
FBgn0032847	Taf13	20.9	FBgn0086895	pea	13.3
FBgn0052831	CG33695	20.5	FBgn0000210	br	13.3
FBgn0001994	crp	20.4	FBgn0017572	Mo25	13.3
FBgn0030007	CG2263	20.3	FBgn0030276	Dlic	13.2
FBgn0265998	Doa	20.0	FBgn0031534	CG2774	13.0
FBgn0002069	Aats-asp	19.9	FBgn0016075	vkg	12.4
FBgn0029936	CG4617	19.7	FBgn0036686	CG7728	11.8
FBgn0086350	tef	19.6	FBgn0265998	Doa	11.1
FBgn0003124	polo	19.5	FBgn0260952	Msp-300	10.1
FBgn0261119	Prp19	19.4	FBgn0000283	Cp190	9.6
FBgn0005674	Aats-glupro	19.3	FBgn0264695	Mhc	9.4
FBgn0034054	CG8366	19.2	FBgn0024836	stan	9.3
FBgn0028968	gammaCop	19.2	FBgn0044324	Chro	8.4
FBgn0002872	mu2	19.1	FBgn0030293	CG1737	8.3
FBgn0052479	CG32479	19.1	FBgn0259785	pzg	8.1

FBgn0004045	Yp1	19.1
FBgn0032149	CG4036	19.1
FBgn0000043	Act42A	19.1
FBgn0001108	Gl	18.8
FBgn0029887	CG3198	18.6
FBgn0004047	Yp3	18.5
FBgn0039209	CG13624	18.4
FBgn0011270	Pglym87	18.3
FBgn0035811	CG12262	18.3
FBgn0035424	CG11505	18.3
FBgn0039710	dgt1	18.3
FBgn0034858	eIF2B-delta	18.2
FBgn0032921	Mpp6	18.2
FBgn0030008	CG2129	18.2
FBgn0002521	pho	18.1
FBgn0011763	Dp	18.1
FBgn0038549	CG17802	18.0
FBgn0031186	CG14614	18.0
FBgn0022699	D19B	18.0
FBgn0003330	Sce	18.0
FBgn0259228	C3G	17.9
FBgn0030010	CG10959	17.9
FBgn0033663	ERp60	17.8
FBgn0031161	CG15445	17.8
FBgn0259712	CG42366	17.7
FBgn0261270	SelD	17.7
FBgn0037328	RpL35A	17.7
FBgn0033948	CG12863	17.6
FBgn0028965	A16	17.5
FBgn0032200	CG5676	17.5
FBgn0000709	flil	17.4
FBgn0030320	CG2247	17.4
FBgn0034029	eIF2B-gamma	17.3
FBgn0263593	Lpin	17.3
FBgn0052506	CG32506	17.3
FBgn0262714	Sap130	17.2
FBgn0004606	zfh1	17.2
FBgn0025874	Meics	17.1
FBgn0022943	Cbp20	17.1
FBgn0039743	CG7946	17.0
FBgn0028690	Rpn5	17.0
FBgn0039250	CG11120	16.8
FBgn0008635	betaCop	7.1
FBgn0028968	gammaCop	7.0
FBgn0003598	Su(var)3-7	6.9
FBgn0010355	Taf1	6.3
FBgn0034967	eIF-5A	5.9
FBgn0032521	CG7110	5.8
FBgn0041188	Atx2	5.5
FBgn0033212	CG1399	5.0
FBgn0033749	achi	4.8
FBgn0028737	Ef1beta	4.8
FBgn0029176	Ef1gamma	4.8
FBgn0026262	bip2	4.7
FBgn0039562	Gp93	4.4
FBgn0001990	wek	4.4
FBgn0015602	BEAF-32	4.3
FBgn0011291	Taf11	4.2
FBgn0010417	Taf6	4.2
FBgn0030364	CG15735	4.1
FBgn0010531	CCS	3.8
FBgn0003687	Tbp	3.8
FBgn0025725	alphaCop	3.8
FBgn0031040	CG14210	3.8
FBgn0040308	Jafrac2	3.8
FBgn0027496	epsilonCOP	3.7
FBgn0024227	ial	3.7
FBgn0000541	E(bx)	3.6
FBgn0003278	Rpl135	3.6
FBgn0032202	CG18619	3.6
FBgn0085451	CG34422	3.6
FBgn0033155	CG1845	3.6
FBgn0027378	MRG15	3.6
FBgn0030842	CG8557	3.5
FBgn0013263	Trl-PF	3.5
FBgn0028274	ns3	3.5
FBgn0036184	PCID2	3.4
FBgn0027605	Vps4	3.4
FBgn0025724	betaCop	3.3
FBgn0023172	RhoGEF2	3.3
FBgn0010607	l(2)05714	3.3
FBgn0085444	CG34415	3.3
FBgn0036973	CG5585	3.3
FBgn0022764	Sin3A	3.2

FBgn0000253	Cam	16.8
FBgn0033233	Kdm4A	16.7
FBgn0051368	CG31368	16.7
FBgn0027617	CG5808	16.6
FBgn0011661	Moe	16.6
FBgn0022027	Vps25	16.6
FBgn0015781	P5cr	16.5
FBgn0001185	her	16.4
FBgn0064122	CG33691	16.4
FBgn0037206	CG12768	16.3
FBgn0002787	Mov34	16.3
FBgn0026566	CG1307	16.2
FBgn0037856	CG4674	16.2
FBgn0267433	kl-5	16.1
FBgn0033191	CG1598	16.1
FBgn0029173	fu2	16.1
FBgn0032348	CG4751	15.9
FBgn0027500	spd-2	15.9
FBgn0028689	Rpn6	15.8
FBgn0038922	CG6439	15.8
FBgn0038981	CG5346	15.8
FBgn0010621	Cct5	15.6
FBgn0032475	Sfmbt	15.6
FBgn0014366	noi	15.6
FBgn0040227	eIF-3p66	15.6
FBgn0034230	CG4853	15.6
FBgn0264324	spg	15.6
FBgn0085208	CG34179	15.6
FBgn0027086	Aats-ile	15.5
FBgn0027279	l(1)G0196	15.5
FBgn0025458	BubR1	15.5
FBgn0030648	CG6340	15.5
FBgn0036258	CG5642	15.5
FBgn0264693	ens	15.4
FBgn0261385	scra	3.2
FBgn0002775	msl-3	3.2
FBgn0011335	l(3)j2D3	3.0
FBgn0024996	eIF2B-beta	2.9
FBgn0265991	Zasp52	2.9
FBgn0050020	CG30020	2.9
FBgn0058045	CG40045	2.8
FBgn0031118	RhoGAP	2.7
FBgn0015778	rin	2.7
FBgn0002645	Map205	2.7
FBgn0004167	kst	2.6
FBgn0031980	RpL36A	2.6
FBgn0000319	Chc	2.6
FBgn0265434	zip	2.5
FBgn0013733	shot	2.5
FBgn0027514	CG1024	2.5
FBgn0037621	CG9797	2.5
FBgn0004636	R	2.4
FBgn0037746	CG8478	2.4
FBgn0035001	slik	2.4
FBgn0034802	CG3800	2.4
FBgn0031229	CG3436	2.4
FBgn0033912	RpS23	2.4
FBgn0010411	RpS18	2.4
FBgn0027598	CG31012	2.3
FBgn0032987	RpL21	2.2
FBgn0010265	RpS13	2.2
FBgn0002781	mod(mdg4)	2.1
FBgn0024491	Bin1	2.1
FBgn0001291	Jra	2.1
FBgn0022768	Pp2C1	2.1
FBgn0014269	prod	2.1
FBgn0053526	PNUTS	2.1
FBgn0035422	RpL28	2.0

List 2: Microarray analysis

Listed are all genes that are upregulated ≥ 2 fold with a false discovery rate ≤ 0.05; fc = fold change

Flybase ID	sel.probeset.id	Name	log_2(fc)	Flybase ID	sel.probeset.id	Name	log_2(fc)
FBgn0031623	1624194_a_at	Taf12L	6.34	FBgn0015229	1628743_at	glec	1.30
FBgn0000565	1625276_a_at	Eip71CD	5.65	FBgn0041180	1634552_at	TepIV	1.30
FBgn0053468	1635486_at	CG33468	5.43	FBgn0086447	1632654_at	l(2)37Cg	1.29
FBgn0011746	1630502_at	ana	5.24	FBgn0032486	1637221_at	CG5705	1.29
FBgn0032136	1628049_at	CG15828	5.18	FBgn0020647	1637517_s_at	KrT95D	1.28
FBgn0004047	1631419_at	Yp3	4.55	FBgn0053108	1631039_at	CG33108	1.28
FBgn0037936	1622946_at	CG6908	4.25	FBgn0032670	1623201_at	CG5783	1.28
FBgn0032405	1623103_at	CG14946	4.21	FBgn0022800	1623418_at	Cad96Ca	1.27
FBgn0051642	1629787_at	CG31642	3.85	FBgn0037550	1638190_at	CG9667	1.27
FBgn0000279	1632719_at	CecC	3.77	FBgn0032191	1623989_at	CG5734	1.27
FBgn0034709	1641413_s_at	CG3074	3.74	FBgn0039687	1639034_at	CG7593	1.27
FBgn0033945	1635030_at	CG12868	3.68	FBgn0001330	1623496_at	kz	1.27
FBgn0037850	1639704_at	CG14695	3.61	FBgn0053158	1624658_at	CG33158	1.26
FBgn0032483	1623979_at	CG15482	3.49	FBgn0036570	1628335_at	CG5222	1.26
FBgn0033927	1639694_s_at	CR10102	3.48	FBgn0035996	1626220_at	CG3448	1.26
FBgn0042627	1639230_at	v(2)k05816	3.46	FBgn0036187	1623855_s_at	CG11660	1.26
FBgn0035434	1627327_at	dro5	3.37	FBgn0023542	1623733_at	Nmd3	1.26
FBgn0002733	1639900_at	HLHmbeta	3.34	FBgn0039328	1638852_at	CHKov2	1.26
FBgn0033115	1626851_at	Spn42De	3.27	FBgn0032935	1628475_at	CG8678	1.25
FBgn0011288	1638558_a_at	Snap25	3.20	FBgn0036819	1637720_at	dysb	1.25
FBgn0260660	1632932_a_at	mp	3.20	FBgn0033781	1627545_at	CG13319	1.25
FBgn0052195	1640590_at	CG32195	3.18	FBgn0030241	1637475_at	feo	1.25
FBgn0041087	1641598_at	wun2	3.15	FBgn0051694	1637307_at	CG31694	1.24
FBgn0261284	1627319_at	bou	3.13	FBgn0032922	1627050_at	CG9249	1.23
FBgn0052625	1623296_at	CG32625	3.08	FBgn0032161	1630640_at	CG4594	1.23
FBgn0260746	1624517_at	Ect3	2.96	FBgn0085446	1628465_a_at	CG34417	1.23
FBgn0026718	1625344_at	fu12	2.96	FBgn0052207	1632978_at	CR32207	1.22
FBgn0039108	1637358_at	CG10232	2.86	FBgn0052681	1633018_at	CG32681	1.22
FBgn0037973	1626248_at	CG18547	2.84	FBgn0033928	1632639_at	Arc2	1.22
FBgn0051633	1623426_at	CG31633	2.77	FBgn0031308	1627204_at	CG4749	1.22
FBgn0015541	1623503_at	sda	2.77	FBgn0053910	1623281_s_at	His2B:CG33910	1.21
FBgn0023549	1626727_at	Mct1	2.73	FBgn0061209	1623281_s_at	His2B:CG17949	1.21
FBgn0027499	1626478_at	wde	2.68	FBgn0053908	1623281_s_at	His2B:CG33908	1.21
FBgn0035480	1639452_at	CG14984	2.67	FBgn0053906	1623281_s_at	His2B:CG33906	1.21
FBgn0033134	1635370_at	Tsp42El	2.66	FBgn0053904	1623281_s_at	His2B:CG33904	1.21
FBgn0051279	1624609_at	CG31279	2.63	FBgn0053902	1623281_s_at	His2B:CG33902	1.21
FBgn0032520	1631756_at	CG10859	2.60	FBgn0053900	1623281_s_at	His2B:CG33900	1.21

FBgn0039277	1630217_at	CG13650	2.59
FBgn0051624	1630811_at	CG31624	2.57
FBgn0031516	1634129_at	CG9663	2.57
FBgn0027348	1634048_a_at	bgm	2.50
FBgn0043799	1628813_at	CG31381	2.49
FBgn0016032	1639406_at	lbm	2.49
FBgn0085438	1633516_at	CG34409	2.48
FBgn0039650	1633159_at	Mesh1	2.44
FBgn0052091	1640991_at	CG32091	2.44
FBgn0031365	1639313_at	CG17650	2.42
FBgn0036369	1633800_s_at	CG10089	2.41
FBgn0039651	1624296_at	CG14508	2.38
FBgn0032002	1632345_at	CG8353	2.36
FBgn0034950	1634631_at	Pask	2.32
FBgn0050010	1637118_at	CG30010	2.24
FBgn0039101	1626889_at	CG16710	2.20
FBgn0037817	1626022_at	Cyp12e1	2.19
FBgn0033926	1639180_at	Arc1	2.16
FBgn0051477	1636925_at	CG31477	2.13
FBgn0015565	1634074_a_at	yin	2.13
FBgn0003162	1639469_a_at	Pu	2.13
FBgn0035049	1623160_at	Mmp1	2.12
FBgn0039155	1628493_at	kal-1	2.11
FBgn0034005	1632299_at	alphaPS4	2.09
FBgn0040364	1634165_at	CG11378	2.06
FBgn0001142	1632852_s_at	Gs1	2.06
FBgn0034496	1631519_at	CG9143	2.05
FBgn0030004	1637127_at	CG10958	2.04
FBgn0033204	1630212_at	CG2065	2.02
FBgn0032981	1640207_at	CG3635	2.02
FBgn0036806	1624953_at	Cyp12c1	2.02
FBgn0031296	1624028_at	CG4415	2.01
FBgn0040602	1629116_at	CG14545	1.98
FBgn0039419	1629035_at	CG12290	1.97
FBgn0032620	1624937_at	CG12288	1.97
FBgn0002543	1636905_at	lea	1.97
FBgn0028373	1628363_at	inx3	1.94
FBgn0033153	1625139_at	Gadd45	1.94
FBgn0038595	1635282_at	CG7142	1.94
FBgn0032618	1626965_at	CG31743	1.92
FBgn0085342	1626965_at	CG34313	1.92
FBgn0037906	1630741_s_at	PGRP-LB	1.88
FBgn0053898	1623281_s_at	His2B:CG33898	1.21
FBgn0053896	1623281_s_at	His2B:CG33896	1.21
FBgn0053894	1623281_s_at	His2B:CG33894	1.21
FBgn0053892	1623281_s_at	His2B:CG33892	1.21
FBgn0053890	1623281_s_at	His2B:CG33890	1.21
FBgn0053888	1623281_s_at	His2B:CG33888	1.21
FBgn0053886	1623281_s_at	His2B:CG33886	1.21
FBgn0053884	1623281_s_at	His2B:CG33884	1.21
FBgn0053882	1623281_s_at	His2B:CG33882	1.21
FBgn0053880	1623281_s_at	His2B:CG33880	1.21
FBgn0053878	1623281_s_at	His2B:CG33878	1.21
FBgn0053876	1623281_s_at	His2B:CG33876	1.21
FBgn0053874	1623281_s_at	His2B:CG33874	1.21
FBgn0053872	1623281_s_at	His2B:CG33872	1.21
FBgn0053870	1623281_s_at	His2B:CG33870	1.21
FBgn0053868	1623281_s_at	His2B:CG33868	1.21
FBgn0058461	1623281_s_at	CR40461	1.21
FBgn0034266	1634872_at	CG4975	1.21
FBgn0034267	1634872_at	CG4984	1.21
FBgn0039485	1628173_at	CG17189	1.21
FBgn0034411	1633916_at	CG18605	1.21
FBgn0037481	1626266_at	MAGE	1.21
FBgn0030878	1632374_at	CG6769	1.21
FBgn0029093	1631493_at	cathD	1.20
FBgn0085203	1640652_at	CG34174	1.20
FBgn0053653	1631142_a_at	Caps	1.20
FBgn0033388	1624467_a_at	CG8046	1.19
FBgn0020909	1638146_at	Rtc1	1.19
FBgn0034422	1638539_at	CG7137	1.19
FBgn0051674	1638368_at	CG31674	1.19
FBgn0039404	1638970_at	CG14543	1.19
FBgn0052368	1636566_at	CG32368	1.19
FBgn0039305	1633856_at	CG11858	1.18
FBgn0039801	1624409_a_at	Npc2h	1.18
FBgn0052579	1634329_at	CG32579	1.18
FBgn0051800	1635027_at	CG31800	1.18
FBgn0037543	1633751_at	CG10903	1.17
FBgn0037923	1641375_at	CG6813	1.17
FBgn0036770	1624752_at	Prestin	1.17
FBgn0031114	1634714_at	cactin	1.16
FBgn0000043	1624471_s_at	Act42A	1.16
FBgn0036973	1627743_at	CG5585	1.16

FBgn0039620	1629346_at	CG1443	1.86
FBgn0041713	1625405_at	yellow-c	1.85
FBgn0035591	1625162_at	CG4611	1.84
FBgn0050046	1628232_at	CG30046	1.82
FBgn0028540	1632019_s_at	CG9008	1.82
FBgn0030816	1636835_at	CG16700	1.82
FBgn0040064	1636180_at	yip2	1.82
FBgn0259711	1632958_a_at	CG42365	1.81
FBgn0036035	1636192_at	CG18178	1.81
FBgn0036997	1625052_at	CG5955	1.80
FBgn0046776	1630660_at	CR14033	1.79
FBgn0036290	1626801_at	CG10638	1.78
FBgn0029986	1627619_at	CG15332	1.78
FBgn0040377	1635610_at	Vha36-3	1.77
FBgn0030518	1641025_at	CG11134	1.75
FBgn0030432	1630130_at	CG4404	1.75
FBgn0034915	1633284_at	eIF6	1.74
FBgn0025525	1624060_at	bab2	1.72
FBgn0031220	1634583_s_at	CG4822	1.72
FBgn0036036	1632139_at	CG14174	1.70
FBgn0036984	1632238_at	CG13248	1.70
FBgn0027843	1625185_at	CAH2	1.70
FBgn0000071	1623950_s_at	Ama	1.67
FBgn0259834	1624181_at	out	1.66
FBgn0052099	1633677_at	eap	1.65
FBgn0039049	1623849_s_at	CG6726	1.63
FBgn0031972	1639085_at	Wwox	1.63
FBgn0039854	1639484_at	CG1635	1.63
FBgn0051713	1635473_at	Apf	1.62
FBgn0038612	1624357_at	cona	1.61
FBgn0034140	1631225_at	CG8317	1.61
FBgn0037561	1639024_at	CG9630	1.61
FBgn0086910	1633807_at	l(3)neo38	1.60
FBgn0039553	1624438_at	CG5017	1.59
FBgn0033374	1628731_s_at	CG13741	1.59
FBgn0051472	1635552_s_at	CG31472	1.59
FBgn0038490	1627348_at	CG5285	1.59
FBgn0038974	1637336_at	CG5377	1.58
FBgn0038828	1634218_at	CG17270	1.58
FBgn0023214	1630707_at	edl	1.57
FBgn0037350	1638431_at	CG2911	1.57
FBgn0039640	1634302_s_at	CG14516	1.57
FBgn0029755	1629933_at	Sas10	1.16
FBgn0038436	1624528_at	Gyc-89Db	1.15
FBgn0003997	1640235_at	W	1.15
FBgn0051793	1631763_at	CG31793	1.15
FBgn0033919	1640747_s_at	CG8547	1.15
FBgn0000152	1640260_at	Axs	1.14
FBgn0027864	1636807_at	Ogg1	1.13
FBgn0039689	1640024_at	CG7598	1.13
FBgn0033605	1623322_at	CG9067	1.13
FBgn0039727	1633846_at	CG15523	1.13
FBgn0037960	1639045_at	mthl5	1.12
FBgn0034718	1641504_s_at	wdp	1.12
FBgn0015393	1640574_at	hoip	1.12
FBgn0034494	1629271_at	CG10444	1.12
FBgn0038673	1627911_at	CG14286	1.11
FBgn0028430	1640654_at	He	1.11
FBgn0037491	1636599_at	CG1227	1.10
FBgn0035063	1626337_at	Eap	1.10
FBgn0030582	1624168_at	CG14411	1.10
FBgn0259896	1639502_at	nimC1	1.10
FBgn0260745	1632298_s_at	mfas	1.10
FBgn0036145	1626684_at	CG7607	1.10
FBgn0031253	1637226_at	CG11885	1.10
FBgn0035346	1637605_s_at	CG1146	1.10
FBgn0261673	1632530_s_at	nemy	1.09
FBgn0038183	1629209_at	CG9286	1.09
FBgn0031713	1641134_at	CG7277	1.08
FBgn0036500	1640460_at	CG7275	1.08
FBgn0033836	1631549_s_at	CG18278	1.08
FBgn0260475	1631549_s_at	CG30059	1.08
FBgn0035889	1622892_s_at	mkg-p	1.08
FBgn0053057	1622892_s_at	CG33057	1.08
FBgn0034626	1639094_at	CG10795	1.08
FBgn0030189	1630975_at	CG2909	1.07
FBgn0041588	1630208_at	ligatin	1.07
FBgn0035588	1640492_at	CG10672	1.07
FBgn0038720	1627000_s_at	CG6231	1.07
FBgn0039564	1627837_at	CG5527	1.06
FBgn0032123	1641063_s_at	Oatp30B	1.06
FBgn0030000	1636433_at	CG2260	1.06
FBgn0034734	1630247_at	CG4554	1.06
FBgn0030410	1627409_at	CG15727	1.06

FBgn0042106	1639169_at	CG18754	1.56
FBgn0033615	1633565_at	CG7741	1.55
FBgn0032819	1640143_at	CG10463	1.55
FBgn0034761	1623364_at	CG4250	1.54
FBgn0051116	1629786_a_at	ClC-a	1.53
FBgn0037290	1633989_at	CG1124	1.52
FBgn0026721	1629572_a_at	fat-spondin	1.52
FBgn0030611	1623724_at	CG15027	1.51
FBgn0036181	1631700_at	Muc68Ca	1.51
FBgn0030340	1632086_at	CG15740	1.51
FBgn0004556	1639810_at	Dbp73D	1.50
FBgn0032668	1633142_at	CG17681	1.49
FBgn0031405	1631783_at	CG4267	1.49
FBgn0038590	1639409_at	CG12320	1.49
FBgn0030799	1634788_at	CG4872	1.48
FBgn0033234	1629732_at	CG8791	1.48
FBgn0016031	1640509_s_at	lama	1.48
FBgn0037440	1624185_at	CG1041	1.47
FBgn0035960	1641092_at	CG4942	1.47
FBgn0032162	1638090_at	CG4592	1.46
FBgn0038166	1629777_at	CG9588	1.45
FBgn0033205	1634019_at	CG2064	1.45
FBgn0010620	1636440_at	Sip1	1.44
FBgn0031805	1623438_at	CG9505	1.44
FBgn0026374	1634557_at	Rhp	1.44
FBgn0035918	1631019_at	Cdc6	1.43
FBgn0034225	1635447_at	veil	1.43
FBgn0033754	1635356_at	Ak6	1.43
FBgn0032793	1627330_at	CG10189	1.43
FBgn0063497	1637129_at	GstE3	1.42
FBgn0051278	1633190_at	CG31278	1.42
FBgn0039357	1626701_at	CG4743	1.42
FBgn0260744	1632259_at	Tango9	1.42
FBgn0010397	1629981_at	LamC	1.42
FBgn0032449	1628221_at	CG17036	1.40
FBgn0032946	1640729_s_at	nrv3	1.40
FBgn0259736	1628867_s_at	CG42390	1.40
FBgn0031611	1627938_at	CG17840	1.39
FBgn0034968	1627312_at	RpL12	1.39
FBgn0037490	1628507_at	CG10053	1.39
FBgn0039627	1631093_at	CG11837	1.38
FBgn0050460	1640703_at	CG30460	1.37
FBgn0051314	1627649_at	Neu3	1.05
FBgn0038744	1633088_at	CG4733	1.05
FBgn0034027	1640115_at	CG8187	1.05
FBgn0037526	1624666_at	CG10092	1.05
FBgn0030310	1628884_at	PGRP-SA	1.05
FBgn0026415	1635389_s_at	Idgf4	1.05
FBgn0051441	1640493_at	CG31441	1.05
FBgn0003888	1639503_at	betaTub60D	1.05
FBgn0039407	1634023_at	CG14544	1.04
FBgn0030610	1637159_at	CG9065	1.04
FBgn0038330	1625817_at	CG14868	1.04
FBgn0031052	1623874_at	CG14215	1.04
FBgn0032811	1633078_at	CG10268	1.04
FBgn0030481	1637048_at	CG1662	1.03
FBgn0033717	1637576_s_at	CG8839	1.03
FBgn0039114	1636510_a_at	Lsd-1	1.03
FBgn0035907	1633106_at	CG6662	1.03
FBgn0030457	1632182_at	CG12096	1.03
FBgn0053803	1626867_at	His3:CG33803	1.03
FBgn0051613	1626867_at	His3:CG31613	1.03
FBgn0053806	1626867_at	His3:CG33806	1.03
FBgn0053809	1626867_at	His3:CG33809	1.03
FBgn0053812	1626867_at	His3:CG33812	1.03
FBgn0053815	1626867_at	His3:CG33815	1.03
FBgn0053818	1626867_at	His3:CG33818	1.03
FBgn0053821	1626867_at	His3:CG33821	1.03
FBgn0053824	1626867_at	His3:CG33824	1.03
FBgn0053827	1626867_at	His3:CG33827	1.03
FBgn0053830	1626867_at	His3:CG33830	1.03
FBgn0053833	1626867_at	His3:CG33833	1.03
FBgn0053836	1626867_at	His3:CG33836	1.03
FBgn0053839	1626867_at	His3:CG33839	1.03
FBgn0053842	1626867_at	His3:CG33842	1.03
FBgn0053845	1626867_at	His3:CG33845	1.03
FBgn0053848	1626867_at	His3:CG33848	1.03
FBgn0053851	1626867_at	His3:CG33851	1.03
FBgn0053854	1626867_at	His3:CG33854	1.03
FBgn0053857	1626867_at	His3:CG33857	1.03
FBgn0053860	1626867_at	His3:CG33860	1.03
FBgn0053863	1626867_at	His3:CG33863	1.03
FBgn0053866	1626867_at	His3:CG33866	1.03
FBgn0259740	1641408_at	CG42394	1.02

FBgn0036754	1630347_at	CG5589	1.37	FBgn0037880	1639946_at	CG17726	1.02
FBgn0037809	1633680_at	CG12818	1.37	FBgn0040078	1635279_at	pont	1.02
FBgn0054003	1634806_at	nimB3	1.37	FBgn0029824	1630308_at	CG3726	1.02
FBgn0052640	1630842_s_at	CG32640	1.37	FBgn0086347	1641074_s_at	Myo31DF	1.02
FBgn0052641	1630842_s_at	CG32641	1.37	FBgn0037778	1636340_at	mtTFB2	1.02
FBgn0010039	1635701_at	GstD3	1.36	FBgn0035636	1627833_at	Cralbp	1.01
FBgn0027602	1627032_a_at	CG8611	1.35	FBgn0032781	1639553_at	CG9987	1.01
FBgn0051159	1633043_at	EF-G2	1.35	FBgn0039702	1633455_at	Vps16B	1.01
FBgn0002962	1632713_at	nos	1.34	FBgn0028695	1637349_at	Rpn1	1.00
FBgn0037354	1633503_at	CG12171	1.34	FBgn0086451	1630466_at	l(2)k09022	1.00
FBgn0020388	1627246_at	Pcaf	1.34	FBgn0037620	1636870_at	ranshi	1.00
FBgn0015376	1627253_at	cutlet	1.34	FBgn0037369	1631223_at	CG2100	1.00
FBgn0023479	1624957_a_at	Tequila	1.32	FBgn0037541	1629748_s_at	CG2747	1.00
FBgn0085470	1639494_at	CG34441	1.32	FBgn0001977	1627249_a_at	l(2)35Bg	1.00
FBgn0250903	1639494_at	Img	1.32	FBgn0036578	1627492_at	CG5018	0.99
FBgn0030796	1638807_s_at	CG4829	1.32	FBgn0053181	1634670_at	CG33181	0.99
FBgn0039774	1639396_s_at	CDase	1.30				

Listed are all genes that are downregulated ≥ 2 fold with a false discovery rate ≤ 0.05; fc = fold change

Flybase ID	sel.probeset.id	Name	log_2(fc)	Flybase ID	sel.probeset.id	Name	log_2(fc)
FBgn0002939	1632705_at	ninaD	-4.99	FBgn0027654	1626174_a_at	jdp	-1.55
FBgn0033268	1639597_at	Obp44a	-4.83	FBgn0031739	1636482_at	CG14005	-1.53
FBgn0031801	1623706_at	CG9498	-4.50	FBgn0039896	1633329_at	yellow-h	-1.53
FBgn0014455	1629222_at	Ahcy13	-4.07	FBgn0260749	1635202_s_at	Utx	-1.53
FBgn0005278	1624083_s_at	Sam-S	-3.92	FBgn0052817	1632762_s_at	CG32817	-1.52
FBgn0036467	1640683_at	CG12310	-3.43	FBgn0029524	1632762_s_at	CG3176	-1.52
FBgn0085359	1639737_at	CG34330	-3.41	FBgn0036454	1623767_at	CG17839	-1.50
FBgn0016756	1624727_s_at	Ubp64E	-3.39	FBgn0001225	1635044_at	Hsp26	-1.49
FBgn0036857	1623216_s_at	CG9629	-3.33	FBgn0040099	1634786_at	lectin-28C	-1.47
FBgn0040096	1637561_at	lectin-33A	-3.32	FBgn0002940	1634786_at	ninaE	-1.47
FBgn0030985	1625531_at	Obp18a	-3.22	FBgn0035084	1623388_at	CG15861	-1.47
FBgn0036169	1635028_s_at	Fuca	-3.22	FBgn0052380	1626584_a_at	SMSr	-1.43
FBgn0036170	1635028_s_at	CG11714	-3.22	FBgn0035721	1623437_at	CG9948	-1.43
FBgn0033821	1637367_at	CG10799	-3.19	FBgn0010042	1626136_at	GstD6	-1.43
FBgn0025697	1635522_a_at	santa-maria	-3.09	FBgn0034290	1640400_at	CG5773	-1.43
FBgn0260658	1633281_at	CG42541	-2.85	FBgn0037433	1628252_at	CG17919	-1.42
FBgn0043070	1634325_a_at	MESK2	-2.77	FBgn0051975	1635578_at	CG31975	-1.42
FBgn0011592	1623827_a_at	fra	-2.76	FBgn0051976	1635578_at	CG31976	-1.42
FBgn0001224	1641055_at	Hsp23	-2.75	FBgn0032082	1638462_at	CG18088	-1.41
FBgn0014135	1627135_at	bnl	-2.69	FBgn0013988	1634574_a_at	Strn-Mlck	-1.40

FBgn0050377	1625421_at	CG30377	-2.68	FBgn0036616	1625388_at	CG4893	-1.39
FBgn0041183	1637734_at	Tepl	-2.66	FBgn0027544	1636293_at	CG2217	-1.39
FBgn0035697	1623681_at	CG10163	-2.66	FBgn0024985	1624881_at	CG11448	-1.37
FBgn0011676	1625574_at	Nos	-2.65	FBgn0020309	1626018_a_at	crol	-1.36
FBgn0051778	1636682_at	CG31778	-2.63	FBgn0052529	1628469_a_at	CG32529	-1.34
FBgn0033978	1624101_at	Cyp6a23	-2.59	FBgn0016123	1636888_a_at	Aph-4	-1.34
FBgn0033924	1632731_at	CG8613	-2.51	FBgn0003520	1633016_a_at	stau	-1.33
FBgn0032024	1628144_at	CG14273	-2.49	FBgn0037623	1641304_s_at	CG9801	-1.33
FBgn0052984	1636449_at	CG32984	-2.47	FBgn0016126	1637380_s_at	CaMKI	-1.33
FBgn0010038	1630258_at	GstD2	-2.47	FBgn0028525	1624856_at	c(2)M	-1.33
FBgn0040503	1626144_at	CG7763	-2.40	FBgn0041607	1633765_at	asp-synthetase	-1.32
FBgn0028433	1637526_s_at	Ggamma30A	-2.38	FBgn0039109	1637983_s_at	CG10365	-1.32
FBgn0035496	1628332_at	CG14990	-2.38	FBgn0003076	1633803_at	Pgm	-1.31
FBgn0046322	1631486_at	p38c	-2.36	FBgn0085466	1626896_at	CG34437	-1.31
FBgn0020303	1629479_a_at	fok	-2.35	FBgn0003071	1634739_a_at	Pfk	-1.31
FBgn0035626	1631236_at	lin-28	-2.30	FBgn0030653	1634351_at	CG7860	-1.31
FBgn0037683	1623903_at	CG18473	-2.29	FBgn0052112	1628887_a_at	CG32112	-1.30
FBgn0034894	1640962_s_at	CG4091	-2.28	FBgn0039494	1641496_a_at	grass	-1.29
FBgn0001226	1628117_at	Hsp27	-2.25	FBgn0052027	1633520_at	CR32027	-1.29
FBgn0050148	1635894_at	CG30148	-2.25	FBgn0029167	1628018_at	Hml	-1.28
FBgn0000527	1639823_at	e	-2.25	FBgn0038088	1627073_a_at	CG10126	-1.27
FBgn0016715	1641722_at	Reg-2	-2.24	FBgn0042206	1627890_at	GstD10	-1.27
FBgn0036534	1632415_s_at	Dcp2	-2.24	FBgn0010395	1630699_at	betaInt-nu	-1.25
FBgn0036837	1626749_a_at	CG18135	-2.23	FBgn0035083	1624153_at	Tina-1	-1.23
FBgn0032820	1641066_s_at	fbp	-2.23	FBgn0001259	1639275_at	in	-1.23
FBgn0033830	1635913_at	CG10814	-2.23	FBgn0030244	1634136_at	CG2157	-1.23
FBgn0015038	1639495_at	Cyp9b1	-2.20	FBgn0020224	1626708_at	Cbl	-1.22
FBgn0031561	1628474_at	CG16712	-2.19	FBgn0004652	1631498_a_at	fru	-1.21
FBgn0038516	1631266_a_at	CG5840	-2.18	FBgn0032955	1626079_a_at	CG2201	-1.21
FBgn0086708	1634364_s_at	stv	-2.18	FBgn0034493	1640231_a_at	CG8908	-1.20
FBgn0051337	1626917_at	CG31337	-2.17	FBgn0020277	1626882_at	lush	-1.20
FBgn0038865	1631523_at	CG10824	-2.16	FBgn0004034	1633285_at	y	-1.19
FBgn0051092	1628032_a_at	LpR2	-2.14	FBgn0036862	1629811_at	CG9619	-1.19
FBgn0028494	1632465_s_at	CG6424	-2.13	FBgn0037560	1635469_at	CR18228	-1.19
FBgn0035312	1623022_at	CG15820	-2.11	FBgn0034997	1639637_a_at	CG3376	-1.18
FBgn0031580	1637589_at	CG15423	-2.08	FBgn0038099	1638935_at	CG7091	-1.17
FBgn0051997	1633712_at	CG31997	-2.07	FBgn0015600	1641048_a_at	toc	-1.17
FBgn0038846	1632045_at	CG5697	-2.06	FBgn0250911	1638162_s_at	CG42245	-1.16
FBgn0032652	1629324_at	CG6870	-2.05	FBgn0035357	1638162_s_at	MEP-1	-1.16
FBgn0051546	1624949_at	CG31546	-2.00	FBgn0003886	1623910_at	alphaTub85E	-1.16
FBgn0033519	1635263_at	CG11825	-1.99	FBgn0028993	1635675_at	scro	-1.15
FBgn0032021	1639596_at	CG7781	-1.99	FBgn0040322	1631633_a_at	GNBP2	-1.14

FBgn0032533	1638220_at	CG16888	-1.98	FBgn0027101	1633143_s_at	Dyrk3	-1.14
FBgn0039844	1626581_s_at	CG1607	-1.97	FBgn0031254	1623065_at	CG13692	-1.14
FBgn0001075	1624125_at	ft	-1.97	FBgn0003310	1638189_s_at	S	-1.14
FBgn0033584	1637758_at	CG7737	-1.94	FBgn0030326	1633607_at	CG2444	-1.12
FBgn0032900	1632212_at	CG14401	-1.92	FBgn0004893	1635803_s_at	bowl	-1.12
FBgn0024315	1628494_a_at	Picot	-1.89	FBgn0022160	1631474_s_at	Gpo-1	-1.12
FBgn0038309	1633393_at	CG6499	-1.88	FBgn0086758	1628005_at	chinmo	-1.11
FBgn0051531	1623254_s_at	CG31531	-1.88	FBgn0250876	1639542_at	Sema-5c	-1.11
FBgn0053346	1630555_at	CG33346	-1.87	FBgn0036302	1631040_at	sowah	-1.11
FBgn0051769	1624128_at	CG31769	-1.87	FBgn0037849	1633126_at	CG4596	-1.10
FBgn0031097	1640107_at	obst-A	-1.87	FBgn0027865	1631105_at	Tsp96F	-1.09
FBgn0036194	1625173_s_at	CG11652	-1.86	FBgn0033749	1630768_s_at	achi	-1.08
FBgn0030574	1634200_a_at	CG9413	-1.80	FBgn0063498	1641429_at	GstE2	-1.08
FBgn0038952	1635951_at	CG7069	-1.79	FBgn0023416	1625072_s_at	Ac3	-1.07
FBgn0086689	1638797_a_at	Hph	-1.79	FBgn0026616	1632936_at	alpha-Man-IIb	-1.07
FBgn0010223	1633439_at	Galpha73B	-1.79	FBgn0040230	1625931_at	dbo	-1.07
FBgn0003074	1638550_s_at	Pgi	-1.76	FBgn0039156	1627423_at	CG6178	-1.06
FBgn0038680	1629771_at	Cyp12a5	-1.76	FBgn0033304	1635110_at	Cyp6a13	-1.06
FBgn0052695	1641434_at	CG32695	-1.75	FBgn0003870	1636673_s_at	ttk	-1.06
FBgn0015513	1631013_at	mbc	-1.75	FBgn0037151	1628660_at	CG7130	-1.06
FBgn0000489	1635928_a_at	Pka-C3	-1.72	FBgn0039804	1641633_at	CG15544	-1.06
FBgn0001258	1635227_at	ImpL3	-1.71	FBgn0052115	1623963_at	CG32115	-1.05
FBgn0001230	1638872_at	Hsp68	-1.70	FBgn0033744	1631164_a_at	CG12370	-1.05
FBgn0031836	1641169_s_at	CG11050	-1.69	FBgn0000289	1630717_s_at	cg	-1.05
FBgn0040636	1635919_at	CG13255	-1.67	FBgn0030576	1626901_at	CG15890	-1.04
FBgn0031914	1626846_s_at	CG5973	-1.66	FBgn0029866	1633814_at	CG3842	-1.04
FBgn0000567	1634440_s_at	Eip74EF	-1.65	FBgn0034010	1638301_at	CG8157	-1.04
FBgn0052017	1634093_at	CG32017	-1.65	FBgn0022774	1627352_at	Oat	-1.04
FBgn0039932	1634195_at	CG11093	-1.65	FBgn0051216	1640214_at	Naam	-1.03
FBgn0015037	1638053_at	Cyp4p1	-1.63	FBgn0038014	1624414_at	CG10041	-1.03
FBgn0002773	1625071_a_at	Mlc2	-1.63	FBgn0005771	1625960_at	noc	-1.03
FBgn0000547	1627506_at	ed	-1.60	FBgn0259823	1624235_at	CG42404	-1.03
FBgn0001228	1629061_s_at	Hsp67Bb	-1.60	FBgn0039831	1628688_at	CG12054	-1.02
FBgn0001223	1629061_s_at	Hsp22	-1.60	FBgn0036134	1634587_s_at	fd68A	-1.02
FBgn0032637	1640348_at	CG5050	-1.60	FBgn0038037	1639944_at	Cyp9f2	-1.02
FBgn0031579	1640827_at	CG15422	-1.60	FBgn0017558	1629515_at	Pdk	-1.02
FBgn0039525	1633039_at	CG5646	-1.59	FBgn0000257	1629509_s_at	car	-1.02
FBgn0033949	1623555_at	CG10131	-1.59	FBgn0035895	1636276_at	Unr	-1.02
FBgn0052706	1641232_s_at	CG32706	-1.58	FBgn0027596	1623036_a_at	CG10249	-1.02
FBgn0030085	1641232_s_at	CG6999	-1.58	FBgn0021800	1624889_a_at	l(2)k16918	-1.01
FBgn0037646	1633770_at	CAHbeta	-1.57	FBgn0026084	1624931_at	cib	-1.01
FBgn0027578	1628258_at	CG14526	-1.57	FBgn0260399	1631785_at	gwl	-1.01

FBgn0051445	1633991_at	CG31445	-1.57	FBgn0029833	1627443_at	CG5941	-0.99
FBgn0066101	1637280_at	LpR1	-1.56	FBgn0015803	1639115_s_at	rtGEF	-0.99
FBgn0050035	1627582_a_at	Tret1-1	-1.55	FBgn0052485	1639640_at	CG32485	-0.99

List 3: Caprotec

In total, 2001 proteins were identified in SAH-CC_{aa} capturing experiments and 1696 proteins in SAH-CC_{aa} capturing experiments, respectively, with a log_2 fold enrichment factor > 2. Listed are the first 200 proteins identified in each experiment:

SAH-CC_{aa}			**SAH-CC_{bp}**		
Flybase ID	**Name**	**log_2 IP (Sam-S/Control)**	**Flybase ID**	**Name**	**log_2 IP (Sam-S/Control)**
FBgn0087021	Spc25	13.8	FBgn0038065	CG6359	17.1
FBgn0040964	CG18661	13.6	FBgn0003687	Tbp	11.7
FBgn0029885	CG3224	13.5	FBgn0028398	Taf10	11.6
FBgn0014022	Rlb1	13.0	FBgn0025638	Roc1a	11.6
FBgn0085192	CG34163	12.8	FBgn0028411	Nxt1	11.5
FBgn0037061	CG12975	12.7	FBgn0001216	Hsc70-1	11.2
FBgn0032822	CG10466	12.4	FBgn0029936	CG4617	11.2
FBgn0021765	scu	12.1	FBgn0035624	Eaf6	11.1
FBgn0051365	CG31365	12.0	FBgn0039874	CG2135	11.0
FBgn0028398	Taf10	12.0	FBgn0032202	CG18619	10.9
FBgn0031390	tho2	12.0	FBgn0035033	CG3548	10.7
FBgn0036254	CG5645	11.8	FBgn0014879	Set	10.7
FBgn0031873	Gas41	11.7	FBgn0037752	RpS29	10.6
FBgn0004363	porin	11.7	FBgn0030680	CG8944	10.6
FBgn0024963	GluClalpha	11.5	FBgn0015299	Ssb-c31a	10.6
FBgn0032847	Taf13	11.5	FBgn0022027	Vps25	10.5
FBgn0039735	CG7911	11.5	FBgn0001297	kay	10.4
FBgn0042213	CG18731	11.4	FBgn0043012	AP-2sigma	10.4
FBgn0030048	CG12112	11.4	FBgn0051184	LSm3	10.4
FBgn0032202	CG18619	11.4	FBgn0035036	CG4707	10.3
FBgn0053107	CG33107	11.3	FBgn0038043	CG17202	10.3
FBgn0043002	Chrac-14	11.3	FBgn0024909	Taf7	10.3
FBgn0016700	Rab1	11.3	FBgn0005640	Eip63E	10.3
FBgn0039943	CG17168	11.2	FBgn0031047	CG14213	10.2
FBgn0026250	eIF-1A	11.1	FBgn0052595	CG32595	10.2
FBgn0033527	CG11777	11.1	FBgn0037439	CG10286	10.1
FBgn0022288	l(2)09851	11.0	FBgn0003511	Sry-beta	10.0
FBgn0033381	GstE13	11.0	FBgn0031603	CG15432	10.0
FBgn0033571	Rpb5	11.0	FBgn0031437	p16-ARC	9.9
FBgn0003687	Tbp	11.0	FBgn0038787	CG4360	9.9
FBgn0031603	CG15432	10.9	FBgn0029867	CG3847	9.8
FBgn0030093	dalao	10.9	FBgn0032924	CG9247	9.8
FBgn0026582	Hmg-2	10.9	FBgn0030142	CG3004	9.8
FBgn0035063	Eap	10.9	FBgn0039977	CG17454	9.7

FBgn0026441	ear	10.9
FBgn0037087	CG7519	10.9
FBgn0032487	Ski6	10.8
FBgn0035110	thoc7	10.8
FBgn0038235	CG8461	10.8
FBgn0029800	lin-52	10.8
FBgn0035624	Eaf6	10.8
FBgn0037543	CG10903	10.7
FBgn0020620	RN-tre	10.7
FBgn0005617	msl-1	10.6
FBgn0036342	CG11279	10.6
FBgn0025185	az2	10.6
FBgn0039163	CG5515	10.6
FBgn0029857	wuho	10.6
FBgn0011290	Taf12	10.5
FBgn0031782	WDR79	10.5
FBgn0038787	CG4360	10.4
FBgn0036405	CG6833	10.4
FBgn0029094	asf1	10.3
FBgn0024909	Taf7	10.3
FBgn0032016	CG7818	10.3
FBgn0038389	CG5516	10.2
FBgn0004636	R	10.2
FBgn0031003	CG7889	10.1
FBgn0003660	Syb	10.1
FBgn0038805	TFAM	10.1
FBgn0063497	GstE3	10.1
FBgn0027495	CG8378	10.1
FBgn0003360	sesB	10.1
FBgn0011289	TfIIA-L	10.0
FBgn0032725	Nedd8	10.0
FBgn0014009	Rab2	10.0
FBgn0010213	Sod2	10.0
FBgn0031832	CG9596	10.0
FBgn0020235	ATPsyn-gamma	9.9
FBgn0031909	CG5181	9.9
FBgn0011207	pelo	9.9
FBgn0037342	CG2931	9.9
FBgn0039827	CG1544	9.9
FBgn0003612	Su(var)2-10	9.9
FBgn0262732	mbf1	9.9
FBgn0259483	Mob4	9.9
FBgn0053107	CG33107	9.7
FBgn0023212	Elongin-B	9.7
FBgn0031782	WDR79	9.6
FBgn0038546	CG7379	9.5
FBgn0030048	CG12112	9.5
FBgn0031238	CG3645	9.4
FBgn0035149	MED30	9.4
FBgn0015521	oho23B	9.4
FBgn0026749	Yippee	9.4
FBgn0010041	GstD5	9.4
FBgn0003330	Sce	9.4
FBgn0015925	csul	9.3
FBgn0034923	Upf3	9.3
FBgn0000615	exu	9.3
FBgn0025634	CG13367	9.2
FBgn0011290	Taf12	9.2
FBgn0020249	stck	9.2
FBgn0001133	grau	9.2
FBgn0004049	yrt	9.2
FBgn0023542	Nmd3	9.2
FBgn0261067	LSm1	9.2
FBgn0030788	Sap30	9.2
FBgn0025790	TBPH	9.1
FBgn0039250	CG11120	9.1
FBgn0051855	CG31855	9.0
FBgn0032321	YL-1	9.0
FBgn0005278	Sam-S	9.0
FBgn0036395	CG17361	9.0
FBgn0035725	Mis12	9.0
FBgn0051955	CG31955	9.0
FBgn0003134	Pp1alpha-96A	9.0
FBgn0033624	CG12384	9.0
FBgn0261238	Alh	8.9
FBgn0036134	Mnf-PK	8.9
FBgn0043002	Chrac-14	8.9
FBgn0030314	CG11696	8.9
FBgn0051974	CG31974	8.8
FBgn0039321	CG10550	8.8
FBgn0039691	CG1972	8.8
FBgn0031711	CG6907	8.8
FBgn0033566	CG18004	8.7
FBgn0039642	CG11882	8.7

FBgn0038519	Prx3	9.9
FBgn0003042	Pc	9.8
FBgn0062442	CG1458	9.8
FBgn0266710	hog	9.8
FBgn0037255	Fip1	9.8
FBgn0037773	CG5359	9.8
FBgn0026324	Taf10b	9.8
FBgn0038795	CG4335	9.8
FBgn0032509	CG6523	9.8
FBgn0039110	RanBP3	9.8
FBgn0261792	snRNP-U1-C	9.8
FBgn0031263	CG2789	9.7
FBgn0052343	Atac3	9.7
FBgn0259742	CG42360	9.7
FBgn0030057	Ppt1	9.7
FBgn0036107	CG7949	9.7
FBgn0014879	Set	9.7
FBgn0033879	CG6543	9.7
FBgn0031893	CG4495	9.7
FBgn0028926	NC2beta	9.6
FBgn0262524	ver	9.6
FBgn0032921	Mpp6	9.6
FBgn0036451	CG9425	9.6
FBgn0050096	CG30096	9.6
FBgn0032346	Csl4	9.6
FBgn0038666	Smu1	9.6
FBgn0037874	Tctp	9.6
FBgn0038369	Arpc3A	9.6
FBgn0053801	His1:CG33801	9.5
FBgn0028479	Mtpalpha	9.5
FBgn0033341	MrgBP	9.5
FBgn0050499	CG30499	9.5
FBgn0041191	Rheb	9.5
FBgn0262114	RanBPM	9.5
FBgn0265192	Snp-PG	9.5
FBgn0032354	CG4788	9.5
FBgn0031238	CG3645	9.5
FBgn0014010	Rab5-PI	9.5
FBgn0010704	rti	9.4
FBgn0032634	Rpb11	9.4
FBgn0031678	CG31918	9.4
FBgn0038767	trem	9.4
FBgn0023097	bon	8.7
FBgn0004901	Prat	8.7
FBgn0259228	C3G	8.7
FBgn0025394	CG32810	8.6
FBgn0036916	Mtr3	8.6
FBgn0033716	Den1	8.6
FBgn0026582	CG9418	8.6
FBgn0036239	Pop2	8.6
FBgn0004652	fru	8.6
FBgn0036263	thoc6	8.6
FBgn0014467	CrebB-17A-PJ	8.6
FBgn0040346	CG3704	8.5
FBgn0041781	SCAR	8.5
FBgn0035902	CG6683	8.5
FBgn0031186	CG14614	8.5
FBgn0261456	hpo	8.5
FBgn0261394	Pros29	8.4
FBgn0033806	CG4616	8.4
FBgn0036237	viaf	8.4
FBgn0028387	chm	8.4
FBgn0260390	CG42516	8.4
FBgn0003141	pr	8.4
FBgn0034814	CG9890	8.4
FBgn0086350	tef	8.4
FBgn0044020	Roc2	8.4
FBgn0037659	CG11033	8.4
FBgn0032940	Mondo	8.4
FBgn0030789	Rrp45	8.4
FBgn0024364	CG11417	8.3
FBgn0054008	CG34008	8.3
FBgn0032156	CG13124-PJ	8.3
FBgn0037379	CG10979	8.3
FBgn0030269	CG18292	8.3
FBgn0014870	Psi	8.3
FBgn0010421	TfIIFbeta	8.3
FBgn0031459	CG2862	8.3
FBgn0020510	Abi	8.2
FBgn0037943	CG14722	8.2
FBgn0034158	CG5522-PF	8.2
FBgn0032390	dgt2	8.2
FBgn0027259	Kmn1	8.2
FBgn0035158	CG13895	8.2

FBgn0011016	SsRbeta	9.4
FBgn0050185	CG30185	9.4
FBgn0026373	RpII33	9.4
FBgn0033092	CG9422	9.3
FBgn0023517	Pgam5	9.3
FBgn0034425	CG11906	9.3
FBgn0036104	CG6418	9.3
FBgn0030451	CG15717	9.3
FBgn0031485	CG9643	9.3
FBgn0036292	CG10646	9.3
FBgn0036973	Rbbp5	9.3
FBgn0001612	Grip91	9.3
FBgn0031309	Tfb4	9.2
FBgn0260390	CG42516	9.2
FBgn0003141	pr	9.2
FBgn0030334	Karl	9.2
FBgn0035035	CG3570	9.2
FBgn0033162	CG1707	9.2
FBgn0026873	MED18	9.2
FBgn0030206	CG2889	9.2
FBgn0036302	sowah	9.2
FBgn0029887	CG3198	9.2
FBgn0036891	CG9372	9.2
FBgn0033233	Kdm4A	9.2
FBgn0261394	Prosalpha3	9.1
FBgn0032321	YL-1	9.1
FBgn0038020	GstD9	9.1
FBgn0024558	Dph5	9.1
FBgn0261562	CG42676	9.1
FBgn0015374	crl	9.1
FBgn0033529	CG17765	9.1
FBgn0003205	Ras85D	9.1
FBgn0036685	CG6664	9.0
FBgn0038043	CG17202	9.0
FBgn0035158	CG13895	9.0
FBgn0036395	CG17361	9.0
FBgn0015286	Rala	9.0
FBgn0015797	Rab6	9.0
FBgn0030611	CG15027	9.0
FBgn0013275	Hsp70Aa	9.0
FBgn0039972	CG17018	9.0
FBgn0039306	RIOK2	9.0
FBgn0053520	Rpb4-PF	8.2
FBgn0032882	ns4	8.2
FBgn0038666	CG5451	8.1
FBgn0039654	Brd8	8.1
FBgn0031494	CG17219	8.1
FBgn0030322	CG15220	8.1
FBgn0043070	MESK2	8.1
FBgn0037317	CG14667	8.1
FBgn0086758	chinmo	8.1
FBgn0015569	alpha-Est10	8.1
FBgn0000257	car	8.1
FBgn0036342	CG11279	8.0
FBgn0034573	CG3295	8.0
FBgn0036909	CG15881	8.0
FBgn0031776	CG13993	8.0
FBgn0031873	Gas41	7.9
FBgn0037638	CG8379	7.9
FBgn0033019	CG10395	7.9
FBgn0033715	CG8490	7.9
FBgn0039403	Sld5	7.9
FBgn0028665	VhaAC39	7.9
FBgn0036249	CG11560	7.9
FBgn0030093	dalao	7.9
FBgn0061515	endos	7.9
FBgn0030877	Arp8	7.9
FBgn0032725	Nedd8	7.8
FBgn0017453	Zn72D	7.8
FBgn0038307	mRpS10	7.8
FBgn0035639	CG5537	7.8
FBgn0000499	dsh	7.8
FBgn0015816	Slh-PF	7.8
FBgn0035251	CG7967	7.8
FBgn0034519	CG18065	7.8
FBgn0259982	l(2)35Cc	7.8
FBgn0035424	CG11505	7.8
FBgn0036135	mRpL2	7.8
FBgn0032634	Rpb11	7.8
FBgn0035063	Eap	7.8
FBgn0031875	CG3430	7.8
FBgn0013531	MED20	7.8
FBgn0265082	Cdep	7.8
FBgn0052016	CG32016	7.7

FBgn0017550	Rga	8.9
FBgn0040467	Dip1	8.9
FBgn0031610	CG15436	8.9
FBgn0039210	CG13625	8.9
FBgn02631	psq	8.9
FBgn0036911	Fibp	8.9
FBgn0037617	CG8145	8.9
FBgn0015818	Spx	8.9
FBgn0035726	CG9953	8.9
FBgn0001123	Galphas	8.8
FBgn0035356	CG16986	8.8
FBgn0004855	RpII15	8.8
FBgn0036277	CG10418	8.8
FBgn0037354	CG12171	8.8
FBgn0029861	CG3815	8.8
FBgn0027259	Kmn1	8.8
FBgn0042712	HBS1	8.8
FBgn0032250	holn1	8.8
FBgn0085208	CG34179	8.8
FBgn0001974	l(2)35Bd	8.8
FBgn0263490	mld-PF	8.7
FBgn0019949	Cdk9	8.7
FBgn0030680	CG8944	8.7
FBgn0004638	drk	8.7
FBgn0035210	msd5	8.7
FBgn0031977	baf	8.7
FBgn0030648	CG6340	8.7
FBgn0034300	CG5098	8.7
FBgn0015789	Rab10	8.7
FBgn0036354	Poc1	8.7
FBgn0039250	Mink	8.7
FBgn0038966	pinta	8.7
FBgn0027590	GstE12	8.7
FBgn0031608	CG15435	8.6
FBgn0261019	moi	8.6
FBgn0035923	CG6511	8.6
FBgn0030316	CG11695	8.6
FBgn0037670	CG8436	8.6
FBgn0036564	Taspase1	7.7
FBgn0031320	CG5126	7.7
FBgn0039509	bigmax	7.7
FBgn0028292	ric8a	7.7
FBgn0035996	CG3448	7.7
FBgn0032229	CG5045	7.7
FBgn0051713	Apf	7.7
FBgn0030364	CG15735	7.7
FBgn0260229	CG42503	7.7
FBgn0032258	CG7456	7.7
FBgn0024833	AP-47	7.7
FBgn0043842	Yeti	7.6
FBgn0034617	CG9754	7.6
FBgn0031610	CG15436	7.6
FBgn0026192	par-6	7.6
FBgn0053300	Muc30E	7.6
FBgn0034210	CG6568	7.6
FBgn0035107	mri	7.6
FBgn0037655	CG11984-PI	7.6
FBgn0031947	CG7154	7.6
FBgn0013759	CASK	7.6
FBgn0002521	pho	7.6
FBgn0026873	MED18	7.6
FBgn0025806	Rap2l	7.6
FBgn0037613	Cks85A	7.6
FBgn0015617	Cdk7	7.6
FBgn0046222	CG1109	7.5
FBgn0037891	CG5214	7.5
FBgn0036697	rogdi	7.5
FBgn0030731	CG3415	7.5
FBgn0028342	l(1)G0230	7.5
FBgn0260444	CG18616	7.5
FBgn0016984	sktl	7.5
FBgn0000139	ash2	7.5
FBgn0040929	CG12659	7.5
FBgn0262737	mub	7.5
FBgn0003744	trc	7.5
FBgn0038805	TFAM	7.5

List 4: *Drosophila melanogaster* methylome

Identified methylation sites on lysine (K) and arginine (R) residues are listed:

Methyl-K				Methyl-R			
Class	**Name_Modification**	**Score H**	**Score L**	**Class**	**Name**	**Score H**	**Score L**
A1	sesB_K_58_di	130.06	132.44	A1	Hsc70-5_R_513_me	167.73	233.37
A1	sesB_K_58_me	107.61	95.43	A1	Pep_R_117_di	130.66	136.57
A1	sesB_K_64_me	107.61	95.43	A1	SmB_R_112_di	113.73	139.17
A1	dys_K_6_me	98.94	83.86	A1	Ars2_R_51_di	105.08	67.14
A1	brm_K_1052_tr	92.30	77.91	A1	dys_R_7_me	98.94	83.86
A1	sle_K_314_me	90.63	124.23	A1	Pep_R_87_di	90.65	76.16
A1	SmD3_K_99_me	72.93	53.68	A1	Pep_R_87_me	83.25	69.15
A1	Ef1alpha100E_K_55_di	72.09	192.15	A1	Pep_R_95_me	83.25	69.15
A1	Ef1alpha100E_K_318_tr	15.64	96.31	A1	SmD3_R_97_di	82.29	53.68
A2	Cdc5_K_165_me	47.08	60.91	A1	Ref1_R_26_di	75.82	96.60
A2	MRP_K_543_tr	40.00	29.09	A1	SmD3_R_97_me	72.93	53.68
A2	CG15100_K_655_me	29.57	19.48	A1	Bap60_R_15_me	69.45	75.82
A2	cert_K_323_me	19.76	18.75	A1	CG7878_R_683_me	65.40	63.41
A2	CG3530_K_489_me	18.78	31.07	A1	CG7878_R_686_me	65.40	63.41
A2	mRpS14_K_175_me	14.56	10.33	A1	caz_R_259_me	64.45	90.71
A2	Spt6_K_668_tr	13.05	13.58	A1	caz_R_223_di	63.89	79.77
A2	dup_K_723_tr	12.05	14.67	A1	ncd_R_138_me	58.67	78.69
A2	sesB_K_58_tr	11.28	33.84	A1	caz_R_223_me	58.07	65.47
A2	CG10208_K_187_di	9.69	3.89	A1	caz_R_229_me	58.07	65.47
A2	Vps2_K_108_di	8.95	3.42	A1	SmB_R_108_me	53.25	106.01
A2	Vps2_K_108_me	8.95	11.53	A2	CG6962_R_201_me	55.19	28.21
A2	Osi12_K_177_tr	8.30	1.90	A2	Ref1_R_214_di	47.89	55.72
A2	CG9740_K_158_me	4.30	56.56	A2	Ref1_R_26_me	36.85	30.00
A2	cue_K_231_di	3.89	3.89	A2	Ref1_R_33_me	36.85	30.00
A2	Mcm2_K_670_di	3.57	13.05	A2	Pep_R_105_di	36.11	24.56
A2	CG10289_K_461_di	3.42	3.42	A2	mre11_R_571_di	34.69	46.38
B	Ef1alpha48D_K_55_di	153.75	-	A2	CG7878_R_683_di	34.39	8.60
B	Ef1alpha48D_K_318_tr	134.48	-	A2	CG6841_R_32_me	34.01	47.81
B	CG30339_K_127_me	115.18	-	A2	CG6841_R_40_me	34.01	47.81
B	CG7362_K_771_tr	97.80	-	A2	CG11337-RD_R_760_me	32.61	42.00
B	Msp300_K_7084_di	89.81	-	A2	Pep_R_98_di	31.42	26.81
B	CG8129_K_107_tr	85.96	-	A2	CG4078_R_623_me	28.40	28.40
B	E(spl)_K_51_tr	83.73	-	A2	rod_R_1945_me	27.74	3.70
B	Sb_K_23_me	77.74	-	A2	Cyp6a20_R_366_me	22.15	9.91
B	alt_K_205_me	77.19	-	A2	nop5_R_183_di	21.51	21.51
B	CG4169_K_415_me	75.80	-	A2	Pep_R_105_me	21.35	58.32
B	CG8407-RA_K_62_di	75.38	-	A2	Pep_R_112_me	21.35	58.32
B	DNApol-alpha180_K_1257_tr	74.16	-	A2	lig_R_241_di	20.65	32.15
B	CG17928_K_400_di	69.72	-	A2	stwl_R_689_me	19.82	9.06
B	CG17387-RA_K_268_tr	67.73	-	A2	lig_R_241_me	15.88	16.14
B	CG2124_K_587_tr	66.07	-	A2	lig_R_248_me	15.88	16.14
B	CG6800_K_146_di	61.24	-	A2	NaCP60E_R_1577_di	14.88	19.13
B	Cyp12a4_K_61_me	60.55	-	A2	vig_R_384_me	8.10	47.89
B	CalpA_K_605_di	59.51	-	A2	vig_R_387_me	8.10	47.89
B	CG1970-RA_K_362_tr	59.19	-	A2	Rab35_R_56_di	7.57	5.16

B	CG10361-RA_K_221_me	57.46	-	A2	AdamTS-A_R_1664_me	4.52	4.52
B	CG9754_K_156_me	57.41	-	A2	AGBE_R_549_me	3.42	3.42
B	CG9754_K_159_me	57.41	-	A2	CG32245_R_11_me	3.42	0.00
B	Msp300_K_6222_di	54.61	-	A2	me31B_R_280_me	3.04	3.04
B	zip_K_1524_me	54.42	-	A2	CG31760_R_824_me	0.00	8.22
B	CG12428_K_493_tr	53.97	-	B	Pep_R_140_di	130.66	-
B	CG17652_K_128_me	53.17	-	B	CG4495_R_363_di	118.71	-
B	pad_K_737_di	53.17	-	B	ncd_R_138_di	92.58	-
B	CG17454_K_30_me	51.82	-	B	Pep_R_110_di	90.65	-
B	inaD_K_236_tr	51.73	-	B	Pep_R_110_me	83.25	-
B	Hmr_K_1303_di	48.88	-	B	Pep_R_118_me	83.25	-
B	Hmr_K_1316_di	48.88	-	B	CG30183_R_273_me	77.38	-
B	Tkr_K_806_me	48.79	-	B	Pabp2_R_162_di	75.02	-
B	CG7094-RA_K_260_di	48.74	-	B	Pep_R_128_di	71.56	-
B	Hsp70Ab_K_326_di	47.82	-	B	Pabp2_R_162_me	68.48	-
B	dor_K_523_di	46.41	-	B	Pabp2_R_164_me	68.48	-
B	l(3)psg2_K_375_me	45.86	-	B	mre11_R_579_di	68.46	-
B	Ndc80_K_557_me	45.86	-	B	Dys_R_2813_me	63.09	-
B	CG12713_K_76_di	45.16	-	B	polo_R_265_di	62.38	-
B	Or65b_K_37_di	44.44	-	B	dar1_R_653_me	61.68	-
B	cathD_K_321_me	44.26	-	B	CG14259_R_148_me	60.49	-
B	Axn_K_594_di	43.00	-	B	CG8419-RA_R_607_me	58.68	-
B	Apoltp_K_1282_me	42.74	-	B	Actn_R_324_di	57.60	-
B	chn_K_802_me	42.19	-	B	CG10361-RA_R_220_me	57.46	-
B	CG31191_K_300_di	42.10	-	B	Slob_R_977_di	57.15	-
B	CG31191_K_305_di	42.10	-	B	tankyrase_R_667_me	56.56	-
B	Mms19_K_891_me	42.00	-	B	CG13127_R_629_di	55.72	-
B	CG10565_K_400_me	41.48	-	B	CG4612_R_241_di	55.68	-
B	CG7264_K_311_di	41.35	-	B	zip_R_1519_me	54.42	-
B	CG8798_K_389_me	40.99	-	B	zip_R_1522_me	54.42	-
B	mRpS33_K_4_me	40.72	-	B	CG13634_R_48_me	54.34	-
B	para_K_1590_me	40.59	-	B	CG13634_R_49_me	54.34	-
B	para_K_1591_me	40.59	-	B	CG17652_R_127_me	53.17	-
B	Cyp4d14_K_26_me	40.50	-	B	CG11155-RA_R_249_di	51.93	-
B	CG6719_K_12_me	39.27	-	B	AdamTS-A_R_1664_di	49.50	-
B	Mhc_K_362_di	39.27	-	B	CG13930_R_255_me	47.68	-
B	enok_K_1056_me	39.01	-	B	CG13930_R_256_me	47.68	-
B	dco_K_8_me	38.29	-	B	Cyp6d2_R_100_me	47.57	-
B	Pgi_K_444_di	38.03	-	B	CG32103-RB_R_374_di	46.96	-
B	CG10793-RA_K_431_me	37.68	-	B	CG32103-RB_R_381_di	46.96	-
B	CG17687_K_9_tr	37.19	-	B	Art6_R_34_me	46.89	-
B	Tim9a_K_3_di	37.09	-	B	ocm_R_1383_di	46.82	-
B	CG9577_K_217_me	36.64	-	B	Sans_R_515_me	45.92	-
B	CG4729_K_91_tr	36.30	-	B	Ndc80_R_555_me	45.86	-
B	Mhc_K_720_me	36.28	-	B	Ndc80_R_558_me	45.86	-
B	CG31612_K_625_me	35.65	-	B	CG32352_R_1270_me	45.33	-
B	CG31612_K_631_me	35.65	-	B	CG13127_R_371_di	45.16	-
B	Mhc_K_1443_tr	35.65	-	B	CG13930_R_120_me	43.38	-
B	Mhc_K_1444_tr	35.65	-	B	CG13930_R_132_me	43.38	-
B	Mhc_K_1446_tr	35.65	-	B	Axn_R_599_di	43.00	-

B	CG13337_K_659_me	35.20	-
B	CG13337_K_667_me	35.20	-
B	CG13337_K_669_me	35.20	-
B	CG13364_K_20_di	34.18	-
B	CG13364_K_30_di	34.18	-
B	Oatp58Da_K_343_me	34.08	-
B	Lpt_K_706_me	33.87	-
B	CG7504_K_1647_me	33.80	-
B	unk_K_201_me	33.32	-
B	ida_K_120_me	32.61	-
B	CG32454_K_108_tr	32.55	-
B	CG32454_K_95_tr	32.55	-
B	Strn-Mlck_K_261_tr	32.28	-
B	Prosbeta5R_K_11_me	31.84	-
B	sec3_K_468_di	31.43	-
B	Rap2l_K_31_me	30.98	-
B	Rap2l_K_42_me	30.98	-
B	Gr92a_K_12_tr	30.87	-
B	Esyt2_K_515_tr	30.59	-
B	uri_K_167_me	30.54	-
B	uri_K_168_me	30.54	-
B	CG3817_K_201_di	30.00	-

	Histones	**Score H**	**Score L**
A1	His3_K_80_di	143.97	122.33
A1	His3.3A_K_28_me	79.66	70.94
A1	His1:CG33807_K_156_me	43.77	150.46
A1	His3_K_28_tr	37.60	69.01
A1	His3_K_80_me	28.17	81.64
A2	His3_R_84_me	55.40	35.68
A2	His3_K_28_di	46.84	46.80
A2	His3_K_37_me	26.97	20.46
A2	His3_K_38_me	26.97	20.46
A2	His3_R_41_me	26.97	20.46
A2	His3.3A_K_28_tr	25.44	25.44

B	Apoltp_R_1278_me	42.74	-
B	CG1847_R_45_me	42.57	-
B	CG1847_R_51_me	42.57	-
B	CG5214_R_327_me	40.88	-
B	ird1_R_1044_di	39.92	-
B	brp_R_718_di	39.02	-
B	vih_R_50_me	38.71	-
B	ens_R_397_me	38.30	-
B	dco_R_10_me	38.29	-
B	dco_R_4_me	38.29	-
B	shark_R_484_di	38.29	-
B	Fmr1_R_418_di	38.02	-
B	CG10793-RA_R_425_me	37.68	-
B	CG10793-RA_R_427_me	37.68	-
B	CG3184_R_72_di	37.56	-
B	Or69a_R_347_di	37.48	-
B	wb_R_1983_di	37.19	-
B	CG18675_R_240_di	36.69	-
B	Apc_R_1479_di	36.40	-
B	Apc_R_1481_di	36.40	-
B	CG5645_R_562_me	36.30	-
B	CG31612_R_630_me	35.65	-
B	CG2225_R_976_me	34.91	-
B	fz_R_125_di	34.75	-
B	fz_R_132_di	34.75	-
B	CG7504_R_1654_me	33.80	-
B	CG14186_R_174_di	33.68	-
B	unk_R_202_me	33.32	-
B	tou_R_1176_me	31.53	-
B	sec3_R_467_di	31.43	-
B	Rap2l_R_41_me	30.98	-
B	uri_R_161_me	30.54	-
B	nmdyn-D7_R_280_me	30.33	-
B	Brms1_R_162_di	30.31	-
B	ArfGAP3_R_311_me	30.21	-
B	ArfGAP3_R_319_me	30.21	-
B	CG3817_R_202_di	30.00	-

Acknowledgements

Als erstes möchte ich Prof. Dr. Axel Imhof ***Danke*** sagen! ***Danke*** für die Möglichkeit an diesem Projekt zu arbeiten und für deine Begeisterung, die du in diese gemeinSAMe Zeit mit eingebracht hast.

Ein großes ***Dankeschön*** geht an Prof. Dr. Peter Becker für die schönen Jahre am ABI mit einer tollen wissenschaftlichen Umgebung und einer freundlichen und kollegialen Atmosphäre, die mich jeden Tag wieder neu motiviert hat. Die zahlreichen retreats, barbecues und Wies'n Ausflüge nicht zu vergessen – ich vermisse die Tage am ABI jetzt schon.

Danke an Prof. Dr. Jerzy Adamski und Dr. Cornelia Prehn für die tolle Zusammenarbeit. Ich habe immer gerne den weiten Weg nach Neuherberg gemacht, wurde freundlich aufgenommen und habe viel in Sachen ‚trouble shooting' gelernt!
Ein besonderer ***Dank*** geht an dieser Stelle auch an Sven Zukunft und Carolin Muchet für das geduldige Beantworten aller Fragen und die Hilfe bei den ein oder anderen Analyst Problemchen.

Thanks to Dr. Tobias Straub, Victor Solis and Dr. Andreas Schmidt for all the bioinformatic analyses including the analysis of the microarray and the analyses of all the possible methyltransferases!

Mille grazie to Dr. Tiziana Bonaldi und Dr. Michael Bremang for the nice collaboration, your knowledge and help in deciphering the *Drosophila* methylome. Hope, this work will be continued!

Für's Korrektur lesen habe ich auch einige Leute eingespannt: Teresa, Gabi und Henni, ***viiiielen Dank***! Thomas, ***Danke*** an dieser Stelle für deine Hilfe bei allen qPCR Belangen. ***Thanks*** Shibo for reading part of the thesis and support.

Vielen Dank, Edith Müller und Caroline Brieger für die stetige Unterstützung in allen bürokratischen Belangen!

A ***BIG thank you*** goes to all past and present Imhof group members and the ZfP for the nice and helping working atmosphere, the scientific discussions and support and the fun we had within these years – you always made my day! Thanks for this incredible time!

Ganz besonders danken möchte ich den Salatclub-Mitgliedern Edith, Gabi, Irene und Miri. Ihr habt jede Mittagspause nicht nur zu einem kulinarischen Highlight werden lassen! Wir haben viel gelacht und uns auch den wichtigen Dingen des Lebens angenommen! Und der kalte Kaffee am Ende gehörte irgendwie auch dazu. Es war mir eine Ehre und **Freu(n)de** zugleich! ***Merci***, dass es euch gibt! Das gilt auch für Teresa, Vio, Henni und Moritz : ***Dankeschön*** und ***Mille grazie*** – I remember lots of funny days and late evening sessions with dinner in lab ("..you raise me uuuup.."). Felicitas!

An dieser Stelle auch ein ***Dank*** an den Rupp-Trupp mit allen ehemaligen Forscher/innen. Als „Adoptiv-Rupp" hatte ich mit euch immer viele Späße, ob mit Doktor Auerbach oder der kalten Ente oder einfach nur so.

To the ‚Istanbulers and Pragers': ***Thanks*** and ***Merci*** to Ze Straubs, Frau Jack, Clemens, Wippo, Dr. Sommer and Manolo for great times besides lab – not only on the roof.

Ganz zum Schluss möchte ich natürlich auch noch meiner Familie ***Danke*** sagen. Ihr habt mich immer unterstützt, in allem was ich tat und seid mir bei jeder Entscheidung immer zur Seite gestanden! ***Danke***, dass ihr immer für mich da seid!